

UNIVERSITY OF CALIFORNIA

Los Angeles

**Channel Coding and Power Control for FH/CDMA
Radios**

A dissertation submitted in partial satisfaction of the
requirements for the degree Doctor of Philosophy
in Electrical Engineering

by

Victor Shiaw-Jong Lin

1995

The dissertation of Victor Shiaw-Jong Lin is approved.

Kirby Baker

Henry Samueli

Kung Yao

Gregory J. Pottie, Committee Chair

University of California, Los Angeles

1995

TABLE OF CONTENTS

LIST OF FIGURES	viii
LIST OF TABLES	xii
ACKNOWLEDGMENTS	xiii
VITA	xv
ABSTRACT OF THE DISSERTATION	xvii
1. INTRODUCTION	1
1.1 Historical Perspective	2
1.2 Scope of Thesis	5
2. TECHNICAL BACKGROUND	7
2.1 Communication Systems	8
2.2 Overview of Cellular Radio Concepts	11
2.2.1 Multiple Access Schemes	12
2.2.1.1 FDMA	13
2.2.1.2 TDMA	13
2.2.1.3 CDMA	14
2.3 Summary	16
3. SYSTEM MODELS	17
3.1 Network Topology	18

3.2	SFH/CDMA Network Model	19
3.3	Radio Link Model	21
3.4	Fading Channel Model	22
3.4.1	Propagation Models	23
3.4.1.1	Median Signal Strength	25
3.4.1.2	Signal Variability	25
3.4.2	Interference Model	27
3.5	Channel Modeling for Power Control Study	27
3.6	Channel Modeling for Channel Code Study	29
3.7	Summary	30
4.	IMPLEMENTATION OF DISTRIBUTED POWER CONTROL	31
4.1	Motivation	32
4.2	Description of Power and Admission Control Algorithm	34
4.3	Network Capacity for Ideal Power Control	40
4.3.1	Simulation Parameters	41
4.3.2	Single Cell Reverse Link Capacity	42
4.3.3	Multiple Cell Reverse Link Capacity	44
4.3.4	Peer-to-Peer Cluster Capacity	46
4.4	Performance Degradation Due to Power Control With Dynamic Range Con- straint	48
4.4.1	Global Algorithm with Dynamic Range Constraint	49

4.4.2	Distributed Power Control With Dynamic Range Constraint ...	51
4.5	Reducing Call Dropping Probability	53
4.6	Summary	62
5.	CODE SELECTION	64
5.1	System Model	65
5.1.1	Performance of Reed-Solomon and BCH Codes	67
5.1.2	Performance of Convolutional Codes	68
5.1.3	Decoding Delay	70
5.1.4	Decoder Complexity	72
5.2	Decoding Metrics	73
5.2.1	Soft Decision Metrics for Fading AWGN Channels	74
5.2.2	Soft Decision Metrics for Multiple-Access Channels	75
5.2.3	Estimation of Channel Parameters	77
5.2.4	Erasure Metric	78
5.2.5	Performance Evaluations	79
5.3	Summary	81
6.	ADAPTIVE METRICS FOR CONVOLUTIONAL CODES	83
6.1	Motivation	85
6.2	System Model	87
6.2.1	Interference Model	88

6.2.2	Receiver Model	88
6.2.3	Diversity and Coding	91
6.3	Performance Analysis	92
6.3.1	Hard Decision Decoding	93
6.3.2	VRT Erasure and Error Decoding	94
6.3.3	Soft Decision Decoding	96
6.3.3.1	No CSI	96
6.3.3.2	Weighted Soft Decision Metric, Perfect CSI	98
6.3.3.3	Weighted Soft Decision Metric, Imperfect CSI	100
6.3.4	Quantized Metric (Single Quantization Interval)	101
6.3.5	Quantized Metric (Multiple Quantization Intervals)	102
6.4	Numerical Results and Discussion	103
6.4.1	Rayleigh Fading Channel	103
6.4.2	Rayleigh Fading, Bi-Level Partial-Band Jammer Channel	108
6.5	Adaptive Algorithm and Performance Results for the WAQ metric ..	114
6.6	Summary	117
7.	CONCLUSION	118
A.	Frequency Reuse with Latin-Squares	121
B.	Derivation of the Exact Pair-wise Error Probability.....	124

C. Glossary	126
C.1 List of Acronyms and Abbreviations.....	126
C.2 Definitions.....	127
Bibliography	131

LIST OF FIGURES

- Figure 2-1 Block diagram of a digital communication system. 8
- Figure 2-2 Temporal variation of the received signal power due to Rayleigh fading. 10
- Figure 3-1 Network model with three clusters and a table showing some $N=NT=8$ latin-square hopping sequences. 20
- Figure 3-2 System model for a radio link. 21
- Figure 4-1 Simple example with two links 33
- Figure 4-2 Outage probability vs. dynamic range 34
- Figure 4-3 Reverse link capacity of the single cell SFH/CDMA 44
- Figure 4-4 Reverse link capacity of the cellular SFH/CDMA system (with and without ACI. The ACI coupling factor is -20 dB). 46
- Figure 4-5 Capacity of single-cluster SFH/CDMA system versus ACI coupling factor 48
- Figure 4-6 Reverse link capacity of the single cell SFH/CDMA vs. dynamic range with and without shadowing 50
- Figure 4-7 Reverse link capacity of the single cell SFH/CDMA vs. dynamic range with shadowing 52
- Figure 4-8 Call blocking and call dropping probabilities vs. dynam-

ic range for a single-cell network 53

- Figure 4-9 Histogram of the initial interference power for three different outcomes for a single-cell network 55
- Figure 4-10 Stacked histograms of the gross power increase conditioned on two outcomes for a single-cell network 56
- Figure 4-11 Flowchart of distributed admission control algorithm 58
- Figure 5-1 System model. 65
- Figure 5-2 BER vs. SNR for rate-1/2, 64 state convolutional code. 69
- Figure 5-3 BER vs. SNR for a convolutional code and a Reed-Solomon code with different decoding strategies. 80
- Figure 6-1 Error probability for soft, E&X and hard decision decoding in bi-level partial-band jamming channel. 86
- Figure 6-2 Conventional non-coherent square-law detector for BFSK. 89
- Figure 6-3 The optimum threshold and cutoff rate vs. SNR per bit for a binary coded system over the Rayleigh fading channel. 104
- Figure 6-4 Coding gain comparison of four different metrics for $L=6, k=1, n=2$ convolutional code over the Rayleigh fading channel. 105

- Figure 6-5 The optimum quantization interval and the corresponding cutoff rate vs. SNR for a binary coded system over a Rayleigh fading channel. (for 3 different number of quantization bits) 106
- Figure 6-6 Coding gain comparison of four different metrics for $L=6$, $k=1$, $n=2$ convolutional code over the Rayleigh fading channel. 107
- Figure 6-7 The optimum threshold and cutoff rate vs. SNR per bit for a binary coded system in a Rayleigh fading, bi-level partial-band jammer channel ($r = 0.25$, $f=0.90$). 108
- Figure 6-8 Coding gain comparison of three metrics using $L=6$, $k=1$, $n=2$ convolutional code over Rayleigh fading, bi-level partial-band jammer channel ($r = 0.25$, $f=0.90$). 109
- Figure 6-9 Comparison of weighted soft metrics with perfect CSI and imperfect CSI decoding for $L=6$, $k=1$, $n=2$ convolutional code for Rayleigh faded, bi-level partial-band jammer channel ($r = 0.25$, $f=0.90$). 110
- Figure 6-10 Cutoff rate vs. SNR per bit for quantized metric decode NC-BFSK system over Rayleigh fading bi-level, partial-band jammer channel ($r = 0.25$, $f=0.90$). 112

- Figure 6-11 Optimum quantization interval vs. SNR per bit for IAQ metric decode NC-BFSK system over Rayleigh fading bi-level, partial-band jammer channel ($r = 0.25$, $f=0.90$). 112
- Figure 6-12 Optimum quantization interval vs. SNR for two quantized metric decoded NC-BFSK system over Rayleigh fading bi-level, partial-band jammer channel ($r = 0.25$, $f=0.90$). 113
- Figure 6-13 Cutoff rate vs. SNR per bit for four different decoding metrics with a NC-BFSK system over Rayleigh fading bi-level, partial-band jammer channel ($f=0.90$, $E_b/N_0=13$ dB). 116
- Figure A-1 19 Hexagonal Cell Layout (Frequency Reuse Factor of $1/3$) 122
- Figure A-2 Hopping pattern by Latin-square construction ($n = 8$ and frequency reuse factor of $1/3$). 123

LIST OF TABLES

Table 4-1	Call blocking and call dropping probabilities with and without distributed admission control for a single-cell network 59
Table 4-2	Call blocking and call dropping probabilities with and without distributed admission control for a single-cell network 59
Table 4-3	Call blocking and call dropping probabilities with and without distributed admission control for a multi-cell network 61
Table 4-4	Call blocking and call dropping probabilities with and without distributed admission control for a single-cluster network 62
Table 5-1	Code performance and delay comparison 71
Table 5-2	E_b/N_0 at $P_b = 10^{-3}$ for different decoding metrics for a dual antenna diversity system. 79
Table 5-3	Code performance for different decoding methods 81

ACKNOWLEDGMENTS

To my advisor, Professor Gregory J. Pottie, I would like to express my deepest gratitude for his guidance, support, and kindness throughout my years at UCLA. I am especially grateful for the extra time and effort he has devoted to shape my research experience and to ensure me continuing successful endeavors in the engineering field.

I would also like to thank the other members of my dissertation committee: Dr. Kirby Baker, Dr. Kung Yao, and Dr. Henry Samueli. I appreciate the collective enthusiasm they have shown toward my research. Additional thanks go to Dr. Samueli for providing me a rewarding consulting assignment with Broadcom.

To all the members of the radio transceiver project, I thank you for your collaboration. I am grateful for the assistance of Dr. Tim Chen and Prof. Nicholas Bambos in the study on power control issues. I am also thankful for the many helpful technical discussions with my colleagues: Chris Hansen, Jaeheyong Kim, Jonathan Min, Eldad Perahia, Ben Tang, and Charles Wang. The follow is a short list of colleagues and friends who made my stay at UCLA more interesting and enjoyable: Bruce Kwan, Steve Chin, Tom Kwon, Jeff Putnum, Eric Berg, Pat Pai,

Robin Joshi, Gordon Yee, James Chang, Glenn Chang, and Kirk Chang. I apologize for leaving anyone out inadvertently. I appreciate the help and efficiency of all the staff members in the Electrical Engineering department.

I would like to thank my extended family at the University Presbyterian Church. I thank especially Pastor Soon Chang and Esther Chung, for their warmth, kindness and prayers. I thank God that they have strengthen my faith in Him.

Lisa, I want to thank God for bring her into my life. She has shown me the meaning of love and spiced my life with laughters. I will always remember how she helped me regain strength and focus when I felt heavy with burdens.

Most of all, I am indebted to my parents for their immeasurable care, support and understanding. Thank God for giving me parents who are so loving and wise. I have been deeply touched by my brother Tom and sister Cathy for their constant prayers and encouragement. Thank God for them and their families.

Lastly, I would like to acknowledge financial support from ARPA.

VITA

January 7, 1967	Born, Taipei, Taiwan
1989	B.S., Electrical Engineering Cornell University Ithaca, New York
1989-1990	Product Development Engineer Hewlett Packard Andover, Massachusetts
1991	M. Eng., Electrical Engineering Cornell University Ithaca, New York
1990	Teaching Assistant Cornell University Ithaca, New York
1992-1995	Research Assistant University of California, Los Angeles Los Angeles, California
1994	Independent Consultant Broadcom Corporation Los Angeles, California

PUBLICATIONS AND PRESENTATIONS

- J. Min, A. Rofougaran, V. Lin, M. Jensen, A. Abidi, G. Pottie, and Y. Rahmat-Samii, "A Low-Power Handheld Frequency-Hopped Spread Spectrum Transceiver Hardware Architecture," Virginia Tech Symposium on Wireless Personal Communications, Blackburg, VA, p. 10/1-8, June 1993.
- V. S. Lin and G. J. Pottie, "Channel Coding for a Frequency-Hopped Wireless Transceiver," Proc. of the 1993 Canadian Workshop on Information Theory, Ottawa, Canada, pp. 109-124, 1994.

- V. S. Lin and G. J. Pottie, "Implementation of Distributed Power and Admission Control for a Frequency-Hopped Wireless Transceiver," International Wireless '95 Conference, July 1995.
- V. S. Lin and G. J. Pottie, "Adaptive Decoding Metrics with Convolutional Coding in FH/CDMA Systems," Submitted to IEEE Transaction on Communications

ABSTRACT OF THE DISSERTATION

Channel Coding and Power Control For FH/CDMA Radios

by

Victor Shiaw-Jong Lin

Doctor of Philosophy in Electrical Engineering
University of California, Los Angeles, 1995
Professor Gregory J. Pottie, Chair

We investigate the issues of adaptive power control, channel code selection and decoding metrics formulation for a slow frequency-hopped/code division multiple access (SFH/CDMA) radio.

We show how to effectively adapt a distributed power control scheme proposed for single-channel narrowband systems to the unique constraints of the SFH/CDMA system. In addition, the performance of distributed power control with a fixed transmit power dynamic range is studied through simulation. Heuristic admission control algorithms for mitigating performance degradations due to the dynamic range constraints are presented. Some of the trade-offs between system capacity and complexity are discussed.

We also present a low-delay channel coding technique and demonstrate the benefits of dual antenna diversity in combination with coding. BCH, Reed-Solomon (RS), and convolutional codes are considered. The basis for code comparison are the system performance, delay and decoder complexity. It is shown that when

binary non-coherent FSK modulation and hard decision detection are used, the BCH, RS, and convolutional codes that can meet the delay and bandwidth constraints have similar performance and comparable complexity. Soft decision decoding for the convolutional code and error-and-erasure correction decoding for the RS code are investigated in terms of the performance-complexity trade-offs. For convolutional codes, it is shown that improvement over hard decision decoding is significant when the right decoding metric is selected.

To improve the effectiveness of coding in SFH/CDMA systems, a new class of decoding metrics is formulated. The performance of new adaptive decoding metrics for convolutional codes is analyzed under Rayleigh fading and bi-level partial-band noise jamming. New tighter probability of error performance bounds are derived. We find that adapting the metric according to the channel condition provides significant performance gain over standard fixed decoding metrics, such as the soft decision and erasure and error decoding metrics. We also describe a simple algorithm for adapting the decoding metric.

Chapter 1

INTRODUCTION

Wireless personal communication systems enable geographically dispersed users to exchange information using a portable terminal, such as a handheld transceiver. Often, the system engineer's design objective is to maximize the transmission rate and number of simultaneous users (capacity) under the constraints of robustness, power consumption and hardware complexity. The tradeoffs among capacity, reliability, signal power, and cost of equipment can be complex. The topic of this thesis is a study of good system tradeoffs in wireless transceiver design.

Future generations of wireless personal communication systems will be based on digital transmission technology. Digital technology has important advantages over traditional analog technology. With digital technology, radio communication systems can be designed to meet more stringent transmission reliability requirements. Furthermore, digital technology enables more efficient sharing of channel resources when multiple users need to access the system through a common channel simultaneously.

1.1 Historical Perspective

What are some important milestones in the history of wireless communications? The birth of wireless communication is generally accepted to have occurred in 1897, when Marconi received credit with the patent for the radiotelegraph, from which the word radio was coined [17]. Since that time, mobile radio communications has been used to navigate ships and airplanes, dispatch police cars and taxis, generate new businesses, and win wars.

The use of radio telephones has evolved rapidly and grown explosively in the last few decades. This evolution of wireless systems can be viewed to have occurred in different stages [19]. The main force driving the evolution is an increasing public demand for wireless services. To meet this ever increasing demand, better communication technologies are required to increase network capacity, to improve quality of service, and to introduce new service features.

The first generation of public wireless systems was developed in the 1970's and the 1980's, based on analog technology. During this period, several systems were built, including Nordic Mobile Telephone (NMT) by Ericsson, Advanced Mobile Phone Service (AMPS) by AT&T, and Mobile Cellular Service L1 (MCS-L1) by Nippon Telephone and Telegraph (NTT) [17]. In order to improve system capacity, the cellular concept [14] was adopted. The main concept of cellular systems is that the service region is divided into smaller areas, called cells. By using more cells, the system can support more users. To further improve capacity, other ideas, such as cell splitting and sectorization, were developed.

As the public appetite for wireless services gets bigger, the capacity of first generation systems, even with improvements, soon became insufficient to satisfy the

demand in some areas. This led to the development of the second generation digital wireless system, built in the 1980's and the 1990's. In this period, digital technology is implemented to improve the system capacity several times over traditional analog systems. At this stage, vehicular cellular radio and cordless telephone are developed and optimized separately to provide service to users with different mobility patterns and communication needs [8]. The typical vehicular radio systems include Global System for Mobile Communications (GSM) in Europe and Digital AMPS (IS-54) in the United States; the typical cordless telephone systems include CT-2 in Europe and some spread spectrum products in the United States.

Among second generation systems, one of the new technologies used to boost system capacity is code division multiple access (CDMA). CDMA, based on spread spectrum technology, is developed to utilize the available spectrum more efficiently in multicell networks. The history of spread spectrum (SS) communications can be traced all the way back to its military origin during early phases of World War II [36]. In military applications, spread spectrum technology is used to combat intentional jamming by an enemy transmitter. The approach to defeat jamming is to transmit over many signal coordinates with large-bandwidth signals, such that the jammer cannot achieve large jammer-to-signal power ratio in all the coordinates. The antijamming properties of SS signals are well investigated and documented [37].

Since spread-spectrum uses large-bandwidth signals that result in the apparent inefficient use of the radio spectrum, people had assumed that commercial applications of SS radios were impractical [42][43]. Cooper and Nettleton, in 1978, were the first ones to recognize that digital spread-spectrum radio had a potentially higher capacity for mobile radio applications than the analog narrowband radios used at that time [7]. More research on digital SS mobile radio soon followed in 1980 [13][39].

By the late 1980's and early 1990's, advances in very-large-scale integrated circuit (VLSI) technologies has made low-cost implementation of spread-spectrum radio possible while the popularity of mobile radio has spurred the market demand for high-capacity systems. These factors contributed to a renewed interest in the application of spread-spectrum technology for mobile radio. The widespread commercial development of SS wireless systems today is sparked by two key events. One of the events is the 1985 FCC ruling which allows the unlicensed use of spread-spectrum radio in ISM bands, which include the 902 to 928 MHz band. Another key event is the well-publicized Qualcomm direct sequence spread-spectrum (DS/SS) CDMA system which has led to the adoption of a second U.S. digital cellular standard, IS-95 [12].

Today, commercial spread-spectrum radios are used in indoor office applications, such as wireless local area networks (WLANs), and wireless cordless phone (PBX) systems. Among the interesting outdoor applications is the Federal Emergency Management Agency's (FEMA) experimental use of spread-spectrum radios to transmit digital video. In some situations, unlicensed spread spectrum radio is used as an emergency backup to wired lines and in many cases, they are used as a more economical substitute for digital leased lines.

Numerous sources have projected that the demand for wireless communication services will continue to grow rapidly well into the next century. One of the key ingredients needed in third generation wireless personal communications systems (PCS) is a low-power wireless access technology. The portability and affordability requirements forces a design focus on power reduction to extend battery life and lower component costs. Developing a low-power handheld transceiver that can provide robust wireless communications presents many technical challenges. To meet some of the

challenges, the UCLA personal communications project began in 1991.

1.2 Scope of Thesis

This thesis arises from work we have performed to develop and validate the system design techniques proposed for the UCLA prototype all-CMOS wireless transceiver handset. A radio signal propagating in a wireless environment suffers from severe corruption due to various channel impairments, making reliable communication difficult. To overcome the radio channel impairments without resorting to high transmitter power, the proposed architecture incorporates many advanced system techniques, such as antenna diversity, slow frequency-hopped/code division multiple access (SFH/CDMA), channel coding, and adaptive power control.

The topic of this thesis is the study of the system tradeoffs in the implementation of adaptive power control, channel code selection, and the formulation of decoding metrics for frequency-hopped transceivers in wireless communication applications. Our investigation has resulted in the specification and validation of a distributed power control scheme for a SFH/CDMA system, the determination of the sufficient transmit power dynamic range to prevent significant system capacity loss and the development of heuristic algorithms for reducing call dropping in a power controlled network with dynamic power range restrictions. We have also performed a study on low-delay channel coding and demonstrated the benefits of dual antenna diversity in combination with coding. In addition, we have designed an adaptive metric that can track variations in channel statistics and a simple algorithm for adapting the metric to changing channel conditions. We will show that adapting the metric according to the channel condition provides significant performance gain over standard fixed decoding metrics, such as the soft decision and erasure and error decoding metrics.

Chapter 2 gives an overview of terrestrial cellular radio communication technologies, with particular attention to CDMA systems. In chapter 3 we outline a framework and describe system models for analyzing CDMA systems. In chapters 4 to 6, we present our new results. In chapter 4 we consider the implementation of distributed adaptive power control. We show how to effectively adapt a distributed power control scheme proposed for narrowband systems to the unique constraints of a SFH/CDMA system. In chapter 5 we consider channel coding options for a frequency-hopped system employing NC-BFSK signaling. Alternative channel codes are compared on the basis of delay, complexity, and bandwidth efficiency. In chapter 6 we propose new adaptive decoding metrics for convolutional code and derive new tighter probability of error bounds. Chapter 7 contains our conclusions and suggestions for future research.

Chapter 2

TECHNICAL BACKGROUND

In a multi-user radio communication system, several users can simultaneously exchange information over different radio links. The system design objective is to establish as many reliable links as possible over an unreliable shared communication medium. The principal impairments in a single link or channel are attenuation due to multipath fading and multiple access interference from other radios. To overcome these impairments, advanced digital transmission techniques are needed.

In this chapter, we outline basic multi-user radio system design principles and techniques. Specifically, we are concerned with the design of digital mobile radio systems based on spread spectrum technology. Spread spectrum techniques have inherent multipath fading immunity and multiple access capability. Section 2.1 briefly reviews the basic principles of a digital communication system, with focus on system design techniques for overcoming impairments in a fading channel. Section 2.2 gives an overview of cellular radio concepts, explaining the characteristics of CDMA that are advantageous for terrestrial personal wireless systems.

2.1 Communication Systems

We assume the reader to be familiar with the basic concept of digital communications, such as digital modulation. Hence, we provide only a brief review of the fundamental principles of a generic digital communication system. The review introduces some of the communication terminologies used in this thesis. A glossary of definitions is provided in the Appendix.

The basic functional elements of a digital communications system are shown in the block diagram in Figure 2-1. The information source generates a message to be sent electronically to the information sink by the transmitter-receiver pair through a medium or channel, e.g. the copper wires in a telephone network. In digital communications, the

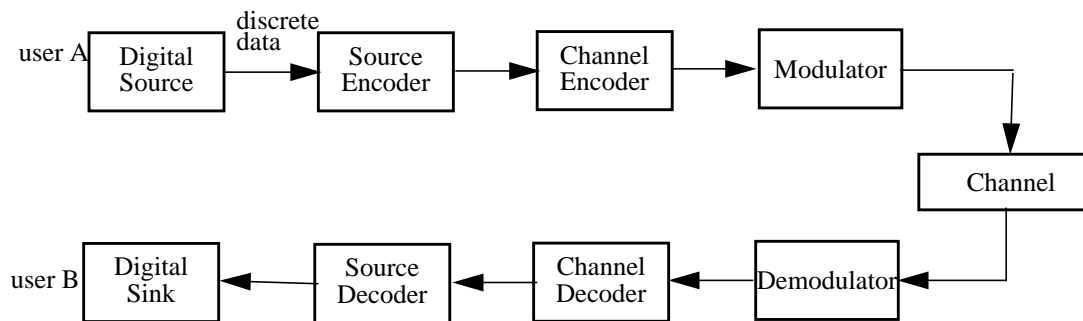


Figure 2-1 Block diagram of a digital communication system.

message consists of a sequence of discrete symbols, e.g. binary digits. The source encoder processes the source output to remove redundancy, compressing the digital sequence into a more efficient representation for transmission.

The channel encoder adds controlled redundancy to the compressed message in order to control the errors caused by channel disturbances. There are a variety of error control coding techniques which have been developed by communication engineers since the 1960's. Selecting an appropriate channel code for a particular system involves

making trade-offs among error performance, transmission delay, channel bandwidth expansion due to added redundancy, and algorithmic complexity.

The modulator converts the digital information sequence into a signal suitable for transmission through an analog waveform channel. The particular method of modulation depends on the channel characteristics. In binary modulation, the modulator may simply map the binary digit 0 onto a waveform $s_0(t)$ and the binary digit 1 onto a waveform $s_1(t)$.

In general, no real channel is ideal. For the terrestrial mobile radio channel, noise disturbances, multiple access interference, and multipath fading corrupt the transmitted signal. The thermal noise generated within the receiver front-end is accurately described by a mathematical model called additive white Gaussian noise (AWGN). In some cases, the interference can also be approximated as Gaussian. In addition to interference and thermal noise, the propagation impairments for terrestrial mobile radio can be separated into two categories—namely, quickly varying or slowly varying with respect to the symbol interval. In the former category is fast fading of desired and interference signals, while in the latter category is shadowing and free space losses. Techniques to deal with both of these conditions will be described in subsequent chapters.

The most damaging type of multipath fading is Rayleigh fading. Multipath fading occurs whenever the received signal consists of various delayed versions of the transmitted signal arising from propagation over multiple paths of different lengths. Depending the relative phases of the delayed signals, the signals could combine to produce a large or small resultant signal, causing large amplitude and power variations in the received signal. Figure 2-2 illustrates typical received power fluctuation due to

Rayleigh fading for a mobile receiver. During a deep fade, the quality of the received

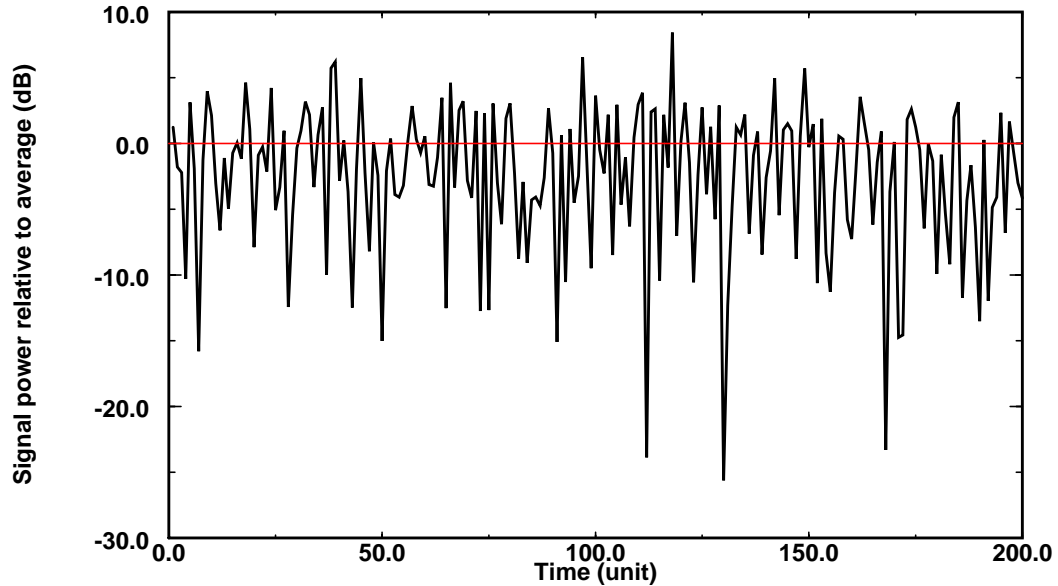


Figure 2-2 Temporal variation of the received signal power due to Rayleigh fading.

signal is severely degraded.

At the receiving end of the communication system, the demodulator processes the channel-corrupted transmitted waveform by frequency shifting and reduces each waveform to a single number that represents an estimate of the transmitted data symbol. A hard decision demodulator decides on whether the transmitted bit is a 0 or a 1. On the other hand, a soft decision demodulator quantizes the decision to more than two levels to enable soft decision decoding, i. e., decoding with more complete signal information. The remainder of the receiver decodes the received information sequence based on knowledge of the code used by the source and channel encoders and delivers the decoded sequence to the user.

The error probability of the decoded sequence is a commonly used measure of the communication system performance. In general, the probability of error is a function of the code characteristics, the types of waveforms used to transmit the

information over the channel, the transmitter power, the characteristic of the channel, and the method of demodulation and decoding.

Whereas in an AWGN channel the bit error rate (BER) of an optimized system drops exponentially with signal-to-noise-ratio (SNR), for a Rayleigh fading channel the BER declines only linearly with SNR. Thus, a huge power penalty must be paid unless diversity techniques are used to mitigate the effects of multipath fading. Diversity is the technical term for reception of different versions of the same information, each with independent fading levels. With L^{th} order diversity, the probability of error declines as the L^{th} power of SNR [29]. Diversity may be achieved in any combination of the space (antenna), time, or frequency domains. Diversity achieved in different domains is multiplicative. A combination of techniques from several domains is an economical means of achieving a high aggregate diversity order, thereby taming the multipath channel and allowing receiver performance close to that achievable in the AWGN channel. These items and their effect on bit error rate (BER) will be investigated in Chapters 5.

2.2 Overview of Cellular Radio Concepts

The public switched telephone network (PSTN) has been developed rapidly in this century, allowing reliable communication of voice and data around the globe. A cellular radio system provides public wireless access to the capabilities of the global wireline network at any time without regard to location or mobility. Subscribers of cellular systems gain access to the wireline network over the service region where cellular coverage is provided. The main feature of cellular systems is that the coverage region consists of smaller disjoint areas, called cells. In each cell, coverage is provided

by one base station. Continuous coverage across different cells is achieved by the seamless transfer of the calls from one base station to another. This procedure is called a handoff. Due to propagation attenuation of radio signals, the same frequency band could be used simultaneously by multiple base-mobile pairs which are far enough apart for the mutual interference to be tolerable. This “frequency reuse” allows a much higher subscriber density per MHz of spectrum than systems using one base station to cover the entire region.

There are two types of channels in cellular systems: downlink channels (from the base station to the mobile user) and uplink channels (from the mobile users to the base station). Under the centralized control of the base station, the downlink is generally operated as a broadcast channel in the Time Division Multiplexing (TDM) mode. On the other hand, the uplink is a multiple access channel that enables dispersed users to share a common resource. The uplink problem poses a more challenging problem than that of the downlink. Hence, in this thesis we focused more attention on the uplink.

2.2.1 Multiple Access Schemes

In the wireless environment, the transmitted radio signal is subjected to various impairments, such as interference, fading, and shadowing, as previously mentioned. A good multiple access scheme should be able to tolerate such impairments while allowing efficient and fair utilization of the available system resources. Depending on the application, there might be many other considerations in designing or selecting a multiple access technique.

In cellular systems, the multiple access channel resource can be parcelled out to users either on a frequency basis using frequency division multiple access (FDMA), on

a time basis using time division multiple access (TDMA), or on a code basis using code division multiple access (CDMA). Hybrid schemes based on combinations of the three basic sharing schemes are also possible. Next, we will describe the three basic schemes briefly.

2.2.1.1 FDMA

In FDMA, a unique frequency channel is assigned to each user for the duration of the call. The channel cannot be shared by other users during the call. With this fixed assignment protocol, the control logic is very simple, but the channel resources are not used very efficiently. To improve capacity, the same frequency channel can be reused in distant cells where there is enough protection from co-channel interference. FDMA is vulnerable to radio channel impairments even at relatively high SNR. The shortcomings of FDMA makes it unsuitable for high capacity wireless systems. FDMA has been used predominately in the first generation cellular systems. Today, it may serve an auxiliary role in a hybrid access scheme.

2.2.1.2 TDMA

In TDMA, time is divided into slots which are grouped into frames. The frame repeats. Each user is assigned a unique time slot in a frame. This slot is usually kept until the connection is released by the user. TDMA suffers from the same inefficiency problem as FDMA since it must rely on spatial attenuation to control intercell interference. Due to excessive worst case co-channel interference, neighboring cells cannot use the same frequency bands. However, it has certain distinct advantages in multimedia applications. By using a flexible slot assignment policy, TDMA can easily support integrated services. TDMA based protocols are used in some second generation systems such as GSM in Europe, ADC in North America, and JDC in Japan.

2.2.1.3 CDMA

Random access protocols require less centralized coordination than fixed assignment protocols. CDMA is a sophisticated random access protocol that uses spread spectrum techniques. Each user is assigned a unique code sequence which modulates the data signal before transmission. With this modulation, the signal is spread over a much wider bandwidth than that required to support the source data rate. At the receiver, a matching code sequence is used to despread the received signal to recover the original data. With this spread and despread procedure, all the other simultaneous transmissions in the channel will act as additive noise to the desired signal [37]. If the codes are orthogonal, the interference can be removed completely.

Based on the spread spectrum technique, CDMA can be divided into Direct Sequence CDMA (DS/CDMA), Frequency Hopping CDMA (FH/CDMA). In DS/CDMA systems, each user occupies the whole bandwidth at the same time with a unique signature code. In FH/CDMA, each user is assigned a unique FH pattern. Users hop around in frequency. FH/CDMA can be further divided according to the hop rate. In Fast FH/CDMA (FFH/CDMA), there are multiple hops per information symbol, and in Slow FH/CDMA (SFH/CDMA), there are multiple information symbols per hop. With well-designed channel coding and interleaving, SFH/CDMA can also obtain interferer diversity and multipath diversity characteristics as DS/CDMA. The main difference in the performance between DS and FH is due to the different forms the intracell interference take in the two methods. While in DS, intracell interference is typically dominant, for FH there is little or no intracell interference since FH can be made approximately orthogonal within a cell.

The performance of DS/CDMA (e.g. IS-95) has been studied extensively. Key advantages of CDMA are well documented in recent papers [12][44]. First in CDMA,

since the whole bandwidth is used in each cell (universal one-cell frequency reuse) the need for complex frequency planning can be eliminated. Second, CDMA allows for the system to be designed based on the average interference, which provides more capacity than the worst case design. Third, voice activity utilization can easily improve system capacity. Multiple access interference (MAI) in CDMA is the dominant factor in the limitation of capacity. A way to reduce MAI is to generate no packets whenever the voice source is silent. By employing voice activity detection, the capacity can be increased. Fourth, since CDMA is interference limited, any interference suppression technique can be directly translated into an increase in system capacity. Fifth, the CDMA systems have soft capacity and soft handoff features [16].

CDMA also has some shortcomings. The major one for DS/CDMA is that the performance is very sensitive to power control. Power control inaccuracy due to imperfect channel measurements can significantly lower the capacity of a real DS/CDMA system [8]. FH/CDMA fares better than DS/CDMA in this respect because FH/CDMA uses power control only to reduce intercell interference and as such, power control can be less accurate.

FH/CDMA has other advantages over DS/CDMA for personal wireless applications, in which a low power implementation of the handheld transceiver is an important goal [26]. For an FH system, the signal processing is performed at the hop rate, which is much lower than the chip rate encountered in a DS/CDMA system. Slower signal processing components in a FH/CDMA system result in less power consumption. Another advantage of FH technique is frequency agility, which means the spectrum does not have to be contiguous. With frequency agility, the effect of narrowband external jammers can be nullified.

The potential problems with FH/CDMA are the need for complex frequency

synthesizer and strict time synchronization requirements to ensure the orthogonality of FH patterns.

2.3 Summary

CDMA has inherent features which make it a good multiple access technique for personal wireless communications. Unlike FDMA and TDMA systems, the capacity of a well-designed CDMA system is interference limited. A spread spectrum radio is designed to tolerate some level of mutual interference. In military applications, interference derives from enemy jammers not under control of the communication system. On the other hand, in commercial applications, interference can be controlled by design techniques such as power control. In multicell systems, it is generally believed that CDMA can fundamentally provide more capacity than either basic TDMA or FDMA schemes. In addition, SFH/CDMA seems to have more merits than DS/CDMA for the implementation of handheld radios. Therefore, SFH/CDMA was chosen as the multiple access scheme for the UCLA low-power handheld transceiver. To achieve robust performance, channel coding is essential in SFH/CDMA systems.

Although we have chosen SFH/CDMA, the merits of various multiple access schemes for wireless personal communications are still the subject of considerable dispute. The debate continues because the comparison results are highly dependent on initial assumptions about system models and requirements. We also note that certain features of CDMA can be implemented in TDMA. For example GSM has an option of slow hopping to make GSM more like an interference-averaging system.

Chapter 3

SYSTEM MODELS

In the last chapter, we outlined the design principles for CDMA wireless systems. In this chapter, we discuss the system models and approaches used to analyze different aspects of the proposed SFH/CDMA architecture. A model is something that describes the objects or processes involved in a system. It can be in several forms, e.g. physical or graphical. We are most interested in mathematical models which represent the system behaviors in terms of mathematical relations. The nature of any object has many facets and no mathematical model can deal with all these facets. Good models should be simple, accurate and suit the purpose of the study.

Using models to predict system performance is a way of exploring design tradeoffs in a fast, inexpensive manner. The purpose of the analysis is to guide the selection of model parameters. Once the system models have been determined, we can invoke analytical and/or simulation techniques to evaluate the performance of the system. When the model is simple enough, elegant formulas that express how model parameters relate to system performance variables could be derived. When the model is

more complex, simulations might be required to evaluate the relationships between system performance and parameters.

In communications, the transmission channel places fundamental limitations on the performance of the system. To properly design a radio communication system, we must have a thorough understanding of the radio channel, which may be quite complex. Choosing and devising a channel model is a very important part of system analysis. In selecting appropriate channel model parameters, factors such as the signal characteristics and the system performance evaluation objectives must be considered.

This chapter is organized as follows. In Section 3.1 we describe two network topologies: cellular and peer-to-peer. In Section 3.2 a multiuser SFH/CDMA system model is presented and frequency hopping is illustrated. The system model for a single user link in the SFH/CDMA system is shown in Section 3.3. Section 3.4 gives a statistical characterization of the radio channel. Section 3.5 and Section 3.6 discuss the appropriate channel models for studying power control and channel coding techniques, respectively.

3.1 Network Topology

Consider two classes of communication networks: cellular and peer-to-peer. The two classes are distinguished by their different link topologies. The cellular concept has been discussed in some detail in Section 2.2. Here, we will describe the peer-to-peer system in reference to the cellular system.

In a peer-to-peer network there are no base stations as in cellular networks and every portable or transceiver can move freely within the service coverage area. The links are organized into separate clusters, which in many ways are similar to cells. One portable from each cluster is designated as a master to provide some network control

services (e.g. a global clock) [11]. During call setup a user should be assigned to the cluster from whose master it receives the strongest signal strength. However, almost all communications takes place directly between the peers, without mediation by the master. The peer-to-peer topology is useful in applications that requires an instant communication infrastructure without cell planning. One example is radio networks for soldiers in combat. These networks needs to be set up quickly, highly secure and self-healing. Another example is wireless local area networks, which allow computers to access any peripherals within communications range, such as printers, file servers, and storage devices. Wireless LAN can reduce cost and difficulty of rewiring.

For both network classes, diversity techniques, such as frequency hopping, and distributed power control are employed. These concepts will be explained in the following subsections.

3.2 SFH/CDMA Network Model

The network model is defined as a group of M radio links, each consisting of one transmitter sending information to the corresponding receiver over a SFH/CDMA channel. In SFH/CDMA systems, the available channel bandwidth is subdivided into a large number of contiguous frequency bins. In any signaling interval, a link occupies one of the available frequency bins. We will assume a time synchronous SFH/CDMA system, in which each link hops among the same set of orthogonal frequencies but with a different hopping sequence that is designed to randomize co-channel interference in order to provide interferer diversity. The latin square construction introduced in [28] is a simple procedure for designing a set of hopping sequences with good interference randomization. By using a latin square hopping pattern, each user suffers collisions from an ensemble of users occupying the nearby clusters, rather than from one

dominant interferer. The following are the key parameters for specifying the hopping patterns generated by latin-squares:

$N_T =$ number of orthogonal frequencies (tones) over which all users hop.

$N =$ number of time slots in a frame.

In a latin square construction, the hopping pattern repeats after each frame.

Figure 3-1 depicts an application of the latin-square construction to a

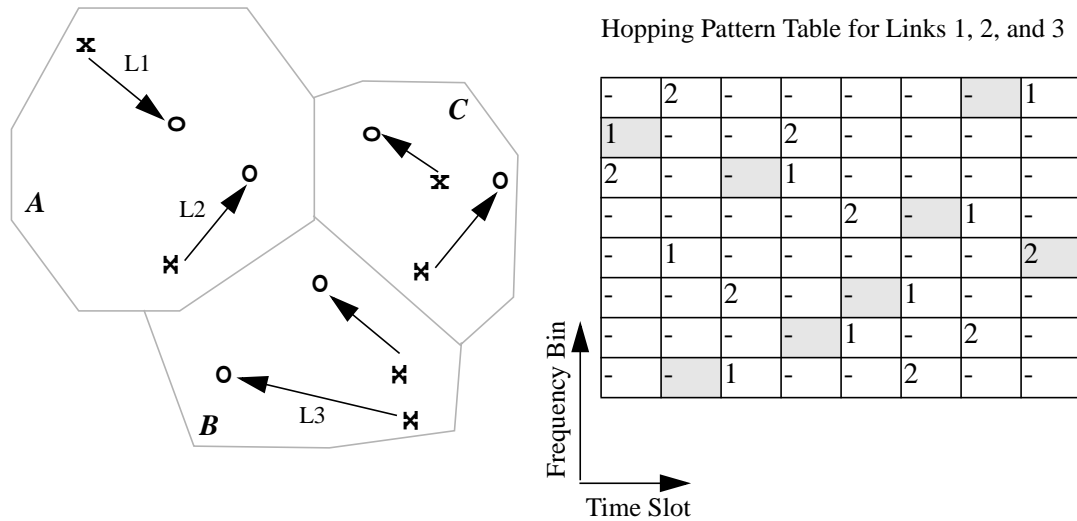


Figure 3-1 Network model with three clusters and a table showing some $N=N_T=8$ latin-square hopping sequences.

hypothetical peer-to-peer network consisting of three clusters, each containing two links. In the figure, transmitters are represented by x's and receivers by o's. The arrows indicate the direction of transmission for each link. Observe that the hopping sequences for the links in cluster A, labelled by indexes 1 and 2, are orthogonal; that is, they do not overlap in any slot. On the other hand, the hopping sequence for link 3 in cluster B, shown by the shaded entries in the hop table, overlaps with each hopping sequence from cluster A only once per frame. In other words, links 1 and 3 will experience mutual co-channel interference only in the first time slot of every frame. Furthermore, for systems

with non-ideal bandpass filters, transmit power will leak into the adjacent frequency bands. If the leakage power is significant in the system of Figure 3-1, link 1 and 2 would emit adjacent channel interference to each other during every first and fourth time slots in a frame. Although this example involves a peer-to-peer system, the latin-square construction can be similarly applied to cellular networks.

3.3 Radio Link Model

Within the network, there are many links. Figure 3-2 outlines the system model for a single radio link. The input bit stream is encoded and fed to the interleaver. The interleaver rearranges the coded sequence in such a way that the fading channel with burst error characteristic is transformed into a channel having independent errors. The coded symbol at the output of the interleaver is transmitted by binary orthogonal FSK signaling. The frequency hopping binary FSK signal is output from a frequency hopper

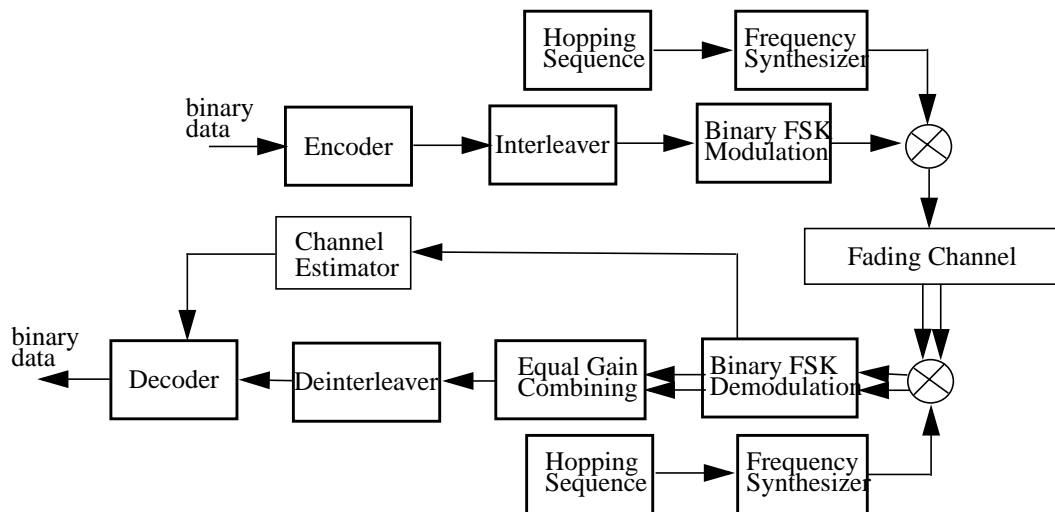


Figure 3-2 System Model.

where the hopping local signal is multiplied by the binary FSK signal. A slow frequency

hop scheme is assumed in which a hop is made in each slot interval consisting of a few symbols. The transmitted signal passes through a radio channel, the characteristics of which are described in the next section.

At the receiver end, the received signal is first dehopped to obtain the baseband binary FSK signal. Non-coherent detection is used for the reception, because the handheld system is designed to allow fast hopping. The receiver employs dual antenna diversity with postdetection equal gain combining to achieve diversity. This was found to outperform selection diversity, and in any case when the channel SNR cannot be estimated with any accuracy for a slot (e.g., fast hopping), two complete receiver branches are required to make antenna diversity effective. Thus, equal gain combining comes essentially for free. We assume that the signals received at the two antennas have low correlation.

3.4 Fading Channel Model

An active radio link will experience transmission impairments. Depending on the bandwidth of the signal relative to the coherence bandwidth, channel models can be classified as wideband or narrowband. In the proposed SFH/CDMA system, the spread bandwidth is much larger than the coherence bandwidth so that frequency diversity can be achieved. However, the aggregate channel resource defined by the bandwidth- time product is divided evenly into subchannels, as illustrated in Section 3.2, and these subchannels are more like narrowband channels; hence, we will concentrate on the characterization of narrowband channels.

In classical AWGN channels, the signal is corrupted by an additive random signal, known as noise. When a signal passes through a multiple access radio channel, besides noise, other random processes, namely propagation phenomena and multiple

access interference distorts the signal. In this section, we will explain the transmission impairments due to propagation and interference and show how these impairments can be modeled for different types of performance evaluations.

3.4.1 Propagation Models

A major propagation mechanism in terrestrial mobile radio channel is multipath fading. Multipath refers to the many paths by which signal energy may arrive at a receiver. The paths are characterized by different delays, phase shifts, and attenuations. The low-pass equivalent impulse response of the multipath radio channel can be modeled by a time-varying linear filter:

$$h(t, \tau) = \sum_i \alpha_i(t) e^{j\theta_i(t)} \delta(t - \tau_i) \quad (3.1)$$

where the i -th path has amplitude α_i , phase θ_i and propagation delay τ_i at time t . As a signal is transmitted through a radio channel, physical characteristics of the propagation environment might be constantly changing. For example, the portables might be moving amongst natural or man-made obstacles which are randomly sited on irregular terrain. It is too complicated and unrealistic to pursue an exact deterministic approach to modeling the propagation effects. To determine the received radio signal, which may be influenced by many random factors, a statistical approach is often used.

The time-varying distortion caused by multipath fading is often characterized by two kinds of spreading: delay spreading (spreading in time) and Doppler spreading (spreading in frequency). Delay spread measured in indoor settings is usually less than 100 ns [9]. For an outdoor microcellular environment, delay spreads on the order of a few microseconds have been observed. The coherence bandwidth, which is defined as

the inverse of the delay spread, ranges from around 1 MHz in outdoors to greater than 10 MHz in indoors. For the proposed SFH/CDMA system, the instantaneous signal bandwidth is less than 1 MHz. When signal bandwidth is narrow relative to the coherence bandwidth of the channel, the channel is frequency-nonselctive. That is, all of the frequency components in the signal undergo the same attenuation and phase during transmission. The impulse response for a narrowband channel can expressed in the form:

$$h(\tau, t) = \alpha(t)e^{j\theta(t)}\delta(t - \tau) \quad (3.2)$$

This flat-fading channel results in multiplicative distortion of the transmitted signal. For such narrowband systems, the symbol period is much longer than the delay spread so that intersymbol interference (ISI) is negligible and ISI reduction by adaptive equalization is unnecessary. Doppler spread due to terminal motion causes time variations in the envelope of the received narrowband signal. For a pedestrian based system, the doppler spread is small (e.g 5 Hz). The coherence time, roughly defined as the inverse of doppler spread, is approximately 0.2 seconds, which is much greater than the frequency dwell time of SFH/CDMA system (e.g. 6 μ s at the hop rate of 160 khops/s). This implies that the channel fades relatively slowly, the condition under which the multiplicative distortion may be regarded as a constant within a hop.

For the purpose of predicting the received strength $\alpha(t)$ for a narrowband signal at a receiver, we use a propagation model that quantifies the phenomena of signal propagation by two factors: the median signal strength, and the signal variability. The prediction is a two step method involving an estimation of both the median received signal within a relatively small area, and the signal variability about the median level.

3.4.1.1 Median Signal Strength

There are a number of models described in the literature for predicting the median signal strength in a small area [27]. In general the models used in the prediction methods are a mixture of empiricism and the application of propagation theory. The empirical approach relies on fitting curves or analytical expressions to sets of measured data and implicitly attempting to take factors such as diffraction, atmospheric effects or irregular terrain into consideration. When the signal variability is averaged out, the path loss has been empirically determined to follow an inverse power law with distance between the transmitter and receiver. That is, the average received signal strength, denoted by $\bar{\Gamma}(r)$, can be written as:

$$\bar{\Gamma}(r) = Ar^{-\gamma} \quad (3.3)$$

where γ is called the path loss exponent, r is the distance, and A is some constant. The values of γ ranged from 1.5 to 6, depending on the propagation environment.

3.4.1.2 Signal Variability

It is often useful to separate the effects of signal variability due to multipath fading on a basis of scale into those which occur over a short distance and those which are apparent only over much longer distance. Although fading is fundamentally a spatial phenomenon, it is experienced as a temporal variation by a receiver moving through the multipath field. Local multipath that can be observed over a short distance on the order of a wavelength causes short-term fluctuation. For a receiver moving at 30 miles/hour, several short-term fades, also known as rapid fading, can occur within a second. The long-term variation, caused by gross changes in the overall path between the transmitter and receiver, occurs over much larger distances on the order of tens of

wavelengths. Because the variations are often caused by the mobile moving into the shadow of buildings or hills, long-term fluctuation is called shadowing.

When shadowing is present, measurements reported by several researchers [30][15][2] suggest that the average received signal strength at distance r , denoted by $\bar{\Gamma}(r)$, has the log-normal distribution:

$$p_{\Gamma(r)}(x) = \frac{1}{\sqrt{2\pi}\sigma} \exp\left\{-\frac{(x - \bar{\Gamma}(r))^2}{2\sigma^2}\right\} \quad (3.4)$$

where all units are in decibels. For similar environmental areas, the standard deviation has been observed to be independent of path length. It ranges from 4-18 dB, with $\sigma = 8$ being a typical value for urban environments.

The signal variability also has a rapid fading component superimposed on the log-normal variation. This is caused by multipath propagation in the immediate vicinity of the receiver. In the absence of a strong line-of-sight path, the central limit theorem arguments may be invoked to show that the received waveform can be characterized as a complex Gaussian process. The envelope of a complex Gaussian process follows a Rayleigh distribution and the phase follows a uniform distribution. The probability density function of Rayleigh fading can be written as:

$$f(y) = \frac{y}{\sigma^2} \exp\left(-\frac{y}{2\sigma^2}\right) \quad (3.5)$$

where $2\sigma^2$, the second moment, represents the average signal power.

The distinction in time scales of the signal variability is extremely useful for engineering. Mathematically, this means that the statistical model of the short-term fading is conditioned upon the instantaneous values of the parameters of the long-term statistics [31]. For most fading channels, only the short-term fading variations influence

the selection of the appropriate method of modulation, diversity, and coding; only the long-term fading variations determine the availability of the channel. The dichotomization of the time scales allows us to analyze network and link issues separately. We will elaborate the practical implication on propagation modeling in Section 3.5 and Section 3.6.

3.4.2 Interference Model

Frequency reuse leads to co-channel interference while spectral leakage produces adjacent-channel interference as described in Section 3.2. The interference and desired signals arrive simultaneously at a receiver and, excluding the thermal noise, their sum is the received signal. Since the interference signals, similarly to the desired signal, pass through the propagation channel, they are impaired by distance loss, log-normal shadowing, and Rayleigh fading. In modeling interference, we assume that all signals are affected by independent but identical statistics.

As with propagation modeling, proper modeling of the impairments due to interference must match the engineering interest. Interference signals can be modeled individually or as a single aggregate process, resulting from the combination of many signals. How to choose the right model for a specific purpose is discussed in the next two sections.

3.5 Channel Modeling for Power Control Study

In CDMA systems, power control techniques are employed to adjust the transmit power from every radio link to the minimum level required for reliable transmission. This saves power and also reduces the interference in nearby cells, thereby increasing capacity. Power control algorithms can be classified as centralized or distributed. To

implement centralized algorithms, there must be some terminals, such as base stations, that can cooperatively control the transmit power of every radio link in the network. On the other hand, under distributed algorithms each radio link adjusts its power locally. Distributed power control is suitable for peer-to-peer systems, such as military and emergency response applications in which base stations may not be deployed and centralized control is impractical. Furthermore, it is desirable from the practical point of view of avoiding burdening higher levels of the network even should base stations be available.

Chapter 4 studies the implementation of a distributed power control algorithm for the proposed SFH/CDMA system. The power control algorithm uses feedback to deal with slowly varying channel conditions, namely shadowing and free space loss. The algorithm adapts with respect to an average signal-to-interference (SIR) threshold, reducing the average transmitted power to the level actually needed for reliable transmission. Power control with respect to a SIR measure requires a closed-loop structure whereby the two parties on occasion exchange messages indicating that an adjustment in transmitted power level is required.

Power control is mainly a network issue. Its effectiveness can be measured by system capacity, often defined as the number of users that can simultaneously access the system with some guaranteed quality of service. Quality of service is related to both reliability and availability requirements. Reliability is usually a function of average SIR. By keeping the mean SIR near a desired threshold through power control, an implicit reliability requirement is established. A link is considered unavailable when it cannot obtain the SIR threshold, which occurs when there is excessive interference from other co-channel users in the system.

One purpose of studying power control algorithms is to determine system

availability as a function of network loading. In addition, the dynamics of the power control algorithm are interesting. Knowing the convergence property of the algorithm is very important. Since power control involves interaction between multiple links, the interference model should treat the signal in every radio link individually. This allows changes in SIR over successive slots and frames to be determined. Since the system model for studying power control is highly complex, a simulation approach is often required to examine the system behavior. For power control simulations, a channel model should include slowly varying propagation effects, namely distance loss and log-normal shadowing, on the individual signals. The rapid fading can be ignored as long as we assume perfect channel measurements.

3.6 Channel Modeling for Channel Code Study

The power control mechanism in the proposed SFH/CDMA transceiver architecture can overcome slowly changing channel impairments. However, the proposed power control algorithm cannot deal with the other dominant transmission impairments in SFH/CDMA systems, namely multipath fading. In order to achieve a high capacity with low power consumption, it is essential that diversity be employed in the transceiver architecture. There are many well-known diversity techniques for mitigating rapid fading. These techniques can be realized into one of three domains: space, frequency, and time. Channel coding provide time diversity. There are many different channel codes and one of the issues in transceiver design is channel code selection. The selection process considers tradeoffs among error performance, transmission delay, channel bandwidth expansion due to added redundancy, and algorithmic complexity.

The effects of rapid fading on communications performance are usually

described by the error-rate performance of the transceiver as a function of mean SNR. In link performance simulations, the total interference statistics could be modeled as an additive white Gaussian process. When there are many significant interferers and the transceiver employs frequency hopping, long interleaving span and a powerful channel code, the randomized interference will appear as an additive white Gaussian noise at the baseband. The AWGN might have a time-varying variance to simulate the behavior of fading interferers. The variance of the noise might also be time varying due to changes in system loading, which could lead to increase or decrease in system interference.

3.7 Summary

In radio communications, the channel is highly complex and causes severe degradation to the transmitted signal. It is important to understand and model how the channel places fundamental limitations on the performance of the system. A good channel model can facilitate the design and development of radio communication techniques for achieving robust transmission. Choosing a channel model depends on many factors, such as the signal characteristics and the goals of the performance analysis.

In general, for the purpose of determining system availability, a channel model might include the slowly-varying propagation effects such as distance loss, and log-normal shadowing. The model need to include all the various signals in the different links in the system. On the other hand, for the purpose of computing bit error performance on a single link the channel model could consists of only the impairments due to rapid fading and AWGN.

Chapter 4

IMPLEMENTATION OF DISTRIBUTED POWER CONTROL

Dynamic control of the transmit powers and channel assignments of the mobiles in a wireless network can greatly improve system capacity and resource allocation. For networks requiring reduced complexity of protocols and infrastructure, distributed power control schemes are more appropriate than centralized ones. For example, distributed power control could be used in peer-to-peer networks which eliminate the complexity associated with base-stations. In this chapter, we describe the implementation of a distributed power control scheme for the prototype SFH/CDMA system. The scheme is based on a distributed power and admission control algorithm developed by Chen et. al [4]. An important feature in their scheme is the protection the operational links by suppressing new links that may cause the quality of service for ongoing calls to fall below a certain target.

In this chapter, we present capacity analysis of different networks, assuming

power control with limited dynamic range. Some analytical results for simplified systems are presented to verify simulation results. The idealized system provides a baseline for comparison against more realistic systems.

The chapter is organized as follows. In Section 4.1, the motivation for studying distributed power control with dynamic range constraints (DPCDRC) is given. A mathematical description of DPCDRC is presented in Section 4.2. Section 4.3 deals with capacity calculation of systems with different power control schemes to provide some benchmarks for comparison. Section 4.4 studies performance degradation with a dynamic range constraint and details the problem of dropped calls. Heuristic algorithms for reducing dropped calls are presented in Section 4.5. Finally, concluding remarks are made in Section 4.6

4.1 Motivation

The following simple example illustrates how a dynamic range constraint affects the outage probability of a network. Outage probability is defined as the average fraction of the service area over which an acceptable transmission quality cannot be maintained [34]. We take this as our principal measure of performance.

In the network of Figure 4-1, there are two links operating in adjacent channels, both receivers are fixed at the origin, and the transmitters are uniformly distributed in a unit circle centered at the origin.

Let the adjacent channel interference emitted from a transmitter be α dB of the power in the transmitter's own channel. Define x as the dynamic range in decibels. When the SIR of a link drops below the acceptable threshold, denoted by γ , outage occurs. That is,

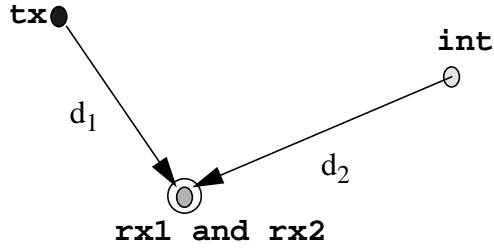


Figure 4-1 Simple example with two links

$$SIR = P_r - P_i - \alpha + x < \gamma \quad (4.1)$$

where P_r = power of the desired signal, and P_i = power of the interference signal.

Assuming that radio propagation attenuation obeys an inverse fourth power law with distance, we can derive a relationship between the distances under the outage condition:

$$d_2 \leq 10^{\frac{(\gamma + \alpha - x)}{40}} d_1 \quad (4.2)$$

Let d_2 and d_1 be modeled as random variables with uniform distributions, then the outage probability is given by

$$\begin{aligned} P\{d_2 - kd_1 < 0\} &= \int_0^{1/ky} \int_0^{ky} dx dy \\ &= 0.5k; \quad k \leq 1 \end{aligned} \quad (4.3)$$

where

$$k = 10^{\frac{(\gamma + \alpha - x)}{40}} \quad (4.4)$$

Figure 4-2 plots the analytical result for a variety of dynamic range values, given $\gamma = 12$ dB and $\alpha = -29$ dB. The -29 dB interference rejection factor is determined

from a functional simulation of the UCLA prototype SFH/CDMA transceiver, taking into account the frequency responses of the transmit and receiver filters.

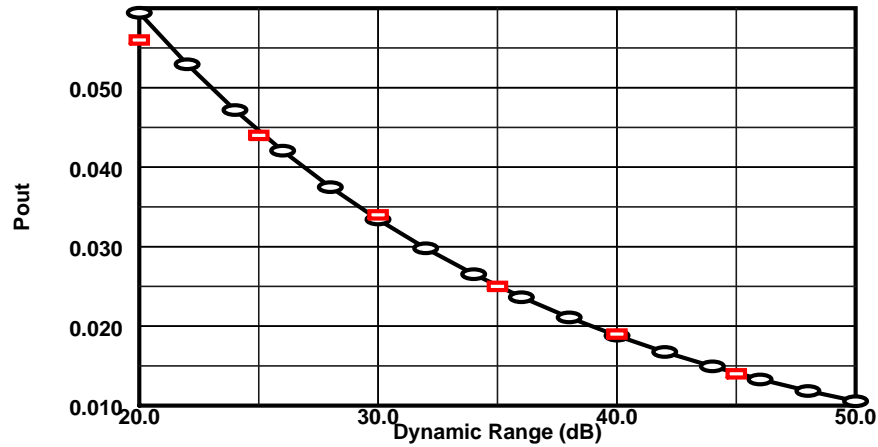


Figure 4-2 Outage Probability vs. Dynamic Range for $\gamma = 12$ dB and $\alpha = -29$ dB

The plot exhibits a general trend in which more dynamic range reduces the outage probability, and also that increasing the dynamic range yields diminishing improvements in the outage probability, which is related to the system capacity. Simulation results (marked by rectangles) for this simple case are in agreement with the analytical result. Next, we consider more realistic networks.

4.2 Description of Power and Admission Control

Algorithm

A general description of the system models for SFH/CDMA network is given in Chapter 3. Here we provide additional details about the models for the purpose of studying power control issues. To implement distributed power control over a SFH/CDMA link, we must be able to reliably estimate the signal-to-interference ratio (SIR) at the receiver. Unreliable SIR information can significantly reduce the benefits of

power control. The non-coherent correlator outputs can be used to implement a maximum-likelihood estimator for the SIR [49]. To obtain reliable measurements of the SIR, the estimator must average over hundreds of samples in a frame instead of ten or less samples in a hop. The RMS error in the SIR estimation, expressed as a percentage of the actual value, is approximately $\sqrt{1/M}$, where M is the number of samples. When the number of samples is greater than 100, the RMS error is less than 10%, which implies a fairly accurate measurement of the SIR. Given the SIR estimate, a signal is sent to the corresponding transmitter to update the transmit power.

In our power control scheme, the power will be adjusted once per frame based on a reliable measure of the “average” SIR, which is mathematically defined below. Given the transmit power is constant across a frame, the SIR can fluctuate in successive hops as multipath and the combination of links causing mutual interference change. Channel coding is thus required to overcome hops with SIR too low for reliable transmission. In other words, our SFH/CDMA system uses power control to mitigate the slowly changing channel impairments such as shadowing and distance loss, and relies on channel coding to combat the rapid channel variations.

In order to study the power control problem with constrained transmit power for SFH/CDMA systems, we propose the following system model as an extension of the models in [10][24]. The performance object is to achieve

$$\bar{R}_i \geq \gamma \quad (i = 1, 2, \dots, M) \quad (4.5)$$

where \bar{R}_i is the SIR of the i -th link averaged over the N time slots within a frame, γ is the prefix SIR target value determined by the lowest acceptable global service quality

of the network, and M is the number of links.

In (4.5), \bar{R}_i is given by

$$\bar{R}_i = \frac{\bar{G}_{ii}P_i}{\sum_{j \neq i} \bar{G}_{ij}P_j + \eta} \quad (4.6)$$

where P_i is the power transmitted by the i^{th} transmitter, \bar{G}_{ij} is the ‘‘average’’ attenuation between the i^{th} transmitter and the j^{th} receiver and η is the power of the additive thermal noise in each receiver. We assume that all receivers have the same noise floors. The average attenuation in (4.6) can be written as

$$\bar{G}_{ij} = \frac{1}{N} \sum_{k=1}^N G_{ij}^{(k)} \quad (4.7)$$

where $G_{ij}^{(k)}$ is the attenuation between the i^{th} transmitter and the j^{th} receiver during the k^{th} time slot within a frame. Equations (4.5) and (4.6) may be combined and stated in matrix form along with the transmit power constraint as follows:

$$\begin{aligned} [\mathbf{I} - \gamma\mathbf{F}]\mathbf{P} &\geq \mathbf{u} \\ P_L &\leq P_i \leq P_U \end{aligned} \quad (4.8)$$

where \mathbf{P} is the vector of transmitter powers which are constrained to be within the interval $[P_L, P_U]$, \mathbf{I} is the $M \times M$ identity matrix, matrix \mathbf{F} is non-negative with elements:

$$\begin{aligned} F_{ij} &= 0 && \text{if } i = j \\ &= \bar{G}_{ij}/\bar{G}_{ii} && \text{if } i \neq j \end{aligned} \quad (4.9)$$

and \mathbf{u} is the vector with elements

$$= \gamma\eta/\overline{G_{ii}} \quad (i = 1, 2, \dots, \Lambda) \quad (4.10)$$

A solution to (4.8) is feasible if at least one solution vector \mathbf{P} exists. Observe that the SFH/CDMA system model reverts to the original TDMA/FDMA model if we let $[P_L, P_U] = [0, \infty]$ and $G_{ij}^{(k)} = G_{ij}$, $\forall k$. That is, (4.8) becomes

$$\begin{aligned} [\mathbf{I} - \gamma\mathbf{F}]\mathbf{P} &\geq \mathbf{u} \\ P_i &\geq 0 \end{aligned} \quad (4.11)$$

Mitra [24] showed that if a solution to (4.8) exists, then a particular solution is \mathbf{P}^* , where

$$\mathbf{P}^* = [\mathbf{I} - \gamma\mathbf{F}]^{-1}\mathbf{u} \quad (4.12)$$

and this solution is Pareto optimal in that any other \mathbf{P} which also satisfies (4.8) is greater than \mathbf{P}^* . Note that finding the solution by (4.12) requires global control to collect measurements of $\overline{\mathbf{G}}$ and the distribution of the power vector after it has been computed. Our objective as formulated in (4.8) is to use power control on a SFH/CDMA network to minimize transmitters' powers *within the dynamic range constraints* while giving each link enough power to satisfy their target average SIR and furthermore, we want to do this in a *distributed manner* to reduce network control complexity.

Foschini [10] proposed a distributed power control algorithm based on an iterative power update approach using the power update equation:

$$\mathbf{P}(n+1) = \gamma\mathbf{F}\mathbf{P}(n) + \mathbf{u} \quad (4.13)$$

Without any dynamic range restrictions, this simple distributed algorithm is guaranteed to converge to the Pareto optimal power solution, whenever a power setting

exists for which all links meet the SIR requirement. That is, when there exists a solution which can be found by the global algorithm (4.12), the solution of the distributed algorithm approaches it geometrically fast [24]. Chen, Bambos and Pottie [4] simplified Foschini's distributed algorithm and showed that the power update equation can be rewritten as:

$$P_i(n+1) = \frac{\gamma_i}{\bar{R}_i(n)} P_i(n) \quad (i = 1, 2, \dots, M) \quad (4.14)$$

Equation (4.14) specifies that the current transmitter power should be adjusted by a factor that is equal to the ratio of the target SIR to the measured average SIR at the receiver.

Computing power updates is an essential part of the distributed power control algorithm. In [4] a power update algorithm is developed to protect the quality of operational links when the set of desired SIR requirements are no longer achievable. The algorithm incorporates a non-linear adjustment function to allow the operational links to increase their powers more rapidly than the new links so that the operational links will always maintain their target SIR while the new links might end up with lower SIR. The power adjustments in [4] are drawn from a set of real numbers. For our implementation, however, we quantized the power update function to four levels. The steps were chosen to preserve the active link protection mechanism. By using discrete adjustment levels, the control traffic in the feedback loop of the power control process is minimized.

Our modified update scheme is formalized below. Define

$$P_i^{\text{dB}}(k+1) = P_i^{\text{dB}}(k) + g_i(\bar{R}_i^{\text{dB}}(k) - \gamma_i^{\text{dB}} - \Delta) \quad (4.15)$$

where the power update functions for an operation link i and a new link j are

given by (4.16) and (4.17), respectively.

$$g_i(x) = \begin{cases} -\delta & x > \delta \\ 0 & 0 < x < \delta \\ \delta & -\delta < x < 0 \\ 2\delta & x < -\delta \end{cases} \quad (4.16)$$

$$g_j(x) = \begin{cases} -\delta & x > \delta \\ 0 & 0 < x < \delta \\ \delta & -\delta < x < 0 \end{cases} \quad (4.17)$$

The only difference between the first and second update function is that the maximum step size is 2δ versus δ , where δ is a quantized adjustment step. In (4.15), a protection margin is provided by raising the effective SIR target of all links by approximately Δ . In addition, the quantization adds a margin of δ so that the effect SIR is actually between Δ and $\delta + \Delta$. Whenever its SIR drops into the protection margin, the operational link can increase its power faster than a new link that is powering up. The protection margin can be optimized for fine tuning the performance of the power control algorithm.

A simple admission control policy algorithm was also derived in [4]. When a set of SIR requirements become unattainable, a new link will see little or no SIR improvements despite increasing its power. The basis of the admission policy is to track the changes in SIR relative to the increase in transmit power and block any new links with small SIR versus power slope in order to relieve network congestion.

When the transmit power is constrained, the admission control will malfunction under certain circumstances. For example, suppose a new link powers up while an operational link, denoted by O, is already at maximum power level. The new link generates interference to active users, causing the SIR of link O to drop below target

SIR. Since link O can no longer increase its power, its transmission quality will decline as the new link, which sees SIR improvements, continues to increase its power to get to the target SIR. If the new link is admitted, link O will terminate prematurely because it can no longer maintain reliable transmission. Thus, failing to reject a new link that causes infeasible SIR requirements forces one or more operational links to drop out. Since call dropping is a more annoying problem than call blocking, in general, we want to keep the call dropping probability lower than the call blocking probability.

4.3 Network Capacity for Ideal Power Control

We use both the number of users per cell and slot efficiency as the measure of capacity performance. Slot efficiency is defined as the ratio of the number of channels occupied to the number of available channels at a certain outage probability. The cellular systems in this section are assumed to have ideal power control. For single-cell systems, we computed the optimum capacity using the global power control algorithm given in (4.12). For multiple-cell systems, the power is controlled so that all reverse link signals are received at the same power level. Although the latter scheme is suboptimal, it is computationally less expensive and the capacity analysis is more tractable. The simulation procedure starts with no calls, and adds calls until the set of SIR requirements becomes infeasible. This is repeated for a large number of trial sets (10000) so that the average efficiency of slot usage can be computed at an outage probability not exceeding 1%. The next section furnishes some additional details about the SFH/CDMA simulation model.

4.3.1 Simulation Parameters

Our simulations include both cellular and clustered systems. The following

assumptions apply to the parameters of the SFH/CDMA model described in Section 4.2:

1. All cells/clusters are of equal size and hexagonal shape. The radius of each hexagon is small enough to ensure the systems are interference-limited.
2. The location of portables (both transmitters and receivers in cluster systems) is uniformly distributed within the coverage area.
3. All portables have a common antenna height and antenna gain.
4. Orthogonal hopping patterns are generated by a 32-element latin square; hence, each cell/cluster can accommodate a maximum of 32 links. In other words, $N_l = 32$, where N_l is the maximum number of links per cell/cluster. Both the number of orthogonal hopping tones and the number of time slots in a frame is also 32. That is, $N_T = N = 32$.
5. A common fourth-power path loss model is used to describe the signal propagation for all transmitter-receiver pairs. All transmitted signals are affected by log-normal shadowing with identical statistics.
6. Adjacent channel interference is specified by the ACI coupling factor. According to the RF transmit and receive filter specifications of the UCLA prototype SFH/CDMA system, the out-of-band emission to an adjacent frequency is approximately 29 dB down from the peak transmitted power in the desired frequency.
7. Thermal noise can be modeled as a constant. It can be calculated assuming a

3 dB noise figure for the low-noise amplifier.

8. Perfect knowledge of the SIR parameters at a receiver is available to the corresponding transmitter.
9. The established SIR requirement includes the gain from coding and antenna diversity. The effectiveness of antenna diversity and error correction coding in mitigating multipath fading is demonstrated in later chapters.

Unless otherwise stated, the above parameters will be the standard for all SFH/CDMA simulations. The next section deals with the basic SFH/CDMA single cell system, and the subsequent sections deal with multi-cell and clustered systems.

4.3.2 Single Cell Reverse Link Capacity

The single-cell capacity formula in [12] can be extended to frequency-hopped single cell systems utilizing an average power control scheme, in which the frame SNR is kept constant and the slot SNR may vary about the mean. When there is ACI, the hopping patterns are no longer completely orthogonal, and so a SFH/CDMA system will experience in-cell interference, similar to a DS/CDMA system.

The capacity of a single-cell SFH/CDMA system with well-designed hopping patterns may be closely approximated as follows. First, find the average SNI per frame.

$$\frac{S}{I} = \frac{S}{(N-1)Sxf + \eta}$$

where f is the adjacency coefficient for the hopping pattern used and x is the ACI coupling factor. In the best case, any pair of users will be in adjacent channels at most twice in each frame. If the hopping patterns has this optimum adjacency property, then

it can be shown that

$$f = \frac{2R}{W}$$

Then,

$$\left(\frac{E_b}{N_o}\right)_{\text{AVG}} = \frac{S/R}{I/W} = \frac{S/R}{[2x(N-1)S + \eta]/W}$$

Finally, solve for N to obtain

$$N = \begin{cases} 1 + \frac{W/R}{2x(E_b/N_o)_{\text{AVG}}} - \frac{\eta}{S} \frac{1}{2x} & \text{if } 2x(E_b/N_o)_{\text{AVG}} > 1 \\ W/R & \text{otherwise} \end{cases} \quad (4.18)$$

where W is the total spread spectrum bandwidth, R is the information bit rate, S is the desired signal power at the base-station, x is the ACI coupling factor, $(E_b/N_o)_{\text{AVG}}$ is the per user average frame SNR requirement, and η is the background noise in the total bandwidth, W . The noise term can be ignored when the system is interference limited. We can look at $W/(2xR)$ as the effective processing gain with respect to the in-cell interference.

To compare the capacity approximation and the exact result obtained by Monte Carlo simulation, we examined a 32-link system with an ACI coupling factor of -10 dB. Figure 4-3 shows that the analytical result accurately predicts the capacity performance.

We note that the simulation and analytical results are in close agreement because the hopping patterns generated by a 32-element latin-square construction have good adjacent interferer randomization. That is, most users interfere with any other user

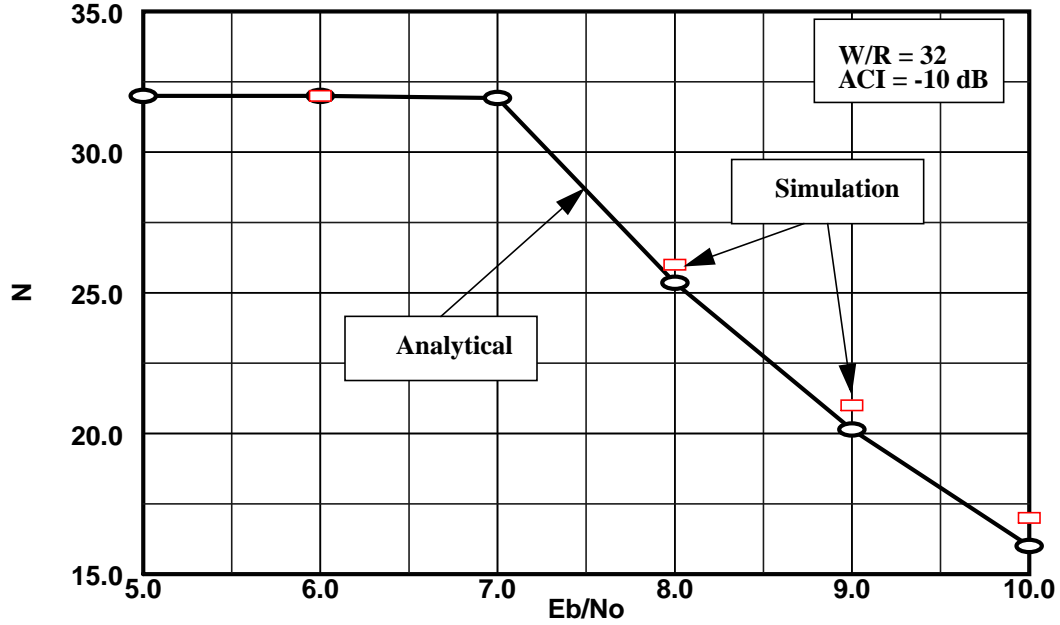


Figure 4-3 Reverse Link Capacity of the Single Cell SFH/CDMA

from the same cell only twice in each frame.

Capacity in terms of number of users per cell can be easily converted to a corresponding slot-efficiency value. For example, at 9 dB SNR, the plot above shows $N = 25$ and since the number of available slots is 32, the slot-efficiency is $25/32 = 0.66$.

4.3.3 Multiple Cell Reverse Link Capacity

It is easy to see that in the absence of ACI, a latin-square based SFH/CDMA cellular system utilizing average power control is similar to a DS-SS/CDMA cellular system without the in-cell interference. Hence, the reverse-link capacity of a SFH/CDMA cellular system could be analyzed using the approach in [12]. This approach assumes that the interference in the SFH/CDMA system has Gaussian statistics. This

assumption is valid when the interference is not dominated by a small number of users. In our analysis, we consider systems with and without ACI. Assuming the effect of thermal noise is negligible, the result is

$$P = \Pr(I_{\text{FRAME}}/S > \delta) = Q\left(\frac{\delta - mN}{\sigma\sqrt{N}}\right) \quad (4.19)$$

$$\delta = \begin{cases} \frac{W/R}{(E_b/N_o)_{\text{AVG}}} & \text{if no ACI} \\ \frac{W/R}{(E_b/N_o)_{\text{AVG}}} - 2x(N-1) & \text{otherwise} \end{cases}$$

where P is the outage probability, and N is the number of users per cell, $(E_b/N_o)_{\text{AVG}}$ is the per user average frame SNR requirement and x is the ACI coupling factor. Given that a certain $(E_b/N_o)_{\text{AVG}}$ is needed to achieve adequate BER performance, (4.19) can be used to upper bound the probability of not achieving this level of performance for N users/cell at any given time (e.g. 1% of the time).

Solving (4.19) for N we obtain:

$$m^2N^2 - \left((\sigma Q^{-1}(P))^2 + 2m\left(\frac{W/R}{(E_b/N_o)}\right)\right)N + \left(\frac{W/R}{(E_b/N_o)}\right)^2 = 0 \quad (4.20)$$

where m is an upperbound on $E(I_{\text{FRAME}}/S)$ and σ is an upperbound on $\text{var}(I_{\text{FRAME}}/S)$, which can be found by numerical integration. $Q(k)$ is defined as

$$Q(k) = \frac{1}{\sqrt{2\pi}} \int_k^{\infty} e^{-x^2/2} dx \quad (4.21)$$

Notice that (4.20) is a quadratic equation in N , the number of users per cell. The larger

root obtained from direct solution is the capacity.

Figure 4-4 plots the capacity expression for the SFH/CDMA system when the “processing gain” is 156. The analytical result shows that the effect of ACI on capacity performance is negligible in comparison to CCI when the ACI coupling factor is less than -20 dB. We also observe that the analysis and simulation results based on a 19 cell

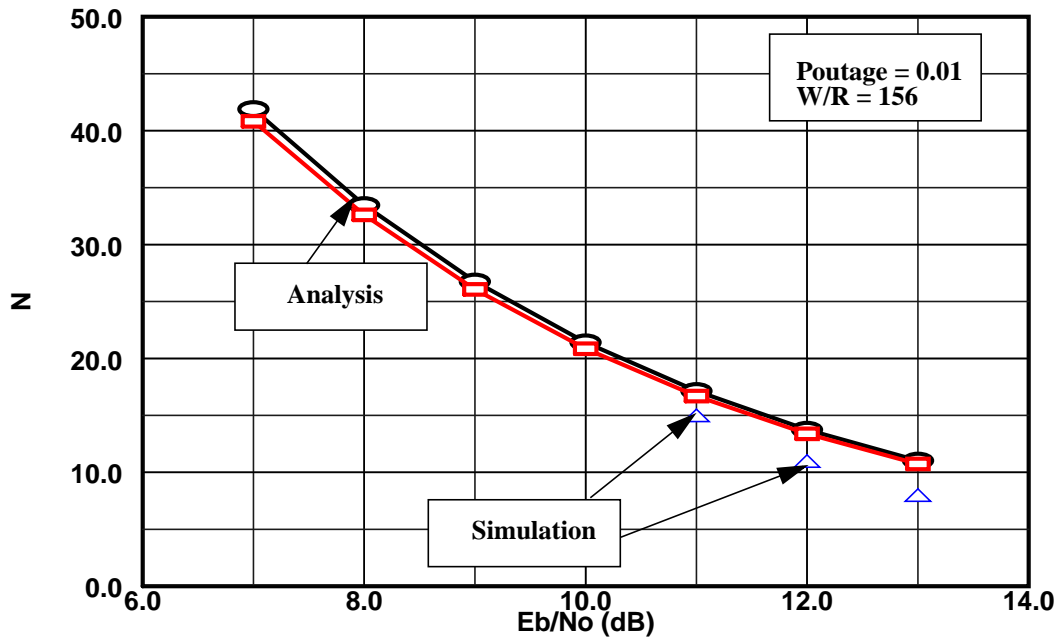


Figure 4-4 Reverse-Link Capacity/Cell of the cellular SFH/CDMA system (with and without ACI. The ACI coupling factor is -20 dB).

network diverge for smaller values of N because the Gaussian approximation used in the analysis becomes less accurate.

4.3.4 Peer-to-Peer Cluster Capacity

This section presents the capacity of clustered peer-to-peer SFH/CDMA networks described in Section 3.1. The lack of regular geometrical structure in a peer-to-peer network renders capacity analysis problematic at best. Hence, we relied on

simulation to calculate the capacity of the standard model described in the beginning of Section 4.3. An algorithm is needed to organize links into clusters. We assume a situation where the algorithm has set up hexagonal boundaries that conforms exactly to the ones in the cellular system. In each cluster, there are an equal number of users. The simulation of a single-cluster network with our distributed algorithm shows that the slot-efficiency is approximately 6% at 1% outage probability when γ is 9 dB. This performance figure is very poor in comparison to the 62% slot-efficiency found when the network contains a base-station. (see Section 4.3.3).

The large disparity in performance between the clustered and cellular systems indicates a fundamental trade-off between capacity and network infrastructure. An intuitive benefit from having a base-station is that most of the time, a transmitter will transmit more signal power to the desired receiver than adjacent channel interference power to the other receivers. However, this is often not true in a clustered system. Although the only source of interference comes from ACI, ACI could be a very severe problem when the links are in a more random configuration.

One way to obtain reasonable capacity for peer-to-peer systems is to add more complexity by doing better frequency planning. For example, the guard band between different frequency slots can be increased to reduce ACI. This would trade-off some spectral efficiency to improve the overall system capacity.

Figure 4-5 shows the effect of reducing ACI within the single-cluster system. Suppose a larger guard band is introduced so that there are fewer channels in the available bandwidth and that the ACI is reduced to -50 dB. Assuming that the guard bands takes up about half of the available bandwidth, then data in Figure 4-5 confirms that a slot-efficiency of about $16/32 = 50\%$ can be achieved.

For multi-cluster systems we can combine frequency reuse with the latin-square

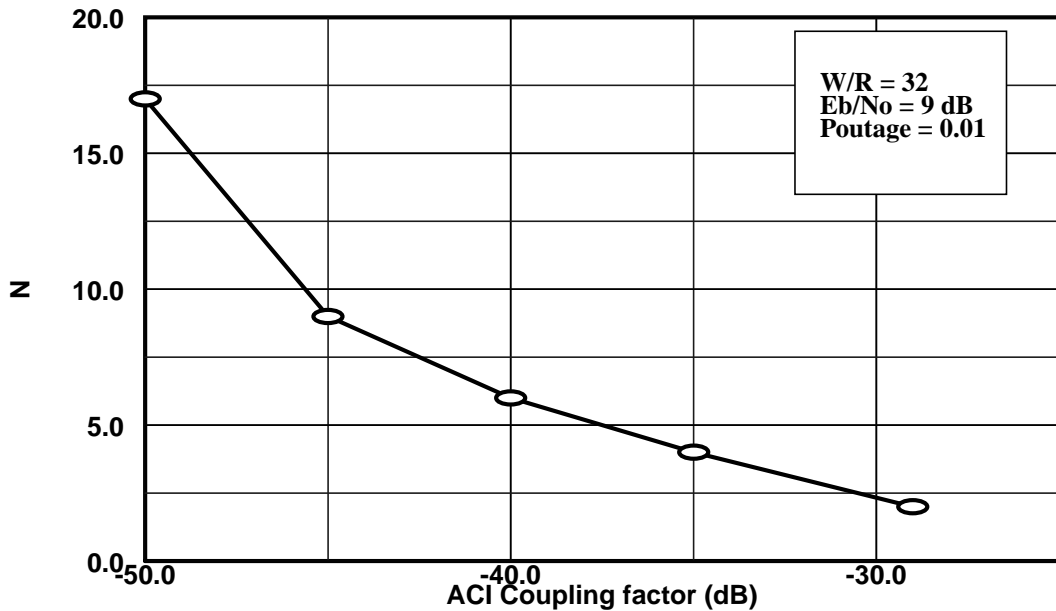


Figure 4-5 Capacity of single-cluster SFH/CDMA system versus different ACI coupling factor

construction to improve system capacity. Appendix A shows how latin-squares can be modified for frequency-reuse with little additional complexity. In general, a SFH/CDMA system does not require frequency planning but simulations show that explicit frequency-reuse is absolutely necessary to obtain reasonable capacity performance for multi-clustered systems. The computed slot-efficiency of a 19-cluster network is a dismal 7.3% at 1% outage probability for a 9 dB SNR requirement. The cost of the frequency planning to make the entire network mobile can be quite high.

4.4 Performance Degradation Due to Power Control With Dynamic Range Constraint

Although in the following sections we will focus mainly on the standard single-

cell SFH/CDMA system, analogous results can be obtained for other SFH-CDMA network configurations. Insufficient transmit power dynamic range could result in two kinds of performance degradations. First, under a centralized power control scheme that has a mechanism to block calls causing dynamic range problems, the network capacity could be lowered to compensate for additional blocked calls in order to maintain the original 1% outage criterion. Second, for a distributed power controlled system, when there is insufficient dynamic range, one or more active calls may be dropped, which also contributes to the outage probability. From the customer's viewpoint, dropped calls are more of a nuisance than a slightly lower network availability. In Section 4.4.1, we will examine the loss in capacity from imposing a dynamic range constraint on the centralized power control algorithm. In the subsequent section, we will study the degradations in performance of the distributed power control algorithm when dynamic range constraints are imposed.

4.4.1 Global Algorithm with Dynamic Range Constraint

In deriving the theoretical capacities formulas (4.18) and (4.20), it was assumed that the portable's transmit power dynamic range is sufficient to ensure that all active portables, regardless of their locations, can deliver equal received power to the base-station. Thus, it can be inferred that the dynamic range requirement is determined by the propagation model and the cell radius. Assuming the propagation loss is an inverse 4-th law with distance, the design rule for the dynamic range is simply:

$$DR^* = 40 \log \left(\frac{R_{\max}}{R_{\min}} \right) \quad (4.22)$$

where R_{\max} and R_{\min} are the maximum and minimum separations between a portable and the base-station, respectively. When the dynamic range is greater than or equal to

DR^* , the theoretical capacity predicted by (4.18) or (4.20) can be achieved. When log-normal shadowing is included in the propagation model, the dynamic range must be increased by some margin.

A Monte Carlo simulation was written to quantify the performance degradation due to a limited dynamic range by computing the capacity of a single-cell network with a dynamic range less than DR^* . We will assume that the global scheme has a mechanism for blocking new calls to prevent dropped calls due to insufficient dynamic range. The other system parameters (e.g. the cell radius) are fixed. Figure 4-6 shows the simulation results. Capacity here is defined to be the maximum slot efficiency that can

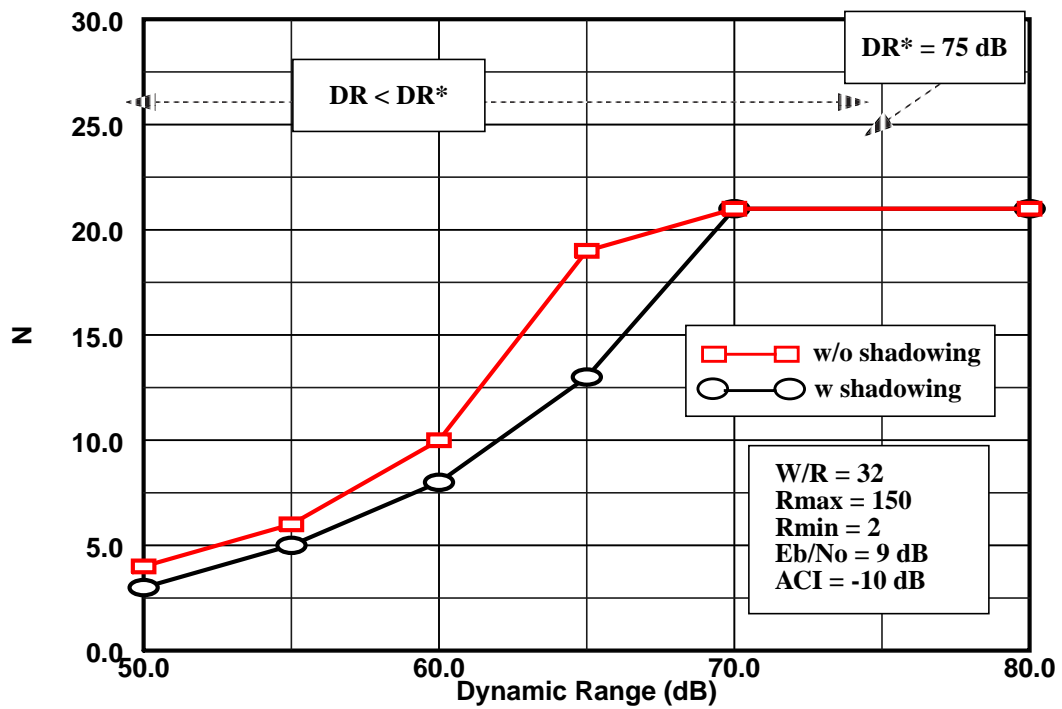


Figure 4-6 Reverse Link Capacity of the Single Cell SFH/CDMA vs. Dynamic Range for Two Different Propagation Models. (With and Without Shadowing)

supported at 1% outage probability. With these parameters, Figure 4-6 shows that the

reverse link can support 22 users with 10^{-3} BER 99% of the time when the dynamic range is above 70 dB. It also shows when signal propagation includes a log-normal shadowing component with $\sigma = 8$ dB, an additional margin in dynamic range would be needed to maintain the same capacity performance. A 10% loss in capacity would be incurred with a dynamic range of only 67 dB.

By observing the simulation results of various systems, some general remarks can be made about the effect of dynamic range. The capacity vs. dynamic range curves illustrate the existence of a breakpoint above which more dynamic range yields diminishing returns in system capacity. The breakpoint phenomenon can be explained by looking at power control as a linear programming problem, in which proper operation of the network corresponds to the existence of a feasible power vector. From the linear programming viewpoint we know there are certain network configurations where no feasible power vector exists for any dynamic range; for these situations, dynamic range becomes a non-issue. The probability that the network does not have a feasible power vector becomes the dominant factor in lowering efficiency of slot usage when the dynamic range is sufficiently large; thus, the efficiency of slot usage is essentially independent of the dynamic range after a certain point.

4.4.2 Distributed Power Control With Dynamic Range Constraint

The capacity of a single-cell SFH/CDMA system utilizing the DPCDRC algorithm is computed using the simulation procedure given in Section 4.3 but here the outages can be caused by blocked as well as dropped calls. The parameters of the power update function (4.10) are fixed: the protection margin $\Delta = 1.5$ dB and the minimum step size $\delta = 0.5$ dB. When a new link is assigned a channel, it stays in the system until the distributed algorithm converges. This is called the initial set up period. The average

number of power update iterations in the set up period depends on several factors, including the dynamic range, the adjustment step sizes, as well as the load on the network. If a new link does not obtain the required SIR after a setup period, it is blocked. When a new link becomes operational, the SIRs of the pre-existing operational links are checked for dropped calls. This is repeated for a large number of trial sets to compute the efficiency of slot usage at an outage probability not exceeding 1%.

Figure 4-7 shows capacity as a function of dynamic range. Compared to the

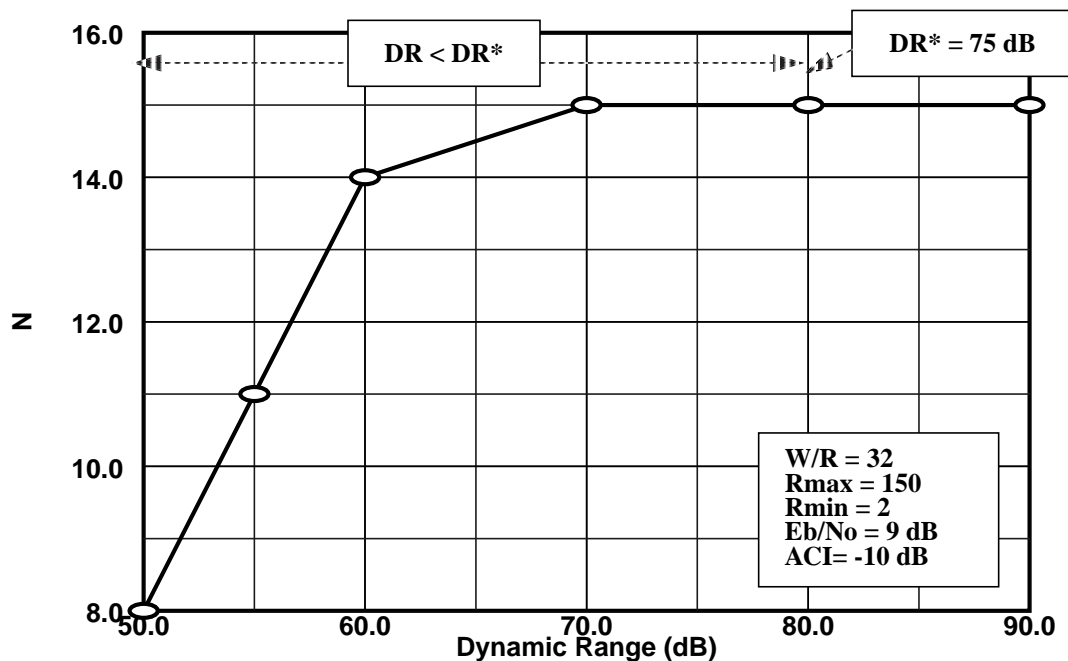


Figure 4-7 Reverse Link Capacity of the Single Cell SFH/CDMA vs. Dynamic Range. (with Shadowing)

previous system with centralized power control, distributed power control suffers a 30% capacity loss due to the protection margin requirement, which raised the effective SIR targets of all links by 1.5dB. Furthermore, if the dynamic range is only 60 dB instead of 75 dB, there is another 10% loss in capacity. The capacity loss due to a more

stringent SIR requirement is one of the drawbacks of the distributed algorithm. The other drawback is that calls can be dropped when the dynamic range is constrained.

Figure 4-8 plots the call dropping and blocking probabilities for four different dynamic ranges. We observe that calls are dropped much more frequently than they are blocked for all dynamic ranges. Although the results in this section pertains to the

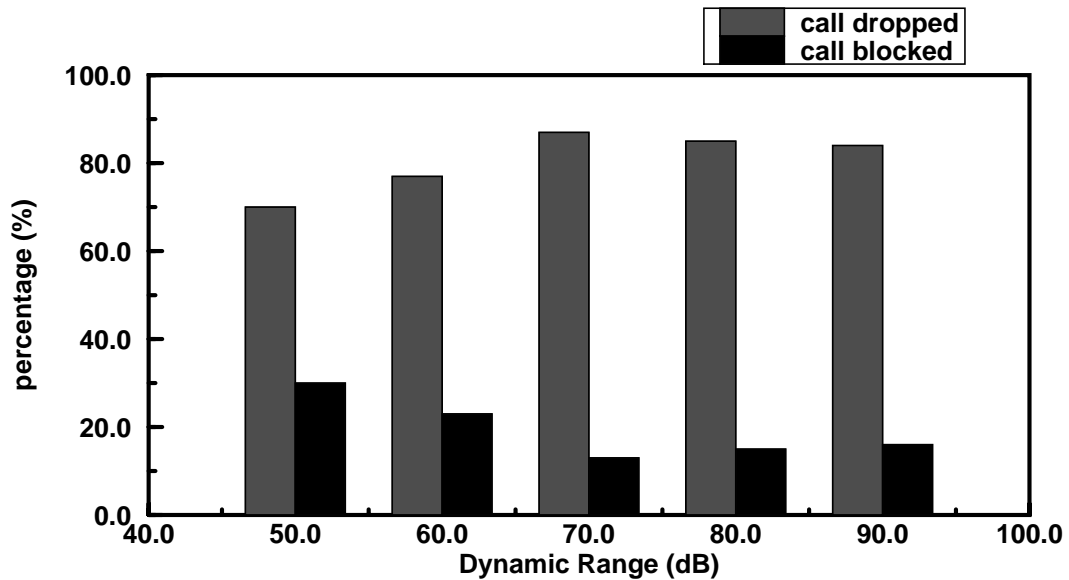


Figure 4-8 Call blocking and call dropping probabilities vs. dynamic range for a single-cell network.

single-cell network, the multi-cell and peer-to-peer networks also exhibit similar behavior. Since call dropping is a severe problem, admission control algorithms for reducing the call dropping rate will be presented in Section 4.5.

4.5 Reducing Call Dropping Probability

One way to reduce the call dropping rate is to decrease the maximum load, trading off some system capacity for fewer dropped calls. A better solution, however, is to employ a distributed admission control policy that allows voluntary termination of

admission attempts when an operational link is in danger of being dropped. A local mechanism to sense the “resistance” of other users is a key element toward implementing a distributed policy. Resistance indicates the network congestion level. Since more calls are dropped at higher congestion levels, blocking or terminating admission attempts that encounter high resistance would effect a reduction in call dropping probability with a slight increase in blocking probability.

To provide a better understanding of the network resistance concept, we can look at each admission attempt as a trial in a random experiment involving a system of links. At the end of a set-up period, one of three system outcomes may occur: call admission, rejection and dropping, which are denoted as c_a , c_b and c_d respectively. A good resistance indicator is a system variable that can accurately predict the outcome of an admission attempt. The correlation between a random variable and a particular event can be quantified through the probability mass function of the random variable conditioned on that event.

To find a good resistance indicator, we evaluated several candidates through simulation. All the simulations in this section involved the single-cell model mentioned in Section 4.3.2. The target SIR is fixed at 9 dB and the dynamic range at 60 dB. One candidate we considered is the initial interference power seen by a new link. The conditional probability distributions of the interference power, conditioned on the three outcomes, were found through simulation. The following definitions will be used in the sequel:

- I^0 is the power of the interference signal detected by the receiver of a new link at the beginning of its set-up period.
- $f_a(I^0)$ the probability mass function of the initial interference power for a success-

ful admission attempt (c_a).

- $f_d(I^0)$ the probability mass function of the initial interference power when an admission attempt results in dropped links (c_d).
- $f_b(I^0)$ the probability mass function of the initial interference power for a blocked admission attempt (c_b).

The histograms of $f_a(I^0)$, $f_d(I^0)$, and $f_b(I^0)$ are plotted in Figure 4-9. For a

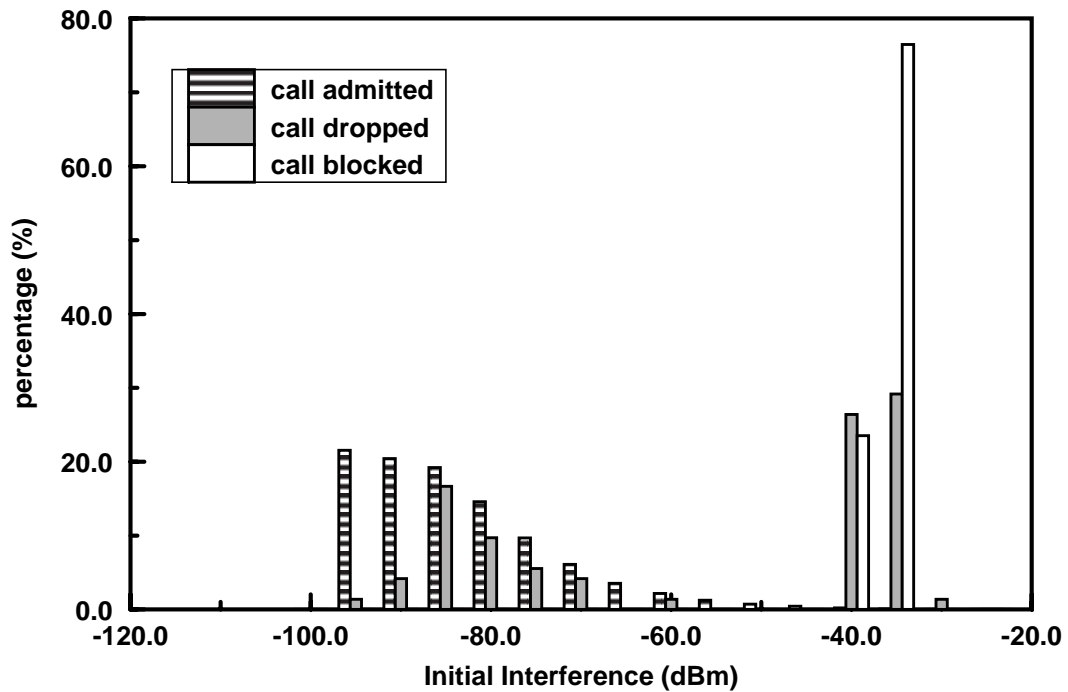


Figure 4-9 Histogram of the initial interference power for three different outcomes. Single-cell network; $N_1 = N_T = N = 32$; Target SIR = 9 dB; Dynamic Range = 60 dB.

resistance indicator to be useful, it must, with high probability, distinguish between admission attempts that will result in dropped links and ones that will not. That is, for good performance, we need $f_a(i)$ and $f_d(i)$ to be very different as functions of i . The result in Figure 4-9 shows that $f_a(i)$ and $f_d(i)$ have different shapes; thus, the initial interference power could be used as a resistance indicator.

Another resistance measure we evaluated is called the gross power increase,

denoted by ΔP . It is defined as the difference in powers transmitted by a transmitter at the beginning and the end of the set-up period. We will use the following notation in the sequel:

- $f_a(\Delta P)$ the probability mass function of the gross power increase for a successful admission attempt.
- $f_d(\Delta P)$ the probability mass function of the gross power increase for an admission attempt resulting in dropped links.

The histograms of $f_a(\Delta P)$ and $f_d(\Delta P)$ are plotted in Figure 4-10. It can be

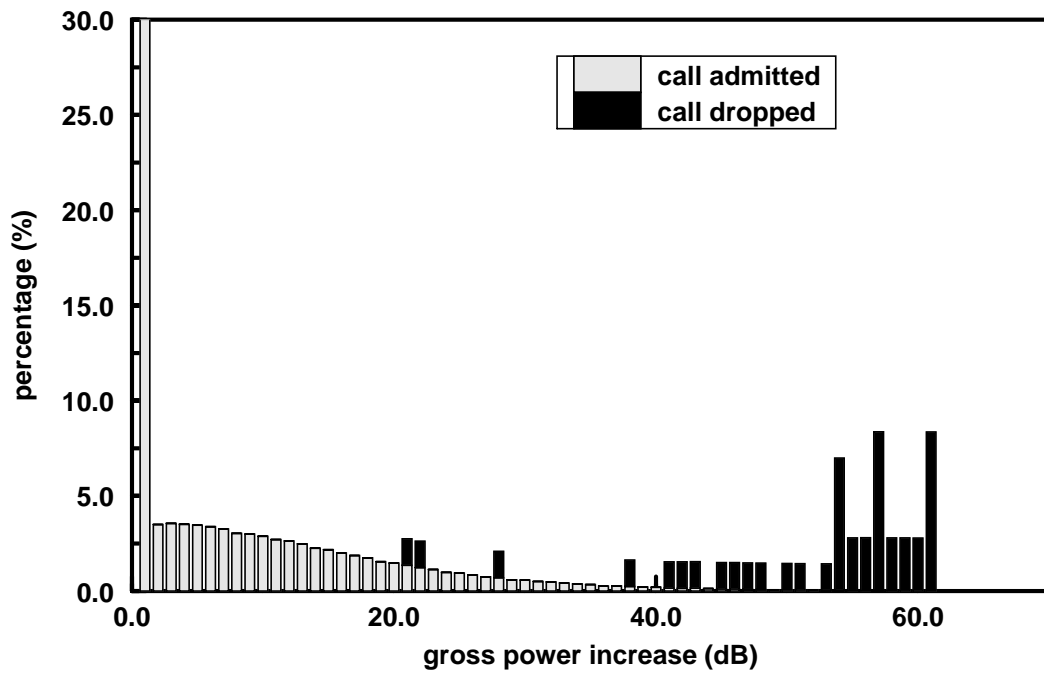


Figure 4-10 Stacked histograms of the gross power increase conditioned on two outcomes.

observed that $f_a(\Delta P)$ is concentrated near $\Delta P = 0$ and that $f_d(\Delta P)$ is concentrated near $\Delta P = 50$. Since $f_a(\Delta P)$ and $f_d(\Delta P)$ are different as functions ΔP , the gross power increase could also be a good resistance indicator.

Other candidates that were evaluated include the initial received power level and the change in interference power. The initial receive power level is denoted by P^0 . The change in interference power, denoted by δi , is calculated at the receiver by subtracting the interference power measured at two different iterations separated by N updates, where N is a small arbitrary positive integer. For example, we set N to six to allow enough time for significant change in interference level to occur.

Given the statistics of potential indicators, we experimented with several admission control algorithms that perform various combinations of threshold tests on the set of resistance indicators. A flowchart of the algorithm that performed well is given in Figure 4-11.

Although the above admission control algorithm, called Algorithm I, is developed heuristically, there is a good physical explanation for why it works. From our experience, we found that reverse link calls are dropped primarily in two kinds of situations. The first occurs when a new call enters the network near the center of the cell while the system is operating near maximum capacity. If the transmit power of the call close to the base-station could not be sufficiently lowered to just meet the SIR requirement, a necessary condition for achieving optimum system capacity, it would generate excess ACI to the other users. The second is when a new call comes up far away from the base-station while the system is also congested. In both cases, the dynamic range required for a feasible power solution will likely violate the given system design specification. From the statistics of initial received power level and initial interference level, we can determine the corresponding thresholds that will indicate when the location of a new call and the system congestion level might cause a dynamic range problem. The values of P_1 and I_1 are thresholds that indicates when a new call

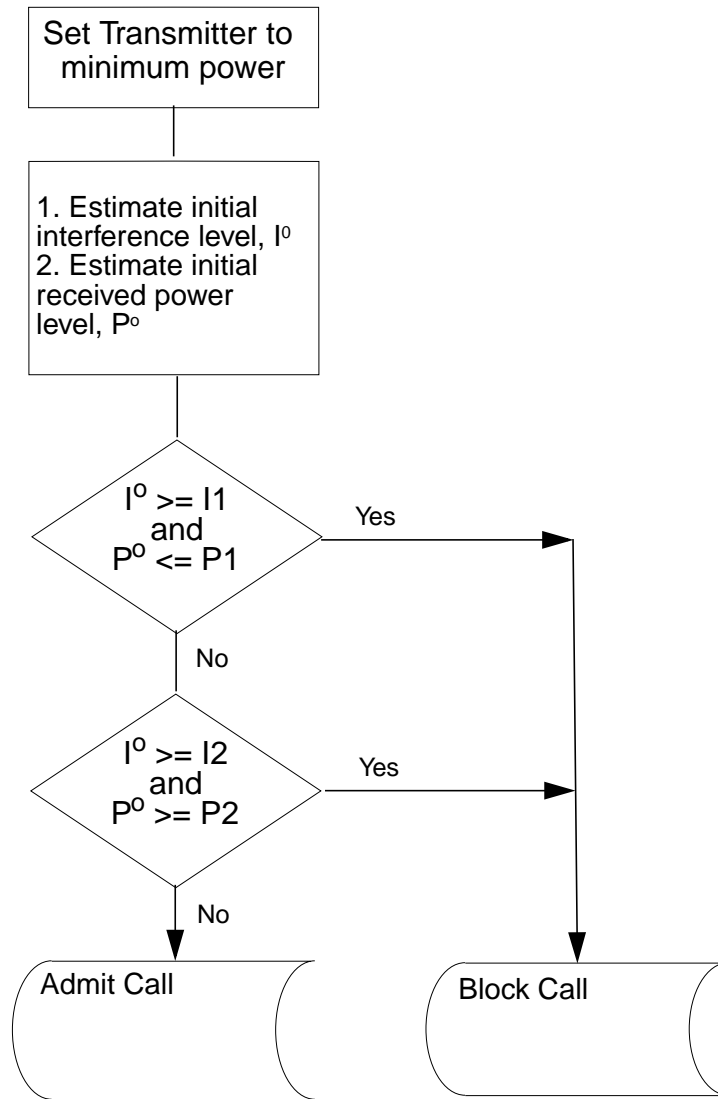


Figure 4-11 Flow-Chart of Distributed Admission Control Algorithm

should be blocked because it is far enough away from the base-station and the system has sufficiently high interference level to potentially cause other calls to be dropped. Thresholds $P2$ and $I2$ applies to calls near the base-station. The dangerous levels of congestion in the two cases are different.

Table 4-1 summarizes the single-cell SFH/CDMA network performance with and without admission control. The thresholds P_1 , I_1 , P_2 , and I_2 of Algorithm I are set to -80 dBm, -86 dBm, -13 dBm, and -43 dBm respectively. These thresholds were chosen to ensure an equal slot-efficiency can be achieved without significantly changing the outage probability. The results clearly show that the admission control mechanism reduced the call dropping probability by raising the blocking probability. Hence, performing a combination of threshold test could be the basis of an effective admission control scheme.

Table 4-1: Call blocking and call dropping probabilities with and without distributed admission control
Single-Cell Network; $N_1 = N_T = N = 32$; Target SIR = 9 dB; Dynamic Range = 60 dB.

	Outage Probability	% Outage due to call drops	% Outage due to call blocks
without admission control	0.0085	84	16
with Algorithm I	0.0104	53	47
with Algorithm II	0.0093	50	50

Note that the outage probability is slightly increased when the admission control algorithm is enabled because the admission control algorithm will sometimes make a wrong prediction, declaring that the network has an infeasible power solution when one actually exists.

A more accurate admission control algorithm was developed by also checking the ΔP variable against a threshold, D . This algorithm, termed Algorithm II, increases the accuracy of prediction of the outcome of an admission attempt. In practice, if a receiver already had the capability to estimate SIR needed for power control, it would also be capable of estimating I^0 , P^0 , or ΔP . The advantage of only checking P^0 and I^0

is that a dangerous congestion level can be detected early enough to quickly terminate an admission attempt to avoid degrading the quality of existing links for a prolonged period. Algorithm II was implemented and tested by simulation. The data given in Table 4-1 shows that the outage probability under Algorithm II is smaller compared to Algorithm I; hence Algorithm II is indeed a slightly more accurate algorithm. By using even more complicated algorithms, it may be possible to further reduce call dropping with a slight increase in outage probability.

With some minor modifications, the admission algorithms developed for the single-cell network can be implemented for multi-cell networks. We repeated the simulation technique to determine the appropriate thresholds, accounting for the effects of both co-channel and adjacent channel interference. Our analysis in Section 4.3.3 showed that for multi-cell systems with a small ACI coupling factor, CCI is the impairment dominating capacity. This fact may allow the admission algorithm to be simplified since the excess ACI generated by calls near the center of a cell might no longer cause other calls to be dropped. To investigate the efficacy of a simplified admission algorithm with only three thresholds (i.e. P1, I1, and D), simulations were employed. The performance measures for a multi-cell network with and without admission control are summarized in Table 4-2. The simulation parameters for the multi-cell network are similar to those for the single-cell network, except there are 19

cells, instead of one, in the multi-cell network simulation.

Table 4-2: Call blocking and call dropping probabilities with and without distributed admission control
Multi-Cell Network; $N_I = N_T = N = 32$; ACI = -29 dB; Target SIR = 9 dB;
Dynamic Range = 60 dB.

	Outage Probability	% Outage due to call drops	% Outage due to call blocks
without admission control	0.0100	60	40
with admission control	0.0140	41	59

The data in Table 4-2 show that the call dropping probability for the multi-cell network can be reduced by using the simplified admission algorithm.

The previous admission algorithms worked well for cell-based networks. For peer-to-peer networks, we found that very different admission algorithms are needed. Simulation experiments showed that blocking new links which see no SIR improvements despite increasing power can significantly reduce dropped calls. This admission policy was described in [4] and here we will call it Algorithm III. To improve the accuracy of Algorithm III, Algorithm IV was developed by testing both P^0 and ΔP against corresponding thresholds to further reduce the call dropping probability. The simulation results for the single cluster peer-to-peer network with different admission control algorithms are summarized in Table 4-3. The dynamic range for the single-cluster system was set to 60 dB because our simulation shows that the system capacity did not improve with a larger dynamic range. We assume the system has a ACI specification of -50 dB to obtain a reasonable capacity. The data in Table 4-3 show the

advantage of using the more complicated Algorithm IV over Algorithm III.

Table 4-3: Call blocking and call dropping probabilities with and without distributed admission control
Single-Cluster Network; $N_I = N_T = N = 32$; ACI = -50 dB; Target SIR = 9 dB;
Dynamic Range = 60 dB.

	Outage Probability	% Outage due to call drops	% Outage due to call blocks
without admission control	0.0104	44	56
with Algorithm III	0.0104	36	64
with Algorithm IV	0.0107	23	77

4.6 Summary

In summary, we considered the implementation of a distributed power control algorithm for a multiple-access frequency-hopped (SFH/CDMA) system employing diversity techniques, such as coding and interference randomization. Our distributed power control/admission scheme fits the unique constraints of this SFH/CDMA system. In our scheme the transmit power is adjusted according to the average SIR of a frame and the power update function uses only four discrete adjustment levels. The system relies on channel coding to overcome hops with poor SIRs.

The performance of the distributed power control scheme with transmit power dynamic constraints, measured by system efficiency and call dropping probability, was computed through simulation. For both the single-cell and single-cluster networks, our simulation shows that a 60 dB transmit power dynamic range is sufficient to obtain most of the available system capacity without the dynamic range constraints. To reduce dropped calls caused by the dynamic range constraint, heuristic admission control algorithms were developed based on the concept of detecting “resistance” of other users

during the call set-up period. We found that cellular and peer-to-peer networks with distributed power control require individually customized admission control solutions. The effectiveness of these algorithms in reducing call dropping probability without significant capacity loss was demonstrated through simulation. Since dynamic power controlled TDMA/FDMA systems must also deal with limited transmit power, the call admission control techniques developed for our SFH/CDMA system may be applied to those other system architectures.

From the simulation of different network topologies using our distributed power control scheme, we can conclude that cellular networks, which contain base-stations, have higher system capacity than the corresponding peer-to-peer networks with similar system parameters. This represents a fundamental trade-off between network complexity and capacity performance.

Chapter 5

CODE SELECTION

In the last chapter we showed that adaptive power control can mitigate slowly-changing variations in the received power by adjusting the transmit power of the desired signal. The proposed power control implementation, however, cannot deal with the other dominant transmission impairment in SFH/CDMA systems, namely rapid fading. Fast fading results in severe fluctuation of the signal level, which can dramatically increase the signal to noise ratio (SNR) required for reliable operation. Because of factors such as geographic proximity and shadow fading, the interference power also displays wide variations across slots.

In order to achieve a high capacity with low power consumption, it is essential that diversity be employed in the transceiver architecture. Dual antenna diversity, frequency hopping, and channel coding are some common diversity techniques. In this chapter, we discuss the selection of the channel codes, and the basic trade-offs in choice of metrics for decoding. There are a variety of error control coding techniques which have been developed by communication engineers since the 1960's. Selecting an

appropriate channel code for a particular system involves making trade-offs among error performance, transmission delay, channel bandwidth expansion due to added redundancy, and algorithmic complexity.

5.1 System Model

Figure 5-1 outlines the system model used in the investigation of alternative channel coding schemes. The input bit stream is encoded into the coded q -bit symbol sequence of a block code or a convolutional code and the resulting coded sequence with a rate of f_c symbols/s is fed to the interleaver. The interleaver rearranges the coded sequence in such a way that the fading channel with burst error characteristic is transformed into a channel having independent errors. The coded symbol at the output of the interleaver, to be transmitted with a rate of $f_c \times q$, is assigned to one of the two binary orthogonal FSK signals.

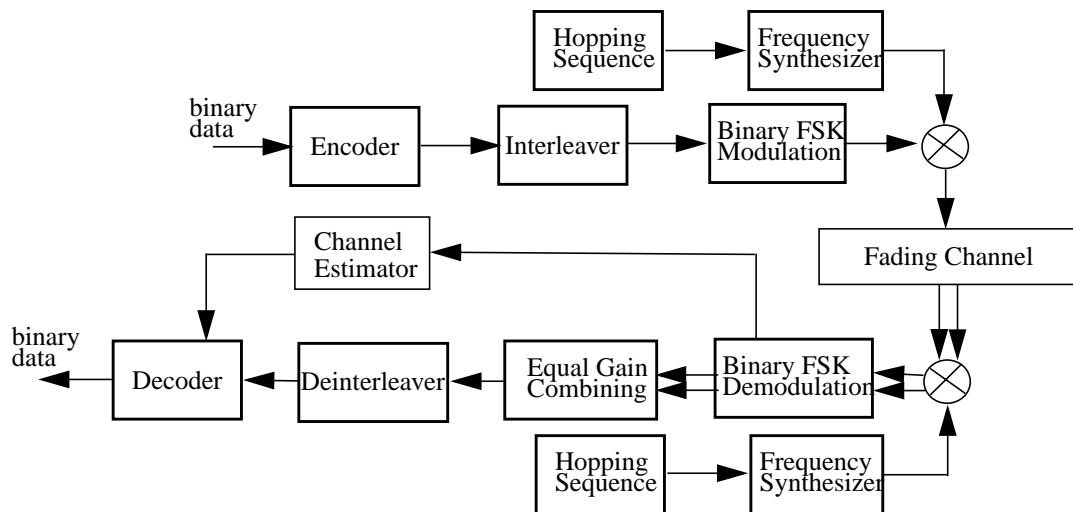


Figure 5-1 System Model.

The frequency hopping binary FSK signal is output from a frequency hopper

where the hopping local signal is multiplied to the binary FSK signal. A slow frequency hop scheme is assumed in which a hop is made in each slot interval consisting of a few symbols. It is assumed that the received signal experiences independent Rayleigh fading slot-by-slot, and that it is perturbed by additive white Gaussian noise. While this model does not yield a capacity estimate, it is sufficient to evaluate the relative effectiveness of coding schemes in a situation where we in fact expect the SNR to be independent from hop to hop as a result of the use of the Latin squares construction. It is possible to perform the link and network simulations independently.

The receiver dehops the signal to obtain the received binary FSK signal. Non-coherent detection is used for the reception, because the handheld system is designed to allow fast hopping. The receiver employs dual antenna diversity with postdetection equal gain combining to achieve diversity. This was found to outperform selection diversity, and in any case when the channel SNR cannot be estimated with any accuracy for a slot (e.g., fast hopping), two complete receiver branches are required to make antenna diversity effective. Thus, equal gain combining comes essentially for free. We assume that the signals received at the two antennas have low correlation.

As a result of interleaving/deinterleaving and frequency hopping, errors within a code word appear to be independent. We assume that a convolutional interleaver is used because it results in less delay than block interleaving. In this section, we consider hard decision decoding for convolutional codes and error correction for block codes. Later, we examine soft decision decoding for convolutional codes and error-and-erasure correction for block codes.

In order to compare the various coding options in terms of BER performance, we assume ideal interleaving so that the channel is memoryless. For non-coherent binary FSK (NC-BFSK) modulation with ideal interleaving, the error rate performance

over a frequency-nonselective, slowly fading channel is

$$P_2 = \frac{1}{2 + \bar{\gamma}_b} \quad (5.1)$$

where $\bar{\gamma}_b$ is the average signal-to-noise ratio, defined as

$$\bar{\gamma}_b = \frac{\xi_b}{N_o} E(\alpha^2) \quad (5.2)$$

The term $E(\alpha^2)$ is the average value of the Rayleigh distributed envelope squared.

When L-th order antenna diversity technique is used, the performance of square-law-detected binary FSK is well approximated by [29]

$$P_2 \approx \left(\frac{1}{\bar{\gamma}_b}\right)^L \binom{2L-1}{L} \quad (5.3)$$

For dual antenna diversity, L is set equal to two.

5.1.1 Performance of Reed-Solomon and BCH Codes

With Reed-Solomon (RS) codes over $GF(2^q)$, q binary channel symbols are used to form one code symbol. Therefore, the probability of code symbol error is $P = 1 - (1 - P_2)^q$, where P_2 is given by (5.1) and (5.2), with and without antenna diversity, respectively. For M-ary ($M = 2^q$) block codes with error correction decoding, the decoded symbol error probability can be approximated as

$$P_{es} \approx \frac{1}{N} \sum_{i=t+1}^N i \binom{N}{i} P^i (1-P)^{N-i} \quad (5.4)$$

where $t = [(d - 1)/2]$ is the number of errors that can be corrected by the code, d is the minimum distance of the code, N is the block length, and $[x]$ is the largest integer less

than or equal to x . The probability of a decoded bit error is

$$P_{eb} = \frac{2^q - 1}{2q - 1} P_{es} \quad (5.5)$$

For BCH codes, the probability of decoded bit error is just $P_{eb} = P_{es}$, where P_{es} is given by (5.4). Thus, by combining (5.4), (5.5) and (5.2) or (5.3), the probability of decoded bit error for block codes can be computed at any signal-to-noise ratio, with or without antenna diversity.

5.1.2 Performance of Convolutional Codes

Next, we consider the error rate performance of convolutional codes decoded using the Viterbi algorithm with a hard decision decoding metric. The decoded bit error probability of a rate b/n convolutional code can be upperbounded by

$$P_b < \frac{1}{b} \sum_{l=d}^{\infty} \beta_l D^l \quad (5.6)$$

where d is the minimum free distance of the code, and β_l is the total information weight of all paths of distance l from the all-zeros path. With hard decision decoding

$$D = \sqrt{4P_2(1 - P_2)} \quad (5.7)$$

where P_2 is given by (5.1) and (5.2), with and without antenna diversity, respectively.

The weight and distance structure of many convolutional codes have been computed and tabulated in the literature. Thus, equations (5.6) and (5.7) can be used to evaluate the performance of a specific convolutional code.

To study the performance advantage of coded systems over an uncoded one, a system simulation was designed and completed. For decoding Reed-Solomon and BCH

codes, the Berlekemp-Massey algorithm and Forney algorithm were implemented. The Viterbi algorithm was employed for decoding convolutional codes.

The simulation results were checked against the corresponding analytical results whenever possible in order to verify the accuracy of our simulation software during the initial phases of the simulation development. It was found that the assumption of ideal interleaving was good. Analytical expressions (5.5) and (5.6) produced fairly tight upper bounds. For each coding scheme, the difference between the performance curves obtained from the upper bound and the simulation is less than 1 dB for $10^{-2} < \text{BER} < 10^{-4}$. The simulation results were used to compute coding gains. Figure 5-2 illustrates typical BER curves generated from the simulation data for a particular convolutional code with and without dual antenna diversity. Some of the

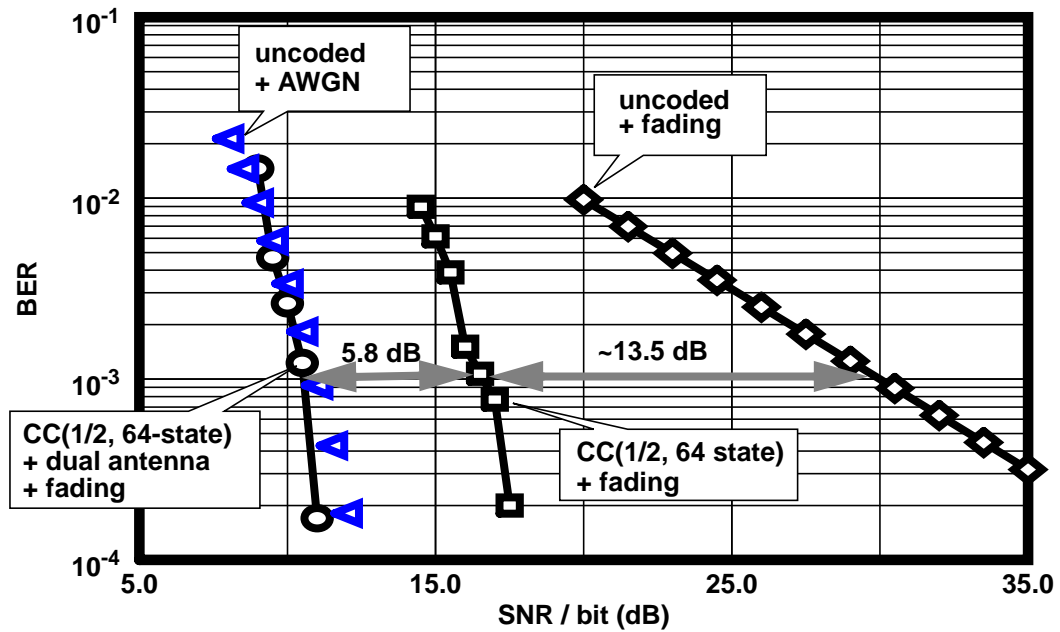


Figure 5-2 BER vs. SNR for rate-1/2, 64 state convolutional code.

coding gain data are summarized in Table 5-1. It shows that using the rate-1/2, 32 state

($v=5$) convolutional code resulted in near minimum SNR at the target BER, with and without antenna diversity. The coding gain achieved is 19.1 dB with antenna diversity, compared to 13.0 dB with a single antenna. This highly motivates the use of both channel coding and antenna diversity in the system architecture.

The code rate and code size for the codes in Table 5-1 were chosen based on their potential to meet code performance with decoding delay tolerable for voice transmission, practical code complexity, and channel bandwidth constraints.

5.1.3 Decoding Delay

To evaluate and compare the delay of the selected codes, we defined three different delay measurements: decoding delay, interleaving delay and overall delay. The delay quantities are specified in signaling interval units, T_s , to provide a normalized delay representation. Denoted τ_d , decoding delay is the waiting time for some number of encoded symbol to be received before starting the decoding process. The interleaving delay, τ_i , for a (I, J) convolutional interleaver is proportional to $(I-1) \times J$, where values of I and J are chosen to randomize the error bursts of the fading channel and depend on the coding scheme, the code parameter, and the number of channel symbols per frequency slot [41]. The overall delay is the sum of the decoding delay and interleaving delay, i.e. $\tau_c = \tau_d + \tau_i$.

In a system with BFSK signaling and $c \times q$ channel symbols per slot, a Reed-Solomon code over $GF(2^q)$ with code symbols interleaved across slots would result in $\tau_d/T_s = (2^q - 1) \times q$, $\tau_i/T_s = (c - 1) \times (2^q - 1) \times q$ and $\tau_c/T_s = (2^q - 1) \times c \times q$. For the same system, a rate-1/2 convolutional code with memory v (no. of states = 2^v) would result in $\tau_d/T_s = 9 \times v$, $\tau_i/T_s = (c \times q - 1) \times 9 \times v$, and $\tau_c/T_s = 9 \times v \times c \times q$ assuming a

truncation depth of $4.5 \times v$ and the interleaving parameters are chosen to guarantee independent fading condition for the successive symbols generated by the encoder with a separation less than truncation depth. It can also be shown that using BCH codes with block length N and bit-by-bit interleaving results in $\tau_d/T_s = N$, $\tau_i/T_s = N \times (c \times q - 1)$, and $\tau_c/T_s = N \times c \times q$.

In general, we note that for similar number of symbols per slot, the overall delays for the BCH and Reed-Solomon codes with equal block lengths are the same. We also note that the overall delay expressions derived above imply that a Reed-Solomon code over $GF(2^q)$ has comparable overall delay to a convolutional code with memory $v = 2^q/9$.

Substituting actual system parameters into the above delay formulae gives the delay values summarized in Table 5-1:.

Table 5-1: Code Performance and Delay Comparison

Code Type RS = Reed-Solomon CC = Convolutional	Gain w/ Single Antenna (dB)	Gain w/ Dual Antenna (dB)	Coding Delay w/o Interleaving (Ts)	Overall Coding Delay (Ts)
BCH (n=31, k=16, d=7)	11.5	17.9	31	310
BCH (n=63, k=36, d=11)	12.3	18.3	63	378
RS (n=31, k=15, d=17)	13.1	18.2	155	310
RS (n=63, k=33, d=31)	13.2	18.7	378	378
CC (r=1/2, v=5)	13.5	19.3	38	380
CC (r=1/2, v=6)	13.6	19.5	54	540

All codes listed in Table 5-1 satisfy the tight delay constraint of 20 ms for voice transmission. In converting normalized delay measure to seconds, it was assumed that

each slot consists of 6 BFSK signals for the length 63 block codes and 10 for remaining codes, and that the channel transmission rate is 16 kb/s. To reduce the delays for the convolutional codes, we use the fact that the full minimum distances of the 32 the 64 state codes are obtained with a truncation depth of 19 and 27, respectively [20].

In addition, to ensure practical code complexity, code selections were limited to block codes with block length less than 255 and convolutional codes with 128 states or less. These are codes which are currently used in various digital communication systems. Channel bandwidth constraints were included in the code selections by limiting the code rate to approximately 1/2; this limits the channel bit rate to a value no larger than twice the user data rate. This limitation was imposed to avoid excessively large bandwidth requirements with high data rates and to decrease link vulnerability from frequency selective fading at high data rates.

5.1.4 Decoder Complexity

Code complexity was quantified in terms of multiplies per decoded symbol for the block codes and additions per decoded symbol for the convolutional code. We found that decoding a single t -error correcting BCH code word required approximately $10t^2 + 3tn$ multiplications, obtained by adding $10t^2$ multiplications for executing the Berlekemp-Massey algorithm to $2tn$ for evaluating the syndrome, and tn for Chien search. For a t -error correcting RS code, the number of multiplications required to decode a code word increases due to the multiplications in the Forney algorithm. However, the number of operations normalized per bit for RS codes is not necessarily higher than BCH codes when the code length and rate are fixed. In fact, our calculation showed that the (63, 33) RS codes required 26 multiplies per bit versus 33 multiplies

per bit for the (63, 36) BCH code. For a 2^V convolutional code, a total of $3 \cdot 2^V$ addition operations are necessary at each stage. This includes two additions to compute the cumulative path metrics of the paths merging at each state and a comparison (subtraction) to determine which incoming path survives. For convolutional codes, in addition, a trace back operation is required to complete the decoding. For the codes parameters listed in Table 5-1, the convolutional codes required more than twice the operations per bit than the comparable block codes. This fact was partly confirmed by the longer simulation times for convolutional codes.

The results of analysis and simulation indicate that for a system architecture employing slow frequency hop and dual antenna diversity to combat multipath fading, a BCH code performs as well as an RS code with a comparable code rate. Our investigation also shows that a rate-1/2, 32 state convolutional code can attain a relatively large coding gain at 10^{-3} BER while meeting the tight delay constraint for two-way speech transmission. In addition, convolutional codes offer the advantage of efficient soft decision decoding. The conclusion is that complexity and performance for the code candidates are similar for hard decision decoding; however, the dependence on soft decision decoding must be determined before deciding which code is the best candidate. We now examine some of the relevant trade-offs.

5.2 Decoding Metrics

For Rayleigh fading channels, soft decision decoding with perfect channel parameters can effectively double the diversity order available through coding [29]. However, for a real system where channel parameters are obtained by an imperfect estimator, the unreliable estimates could significantly degrade the performance benefits

of soft decoding with side information. The reliability of the channel parameter estimator, the modulation scheme, and the channel condition are some of the factors that affect the formulation of a good soft decoding metric. Furthermore, the trade-offs in performance and complexity should be considered when selecting a decision metric for NC-BFSK systems because most soft decoding schemes require much higher receiver/decoder complexity than hard or erasure decoding.

5.2.1 Soft Decision Metrics for Fading AWGN Channels

The optimum soft decision metric is derived from the likelihood function of the decision variables. For a NC-BFSK system, in which one of two frequencies is transmitted with equal probability to a receiver and the transmitted signal is corrupted by additive white Gaussian noise with spectral density $N_o/2$, a model of the received signal is

$$r_i(t) = \alpha \sin(\omega_i t + \phi) + n(t); \quad i = 0, 1 \quad (5.8)$$

We assume that the amplitude, α , is known and the phase, ϕ , is a random variable uniformly distributed in the interval $[0, 2\pi]$. It can be shown that when the constant terms are eliminated, the log-likelihood functions may be written

$$M_{ML} = \ln(p_i(r)) \sim \ln\left(I_0\left(\frac{2\alpha z_i}{N_o}\right)\right); \quad i = 0, 1 \quad (5.9)$$

where z_i is the decision variable produced by a square law detector (the optimum demodulator for NC-FSK), and $I_0(\bullet)$ is the modified Bessel function [45].

The mapping of the decision variables into the maximum-likelihood (ML) soft metric involves a very complicated function, $\ln(I_0(x))$. To implement the branch computation part of the Viterbi decoder, a look-up table will be required to transform

the decision variables into branch metrics. Since the transforming function has a linear and a non-linear region, one way to reduce the size of the look-up table is by storing the values of the function over the non-linear region and use a linear approximation formula, which does not require costly memory storage, to compute the function over the linear region. Using this procedure, the size of the look-up table used in our study is about 2 Kilobytes.

Besides the ML decoding metric, we consider two suboptimal but less complicated soft decision metrics. The first is based on the Euclidean distance concept. The Euclidean distance metric has been shown to be the optimal soft metric for coherent PSK systems in AWGN channels, but it is not optimal for NC-BFSK systems. It may be written:

$$M_E = (z_i - \alpha)^2 + (z_j)^2 \quad (5.10)$$

where $i = 0$ and $j = 1$ for the hypothesis that z_0 was received, and vice versa for the hypothesis that z_1 was received. The metric is simpler not only because it does not involve any complicated functions but also the fade magnitude of the signal is the only channel parameter appearing in the metric. The other metric we considered required even less processing and complexity by using a simple linear combining scheme:

$$M_{LC} = z_i - z_j \quad (5.11)$$

where values of i and j are defined as in the previous metric. The linear combining metric does not require any channel state information.

5.2.2 Soft Decision Metrics for Multiple-Access Channels

FH/CDMA systems experience background thermal noise, as well as,

interference from other users. We use the following model of the received signal for the multiple-access channel:

$$r_i(t) = \alpha \sin(\omega_i t + \phi) + \beta i(t) + n(t); \quad i = 0, 1 \quad (5.12)$$

where the fade levels α and β are independent Rayleigh distributed random variables $i(t)$ and $n(t)$ are independent narrowband white Gaussian processes. Since interference is typically the dominant impairment in multiple-access environments, we can assume that the noise term is negligible and set the two-sided spectral density of $i(t)$ to $N_o/2$. Thus, when $E[\beta^2]$ is normalized to one, then

$$E[\beta i(t)\beta i(\tau)] = E[\beta^2]E[i(t)i(\tau)] = \frac{N_o}{2}\delta(t - \tau) \quad (5.13)$$

Note that for the FH system under consideration, the only real difference between the fading AWGN channel and the multiple-access channel is that the power of the “noise” in the latter is changing from hop to hop.

To perform well for the multiple-access channels, metrics (5.9) and (5.10) were re-formulated to account for the variation in noise power in each symbol interval. The re-formulations are given by (5.14) and (5.15), respectively:

$$M_{L,1} = \ln \left[\text{Io} \left(\frac{2\alpha z_i}{\beta^2 N_o} \right) \right] \quad (5.14)$$

$$M_{E,1} = \frac{(z_i - \alpha)^2 + (z_j)^2}{\beta^2 N_o} \quad (5.15)$$

For NC-BFSK, the relevant quantities for soft decision decoding are the decision variables for the two frequencies, the received signal power, and the noise

power for each slot. We next present ways of obtaining the channel parameters for slow-hopped systems.

5.2.3 Estimation of Channel Parameters

The estimation of channel parameters from the data and with training sequences was investigated in [28], in the context of DQPSK. It was found that it is better from the point of view of capacity to form estimates directly from the data-bearing signals for short slots of 8-16 symbols, rather than appending a training sequence. In addition, it was found that for some combinations of cell loading and channel codes it was better to use an erasure-declaring mechanism than to use the soft metric proposed; but in any case performance was always better than using simple hard decisions for a properly chosen erasure threshold. Simulations were also conducted using the soft metric with perfect channel knowledge, revealing a very large gap in performance. Thus, channel state information can be very valuable in decoding.

For NC-BFSK signaling with square-law detection, the signal power for a slot can be estimated by accumulating the larger decision variable, z_i , for each received symbol in the slot. This type of estimation involves hard decision demodulation. While it is relatively easy to estimate the power of the desired signal for useful signal to interference ratios, it is more difficult to accurately estimate the interference power. For NC-BFSK, an orthogonal signaling scheme, one way to form an estimate of the noise (or interference) power for a slot is to accumulate the smaller decision variable, z_j , in the slot. The reliability of the signal power and noise power estimates depends on the sample size of the estimator, which is equal to the number of symbols per slot.

5.2.4 Erasure Metric

When the channel state information is not so reliable, performing error-and-erasure correction decoding is a way to increase code performance gains without incurring increased cost in system complexity. The mechanism we have chosen for erasing unreliable NC-BFSK symbols is based on a ratio threshold test, in which channel symbols having a signal envelope ratio (i.e. the ratio between the decision variables) below a certain threshold are erased. This erasure declaration mechanism does not use any channel state information; hence, requires very little additional complexity in comparison to hard decision decoding. In the branch metric computations, erasures are assigned a value half-way between the binary values for the expected symbols.

We also investigated error-and-erasure correction decoding for RS codes, which achieves some performance benefit with a trivial increase in decoding computation in comparison to error correction decoding [3]. The mechanism for declaring erasures is again based on a ratio threshold test, in which the code symbols having the lowest signal envelope ratio, z_0/z_1 (assuming that $z_0 > z_1$), is erased. When $z_0/z_1 > \theta > 1$, the decision corresponding to z_0 appears to have a good quality. This erasure declaration metric recognizes that the worst BFSK symbol in each q-bit code symbol is the weak link but it will inevitably fail to erase some symbols which are in error, and will erase some symbols which are not in error. There is an optimum range of values for the number of erasures, N_e , declared so that residual error correcting capability, N_c , is sufficient to correct the remaining errors in the received word. The optimum range of values was found during simulation.

5.2.5 Performance Evaluations

Performance evaluation by simulation for a NC-BFSK system over fading AWGN channels, as well as, multiple-access channels using soft decision decoding metrics given in (5.9), (5.10), (5.11), (5.14) and (5.15) was performed. Receivers with perfect knowledge of channel parameters α and N_o , and ones with estimated channel parameters were simulated. Table 5-2 summarizes the relevant E_b/N_o data for a rate-1/2, 32-state convolutional coded system with dual antenna diversity.

Table 5-2: E_b/N_o at $P_b = 10^{-3}$ for different decoding metrics for a dual antenna diversity system.

Metric Type	Fading AWGN Channel		Multiple-Access Channel	
	Perfect	Estimated	Perfect	Estimated
Maximum Likelihood	8.25	9.25	8.25	9.10
Linear Combining	8.50	8.50	10.0	10.0
Euclidean	8.25	9.0	8.75	9.50

The data in Table 5-2 shows that there is no single metric that out-performs all others in every scenario. For the fading AWGN channel, the linear combining metric is clearly a very good selection in terms of having a good complexity-performance trade-off. However, for the multiple-access channel, the maximum-likelihood (ML) metric might be the better choice since it holds a slight performance advantage over the other two metrics. In short, when fading interferers are the dominant impairment, the metrics using imperfect estimates of channel parameters performed better than the one using no channel parameters at all. For single antenna systems, the performance gap between the alternative metrics is even bigger.

For comparing soft decision decoding against hard decision decoding, the simulation showed that soft decoding with the ML metric performed 3.5 dB better than hard decision decoding for a rate-1/2, 32 state convolutional code for a single antenna system. When dual antenna diversity was employed, the improvement decreased to approximately 2 dB. Figure 5-2 illustrates the improvements in SNR of soft decision decoding over hard decision decoding for SNR ranging from 8 to 10 dB.

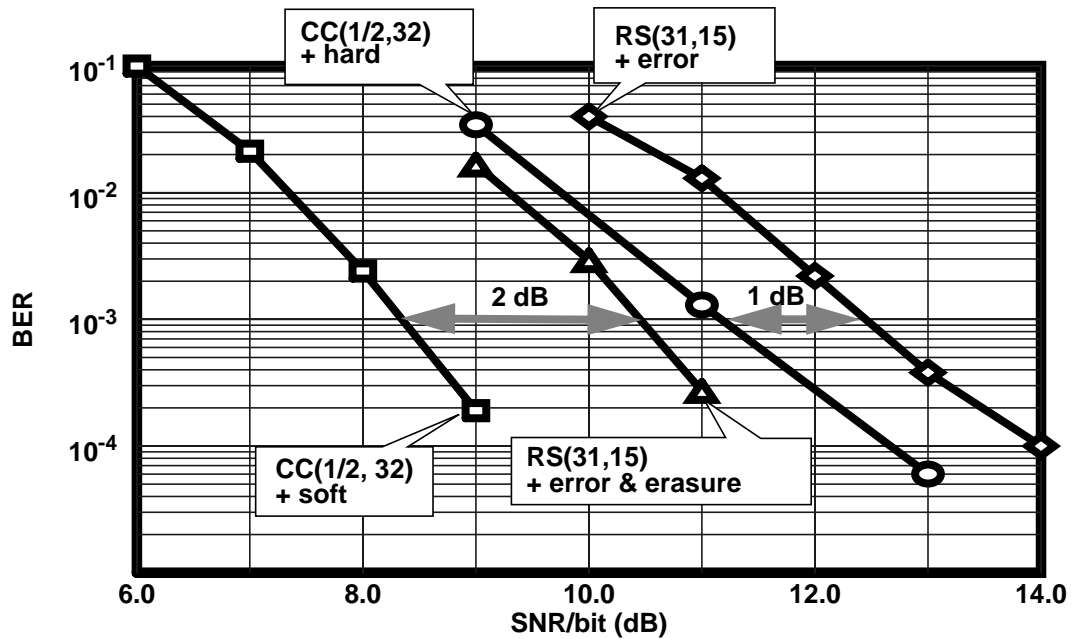


Figure 5-3 BER vs. SNR for a convolutional code and a Reed-Solomon code with different decoding strategies.

Simulation of the error-and-erasure correction decoding for a RS code was also carried out and the results are included in Table 5-3, where the performance of coded

systems for various coding schemes and decoding methods are summarized.

Table 5-3: Code Performance for Different Decoding Methods

Code Type RS = Reed-Solomon CC = Convolutional	Decoding method	Gain w/ Single Antenna (dB)	Gain w/ Dual Antenna (dB)
RS (n=31, k=15, d=17)	Error Correction	13.1	18.2
	Error & Erasure Cor- rection	14.9	19.5
CC (r=1/2, v=5)	Hard Decision Decod- ing	13.5	19.3
	Error & Erasure Decoding	15.0	20.0
	Soft Decision Decod- ing	17.0	21.5

The simulation data showed that a rate-1/2, 32 state convolutional code with soft decision decoding requires approximately 2 dB less signal-to-noise at 10^{-3} BER than a length 31, RS code with error-and-erasure correction decoding on a Rayleigh fading channel, both with and without dual antenna diversity. Thus, a convolutional code with soft decision decoding using channel state information appears to be a suitable code selection for the proposed frequency-hopped system under the assumption that the channel can be modeled by Rayleigh fading with AWGN.

5.3 Summary

We have considered channel coding options for a frequency-hopped system employing NC-BFSK signaling. We have concluded that the hopping patterns should be selected so as to randomize the interference encountered in successive hops, and

have observed the advantages offered by the Latin squares construction for synchronous systems. Alternative channel codes were compared on the basis of delay, complexity, and bandwidth efficiency, with the conclusion that when hard decision decoding is employed, the BCH, RS, and convolutional codes that can meet the delay and bandwidth constraints have similar performance and comparable complexity. At the desired bit error rate, the convolutional codes are slightly better since they required approximately one dB less signal-to-noise ratio than the best performing block codes. Furthermore, the performance gain obtained by soft decoding of the convolutional codes with the maximum-likelihood metric was shown to be more significant than the gain obtained by error-and-erasure correction decoding of block codes. This was true even with imperfect channel state estimates. The benefits of dual antenna diversity in combination with coding were demonstrated.

One way to form an estimate of the SNR for a slot is to accumulate the mean squared error between the received signal and hard decision demodulation. The larger the mse, the less reliable the slot. The selection of a soft decision metric depends on the reliability of the channel parameters estimator. That is, the number of levels of quantization to be used in subsequent decoding depends on the application. For example, with a very slowly changing channel, results could be accumulated over several slots, and many bits of soft decision information extracted. At the other extreme, for only a small number of data symbols per slot the best that can be expected is to be able to declare erasures. The same is true of fast hopped systems, where all that could be done is to monitor the received signal strength and declare erasures when it is below some empirically determined threshold. In the next chapter, we consider decoding metric formulation under more general fading statistics and algorithms for adapting the metric to changing channel conditions.

Chapter 6

ADAPTIVE METRICS FOR CONVOLUTIONAL CODES

In the previous chapter, we considered channel code selection for the SFH/CDMA system under the assumption of a Rayleigh fading channel model. The results show that the performance gain obtained by soft decoding of the convolutional codes with the maximum-likelihood metric was more significant than the gain obtained by error-and-erasure correction decoding of block codes. Unlike convolutional codes, block coding with algebraic decoders are not well suited for efficient soft decision decoding.

In the last chapter we also observed that the selection of a soft decision metric for the convolutional code might depend on the reliability of the channel estimates. Since the branch metric computation of the Viterbi decoder can be changed easily and quickly to implement different decoding strategies, the selection could be done on-line during transmission. For example, to switch between hard decision decoding and soft

decision decoding, only the number of quantization levels following the detector needs to be modified. Depending on the quantization of decision statistics (soft or hard) at the output of the demodulator, the decoding metric will compute either the Hamming distance or the Euclidean distance between the received symbol sequence and the hypothetical transmitted symbol sequences. Unlike convolutional codes, decoding block codes, such as BCH and Reed-Solomon codes, with different metrics would require several decoding algorithms with different structures. As a result, switching decoding metrics for block codes on-line would be very difficult and expensive to implement. In this chapter we focus on the convolutional code to show how the metric computation can be adapted to the time-varying transmission impairments in a multiple-access channel in order to achieve improved code performance. To generalize the decoding metric problem to consider a variety of fading statistics, we model the channel with Rayleigh fading and a bi-level partial-band noise jammer.

From among the conventional decoding metrics, we pick the standard soft, hard, and error-and-erasure metrics for comparison against the new adaptive decoding metric. The performances of some of the metrics will be computed using cutoff rate analysis, put forward by Wozencraft [46] and Massey [23], based on the Chernoff bound. The Chernoff bound is not always especially tight but it does provide a relatively simple general expression for upper bounds on coded bit error probabilities. It applies to all coded communication systems that use enough interleaving and deinterleaving so that the channel can be modeled as memoryless. Another merit of cutoff rate analysis is the decoupling of coding from the rest of the communication system so that codes can be evaluated separately. For anti-jamming FH/SS systems, there has been considerable investigation of convolutional code design [5][34][38][18][36][37]. Although some coding design principles developed for anti-jamming systems can be applied to land-

mobile and PCS systems, in general, we should exploit the unique requirements and characteristics of commercial wireless applications in the channel code design.

This chapter is organized as follows. In Section 6.1 we motivate the investigation of adaptive metrics. In Section 6.2 we introduce the channel and receiver model the SFH/CDMA system. The model used here is slightly different from the one used in previous chapter in order to facilitate cutoff rate analysis. In Section 6.3 the bit error probability performance for all the metrics considered in this chapter is derived. Section 6.4 presents numerical results on the performance of the various metrics. Section 6.5 describes an algorithm for the metric adaptation and the cost to implement the algorithm. Conclusions and comparisons are drawn in Section 6.6.

6.1 Motivation

The following example provides some of the motivation for investigating adaptive metrics for wireless applications. We consider the error probability performance for three different decoding metrics for a system using non-coherent BFSK signaling over a channel that is impaired by Rayleigh fading and an on-off partial-band noise jammer. The average SNR is set to 13 dB. Figure 6-1 plots the

performance of each metric as a function of the jammer parameter ρ .

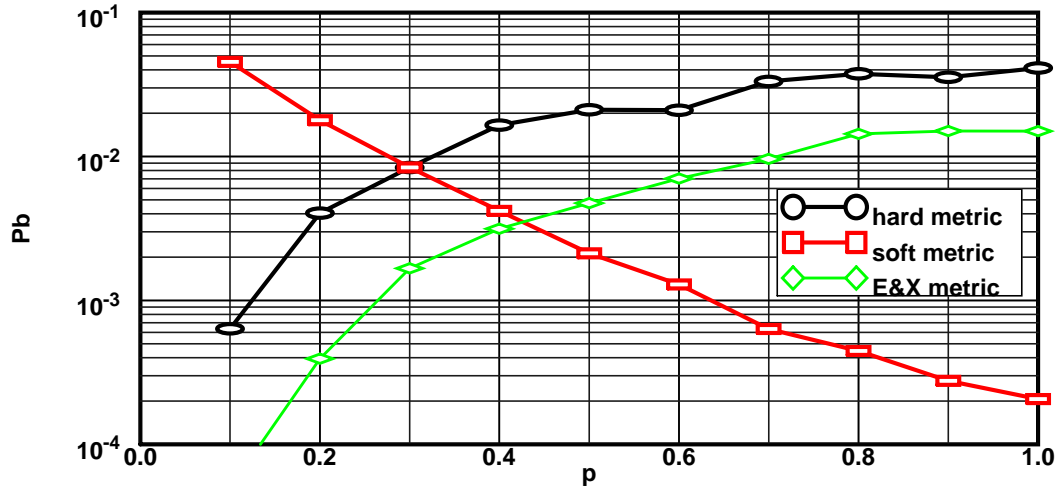


Figure 6-1 Error probability for soft, E&X and hard decision decoding in bi-level partial-band jamming channel.

The data show that the error and erasure (E&X) metric always results in a lower error probability than the hard decision metric. In other words, the E&X metric performs better than the hard decision metric for all ρ . For ρ above a certain threshold, the soft decision metric performs better than the E&X metric, but below the threshold, the E&X metric does better. The soft decision metric does not do well for small ρ because high jamming energy can be injected on a small number of symbols of a coded transmission sequence and lead to a large number of decoding errors. If the value of the jammer parameter is known by the system, the system should be designed to select and use the metric with the best performance for the given ρ .

In military scenarios, the jammer parameter is under the control of the enemy's system and cannot be easily obtained. This means that anti-jam systems should use metrics designed to be robust against all jammer parameters. Usually, these metrics are

designed by using the minimax approach. On the other hand, in civilian cellular FH/CDMA networks, unintentional jamming arises from multiple-access interference generated by similar communication systems which have established links over a shared radio spectrum. Since multiple-access interference is usually slowly-varying with respect to the baud rate, each receiver can estimate some jammer (interference) parameters in a distributed manner. For example, in a SFH/CDMA network, ρ would correspond to the fraction of the frequency-slots occupied by users of the network. As ρ changes on the order of user arrival and service times, which are typically much longer than the baud interval, it could be estimated locally by every receiver. Our design approach, as described in this chapter, is to adapt the decoding metric in each communication link according to the estimated jammer parameters in order to effectively combat the prevailing interference characteristic.

6.2 System Model

As described in Section 5.1, frequency hopping, NC/BFSK, interleaving, antenna diversity, and channel coding are parts of the SFH/CDMA transceiver architecture. In this chapter, we model the transmission channel with Rayleigh fading and bi-level partial-band noise jamming, which generalizes the metric formulation problem to various fading statistics. This model is complex enough to represent realistic channel conditions encountered in SFH/CDMA systems; at the same time, it is simple enough to allow the cutoff analysis to be tractable mathematically. Although we carry out the analysis for a system with only one antenna, the results can be easily extended to multiple antenna diversity with slight modifications.

6.2.1 Interference Model

We assume that the multiple-access interference in the SFH/CDMA system can be modeled as a bi-level partial-band noise jammer. The model also take into account the background thermal noise in the receiver front-end. The jammer model consists of two states 0 and 1 with corresponding interference powers, N_{j0} and N_{j1} . When the state of the channel, denoted by z , is 0 (or 1), each symbol transmitted over the channel will undergo flat fading as well as perturbation by AWGN with variance N_{j0} (or N_{j1}). There is a probability ρ that the channel will be in state 1 and a probability of $1 - \rho$ that the channel will be in state 0.

The bi-level partial-band noise jammer model is particularly well-suited for modeling the impairments arising from interference and thermal noise in the reverse-link of single-cell type systems [22]. The interference in single-cell type systems are caused by adjacent channels spectral spillage. Under power-control, the average received powers from different portable transmitters in the same cell will be approximately equal at the base-station. In this chapter, we will focus on demonstrating the advantage of an adaptive decoding metric in a partial-band noise jamming environment.

6.2.2 Receiver Model

The conventional non-coherent square-law detector for BFSK has the form

shown in Figure 6-2:

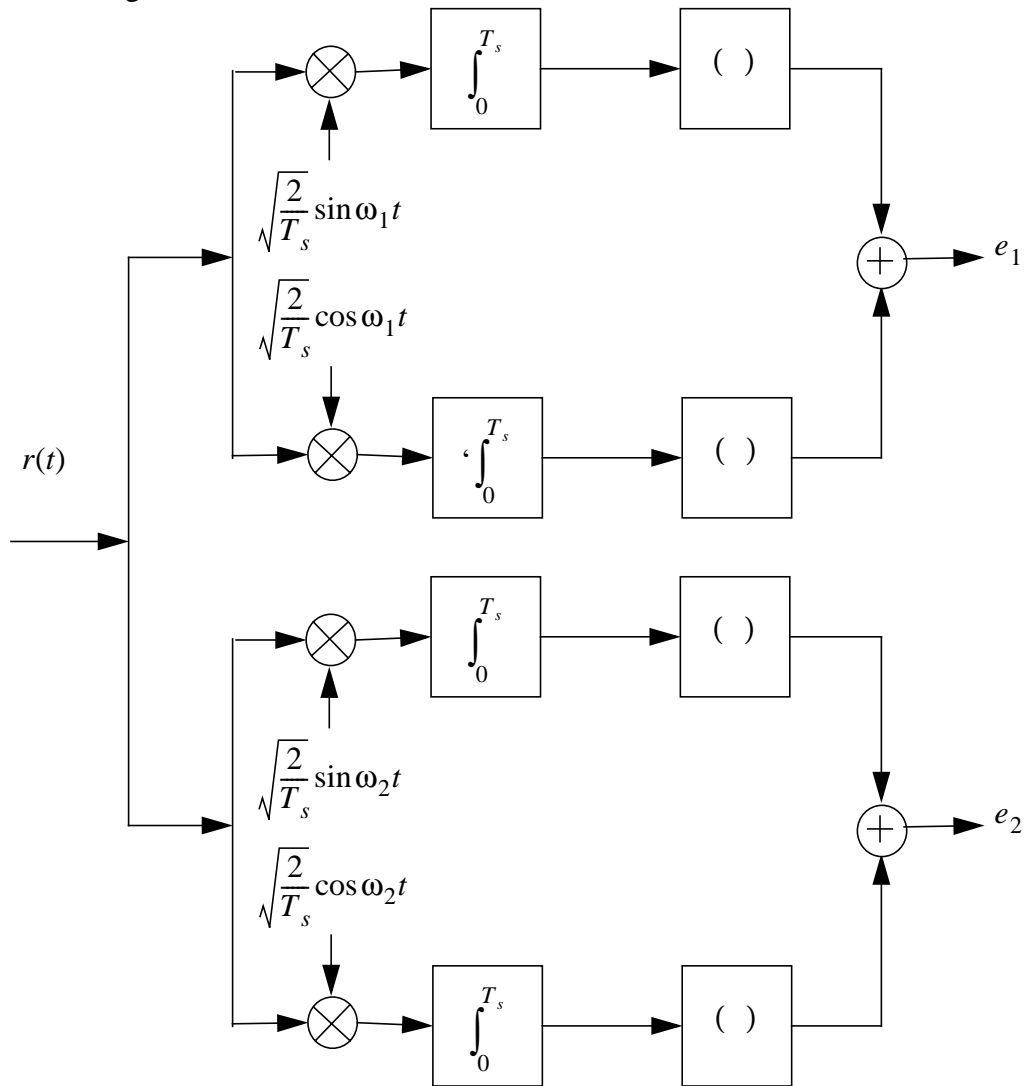


Figure 6-2 Conventional non-coherent square-law detector for BFSK.

The detector output consists of

$$y = (e_1, e_2) \quad (6.1)$$

where e_i is the output of the i -th frequency energy detector. We denote the modulation symbol by $x \in \{0, 1\}$, where $x = i$ corresponds to the i -th frequency tone being

transmitted.

We assume that the sequence of BFSK signals is transmitted over a slowly varying Rayleigh fading channel in the presence of a bi-level partial-band noise jammer. Consider a CW signal of T seconds duration at frequency ω_0 with amplitude α and phase ϕ . The channel impairments include white Gaussian noise $n(t)$ of double-sided power spectral density $N_0/2$ and a bi-level partial-band jammer $i(t)$ of double-sided power spectral density $N_{j0}/2$ and $N_{j1}/2$. The received signal $r(t)$ is modeled as:

$$r(t) = \alpha \sin(\omega_0 t + \phi) + n(t) + i(t) \quad 0 \leq t \leq T \quad (6.2)$$

To simplify the analysis, we can combine the effect of thermal noise and the partial-band noise jammer. In other words, the power spectral density of the partial-band jammer is increased to account for the effect of white noise.

Without loss of generality, assuming that $x = 0$, the statistics at the output of the energy detectors are given by:

$$p(e_0 | \{x=0, z\}) = \frac{1}{\bar{E} + N_{jz}} e^{-\frac{e_0}{\bar{E} + N_{jz}}} \quad (6.3)$$

$$p(e_1 | \{x=0, z\}) = \frac{1}{N_{jz}} e^{-\frac{e_1}{N_{jz}}} \quad (6.4)$$

where $\bar{E} = (1/2)E[\alpha^2]$ is the average energy per BFSK signal and the channel state z is equal to 0 with probability ρ and 1 with probability $1 - \rho$. Thus, in a Rayleigh fading with a partial-band noise jammer, the detector output statistics are exponentially distributed.

Another parameter, f , is used in the bi-level partial-band jammer model to

parameterize the difference in the power spectral density between the two channel states. We define:

$$N_{j0} = \frac{N_0 f}{\rho} \quad N_{j1} = \frac{N_0(1-f)}{1-\rho} \quad (6.5)$$

where $f \in [0,1]$ represents the fraction of the average noise power concentrated in channel state 0. Note that setting $f = 1$ will result in an on-off partial-band jammer model since all the noise power will be concentrated in the jammer on state. Furthermore, it can be observed that letting $f = 1/2$ and $\rho = 1/2$ will result in a broadband noise jammer model, which is more commonly known as the Rayleigh fading channel.

6.2.3 Diversity and Coding

The common definition of an L -th order diversity system is that the transmitter sends replicas of each data bit over L independent channels. With all diversity-combining techniques, including error control coding (a form of time-diversity), the final decision statistic is formed by taking a weighted sum of the square-law detector output for the sequence of transmitted signals corresponding to each data bit. That is,

$$\vartheta_l = \sum_{k=1}^L w_k(z) e_{lk} \quad l = 0, 1 \quad (6.6)$$

where e_{lk} is the energy of the l -th tone in the k -th channel signal interval and $w_k(z)$ is a weighting factor that depends on the k -th channel state. For example, without any knowledge of the channel state, the weight factors are all equal to a constant value and the resulting sum is the basis for the well-known square-law combining metric. In

practice, there might be some post processing on the detector output; hence, we rewrite (6.27) as

$$\vartheta = \sum_{k=1}^L w_k(z) m(y_k, x_k) \quad (6.7)$$

where $m(y, x)$ denotes the post-processing function or the metric. For example, for hard decision decoding, the maximum-likelihood metric is:

$$m(y, x) = \begin{cases} 1 & e_x \geq e_{\hat{x}} \\ 0 & e_x < e_{\hat{x}} \end{cases} \quad (6.8)$$

where $\hat{x} \neq x$. If x is a binary digit, \hat{x} is the complement of x .

6.3 Performance Analysis

In this section, we consider the error probability of convolutional codes decoded using various metrics. In most cases, the analysis is based on the transfer function bound using exact pairwise error probability. The Chernoff bound, which is easier to compute, is used in some cases.

The bit error probability of rate $1/n$ convolutional codes is bounded by:

$$P_b < \sum_{d=d_{\text{free}}}^{\infty} \beta(d) P_2(d) \quad (6.9)$$

where $\beta(d)$ is the number of information symbol errors in two paths separated in distance by d , and $P_2(d)$ is the pairwise error probability between two paths separated in distance by d . d_{free} is the minimum free distance of the code. Notice that $P_2(d)$ is

just the error probability of a repetition code of length d .

When the exact pairwise error probability is hard to obtain, we may use the Chernoff bound to upperbound the solution. The Chernoff bound is given by:

$$P_2(d) \leq D^d \quad (6.10)$$

where the Chernoff parameter is defined by

$$D = \max_{\lambda \geq 0} E\{\exp(\lambda(m(\mathbf{y}, \hat{x}; z) - m(\mathbf{y}, x; z))) | x\} |_{\hat{x} \neq x} \quad (6.11)$$

Here $m(\mathbf{y}, x; z)$ is the metric corresponding to symbol x given that \mathbf{y} is the received vector and the side-information is z .

The Chernoff parameter is directly related to the cutoff rate. For binary modulation, the cutoff rate is defined as:

$$R_0 = 1 - \log_2(1 + D) \quad (6.12)$$

Next we present the performance analysis for the following metrics: hard decision metric, erasure and error metric, soft decision metric (with and without channel state information), and (non-adaptive and adaptive) quantized metric.

6.3.1 Hard Decision Decoding

The first system we consider makes hard decisions on each of the diversity transmissions by deciding that the symbol corresponding to the larger energy was sent. The hard decision metric is given mathematically by (6.8).

Without channel state information, the pairwise error probability can be approximated by:

$$p_2(d) = \sum_{i=0}^d \left[\binom{d}{i} \rho^i (1-\rho)^{d-i} \times \sum_{j=0}^i \sum_{k=k_0}^{d-i} \binom{i}{j} p_1^j (1-p_1)^{i-j} \binom{d-i}{k} p_2^k (1-p_2)^{d-i-k} \right] \quad (6.13)$$

where $k_0 = \max(0, \lfloor (d+1)/2 \rfloor - j)$. p_1 and p_2 are the cross-over probability of the BSC, one for each corresponding channel state.

(6.13) can be combined with (6.9) to produce an upperbound on the bit error rate performance of the system with hard decision decoding.

6.3.2 VRT Erasure and Error Decoding

Viterbi ratio thresholding erasure and error (VRT E&X) decoding is considered an effective method to improve the code performance. In this system, the detector output is mapped to a ternary symbol, -1, 1 and 0 as follows:

$$m(y, x) = \begin{cases} 1 & e_x > \theta e_{\hat{x}} \\ 0 & e_{\hat{x}} < e_x < \theta e_{\hat{x}} \\ -1 & \theta e_x < e_{\hat{x}} \end{cases} \quad (6.14)$$

where θ , called the energy erasure threshold, is some value greater than one. In essence, the detector erases unreliable symbols (i.e. mapping it to the 0 value) by a ratio threshold test. Analysis by Viterbi [40] shows that the receiver designed with an appropriate choice of θ is robust in the sense that θ does not need to be re-adjusted for different jamming environments or system parameters.

Denote the probabilities of making correct and erroneous decisions for the resulting coding channel by p_c and p_e respectively. We can compute $p_c(\theta|z)$ and

$p_e(\theta|z)$ as functions of the threshold θ and the channel state z . Then $p_x = 1 - p_c - p_e$ can be used to determine $p_x(\theta|z)$. The results are:

$$p_c(\theta|z) = \frac{(E_c/N_{jz} + 1)}{(E_c/N_{jz} + 1) + \theta} \quad (6.15)$$

$$p_e(\theta|z) = \frac{1}{(E_c/N_{jz} + 1)\theta + 1} \quad (6.16)$$

The Viterbi decoder that ignores the erased positions and minimizes Hamming distance among the non-erased positions is the maximum likelihood decoder. Hence, the Chernoff bound reduces to the Bhattacharayya bound. For a broadband noise jammer, the Chernoff parameter, which is a function of the θ , is given in [46]. Here when we extended the result to a bi-level partial-band jammer, the Chernoff parameter is given by:

$$D(\theta) = \frac{[p_x(\theta|0) - 2\sqrt{p_e(\theta|0)p_c(\theta|0)}]\rho + [p_x(\theta|1) - 2\sqrt{p_e(\theta|1)p_c(\theta|1)}](1 - \rho)}{[p_x(\theta|0) - 2\sqrt{p_e(\theta|0)p_c(\theta|0)}]\rho + [p_x(\theta|1) - 2\sqrt{p_e(\theta|1)p_c(\theta|1)}](1 - \rho)} \quad (6.17)$$

The optimal value of the erasure threshold should minimize the Chernoff parameter.

Although (6.17) can be substituted into the Union-Chernoff bound (6.10) to obtain an upperbound on decoded bit error probability for erasure and error decoding, the bound is not particularly tight for all values of ρ and f . We have therefore derived a tighter bound by using the pairwise error probability given by:

$$\begin{aligned}
& \sum_{d_1=0}^d \left[\binom{d}{d_1} \rho^{d_1} (1-\rho)^{d-d_1} \times \right. \\
p_2(d) = & \sum_{l=0}^{d_1} \sum_{m=0}^{d-d_1} \left\{ \binom{d_1}{l} p_{x0}^l (1-p_{x0})^{d_1-l} \binom{d_2}{m} p_{x1}^m (1-p_{x1})^{d_2-m} \times \right. \\
& \left. \left. \sum_{j=0}^{d_{11}} \sum_{k=k_0}^{d_{22}} \binom{d_{11}}{j} p_{e0}^j (1-p_{c0})^{d_{11}-j} \binom{d_{22}}{k} p_{e1}^k (1-p_{c1})^{d_{22}-k} \right\} \right] \quad (6.18)
\end{aligned}$$

where $d_{11} = d_1 - l$, $d_{22} = d_2 - m$ and $k_0 = \max(0, \lfloor (d - l - m + 1)/2 \rfloor - j)$. p_{x0} and p_{x1} are shorthands for the conditional probabilities, $p_x(\theta|0)$ and $p_x(\theta|1)$, respectively. Similarly, p_{e0} , p_{c0} , p_{e1} and p_{c1} are shorthands for the corresponding conditional probabilities.

6.3.3 Soft Decision Decoding

6.3.3.1 No CSI

In this system, the unquantized detector output is fed directly to the Viterbi decoder. Without additional channel state information, the square-law combining metric is used in the decoder. That is,

$$y_l = \sum_{k=1}^m e_{lk} \quad l = 1, 2 \quad (6.19)$$

It is well-known that this metric is optimum for a Rayleigh fading channel with a broadband noise jammer. For the Rayleigh fading channel, the error probability expression is given in [29].

To facilitate the derivations of the exact pair-wise error probability for a bi-level partial-band jammer, instead of a broadband noise jammer, we first derive the

conditional pdf of the decision statistics, $y_l, l = 1, 2$. The condition is that given the number of transmitted symbols in the sequence is $m = m_1 + m_2$, m_1 symbols have been transmitted over the 0-state channel and m_2 symbols in the 1-state channel. The pdf of y_l can be written as:

$$p(y_l) = \left(\frac{1}{\sigma_{l,1}}\right)^{m_1} \left(\frac{1}{\sigma_{l,2}}\right)^{m_2} \times \left[\sum_{z=1}^2 \sum_{s=1}^{m_z} \frac{(-1)^{s-1} (m_{\hat{z}} + s - 2)!}{(s-1)! (m_z - s)! (m_{\hat{z}} - 1)!} \left(\frac{1}{\frac{1}{\sigma_{l,z}} - \frac{1}{\sigma_{l,\hat{z}}}}\right)^{m_z + s - 1} y_l^{m_z - s} e^{-\frac{y_l}{\sigma_{l,z}}} \right] \quad (6.20)$$

where $\sigma_{l,z}$ depends on the channel parameters. The derivation of (6.20) is included in Appendix B.

Assuming that $x_k = 0$ for $\forall k$, we can show that: $\sigma_{1,z} = \bar{E} + N_{jz}$ and $\sigma_{2,z} = N_{jz}$. The probability of error $p_2(m)$ can be found by first calculating the conditional probability of error, $p_2(m|m_1, m_2)$:

$$\begin{aligned} p_2(m|m_0, m_1) = \Pr[y_2 > y_1|m_1, m_2] &= \int_0^{\infty} \int_0^{\infty} p(y_1, y_2) dy_2 dy_1 \\ &= \int_0^{\infty} \int_0^{\infty} p(y_2) p(y_1) dy_2 dy_1 \end{aligned} \quad (6.21)$$

The double integration can be simplified to:

$$p_2(m|m_1, m_2) = \left(\frac{1}{\sigma_{1,1}\sigma_{2,1}}\right)^{m_1} \left(\frac{1}{\sigma_{1,2}\sigma_{2,2}}\right)^{m_2} \times \sum_{z=1}^2 \sum_{s=1}^{m_z} \kappa_1(z, s) \left\{ \sum_{\zeta=1}^2 \sum_{t=1}^{m_\zeta} \left[\kappa_2(\zeta, t) \Xi(m_z - s, m_\zeta - t, \frac{1}{\sigma_{1,z}}, \frac{1}{\sigma_{2,\zeta}}) \right] \right\} \quad (6.22)$$

where

$$\kappa_i(z, s) = \frac{(-1)^{s-1} (m_{\hat{z}} + s - 2)!}{(s-1)! (m_z - l)! (m_{\hat{z}} - 1)!} \left(\frac{1}{\frac{1}{\sigma_{i,z}} - \frac{1}{\sigma_{i,\hat{z}}}} \right)^{m_{\hat{z}} + s - 1} \quad (6.23)$$

and

$$\Xi(m, n, a, b) = \sum_{r=0}^m \frac{m!}{(m-r)!} \frac{(n+m-r)!}{a^{r+1} (a+b)^{n+m-r+1}} \quad (6.24)$$

Averaging $p_2(m|m_1, m_2)$ over the probability density of the conditioning event results in

$$p_2(m) = \sum_{i=0}^m \binom{m}{i} \rho^i (1-\rho)^{m-i} p_2(m|i, m-i) \quad (6.25)$$

(6.25) can be combined with (6.9) to produce an upperbound on the bit error rate performance of the system with soft decision decoding. The above bound is much tighter than the one derived using the Chernoff parameter from [37].

6.3.3.2 Weighted Soft Decision Metric, Perfect CSI

We consider two systems that have different perfect channel state information (CSI). The first system has perfect knowledge of the jammer power spectral densities

and the jammer state, i.e. $N_{j0}/2, N_{j1}/2$ and z . We denoted the CSI in the first system by the vector \mathbf{J} . The second system has perfect knowledge of the channel fade level, α , in addition to \mathbf{J} . In both systems, the available channel state information is used to improve the decoding process.

The ML metric for the first system with the CSI, \mathbf{J} , can be shown to be [1]

$$m(y, x|\mathbf{J}) = \frac{\bar{E}}{N_{jz}(\bar{E} + N_{jz})} e_x \quad (6.26)$$

Using (6.27) the final decision statistics can be written as:

$$\vartheta = \sum_{k=1}^L w_k(z) e_{lk} \quad (6.27)$$

where

$$w_k(z) = \frac{\bar{E}}{N_{zz}(\bar{E} + N_{zz})} \quad (6.28)$$

To derive the pair-wise error probability for the first system, we note that the weighting factors in (6.27) scale the detector output statistics in the summation. It can be shown that formula (6.25) can still be used to determine $P_2(d)$ for this system after a slight modifications of the parameters, $\sigma_{1,z}$ and $\sigma_{2,z}$. More specifically, the parameters should be changed to:

$$\sigma_{1,z} = \bar{E}/N_{jz} \text{ and } \sigma_{2,z} = \left(1 + \frac{N_{jz}}{\bar{E}}\right)^{-1} \quad (6.29)$$

Thus, an upperbound on the bit error rate performance of the first system with weighted soft decision decoding can be easily obtained.

The ML metric for the second system with CSI α and \mathbf{J} can be shown to be

[21]:

$$m(y, x|\mathbf{J}, \alpha) = \ln(I_0(\frac{2\alpha\sqrt{e_x}}{N_{jz}})) \quad (6.30)$$

For high SNR, this highly nonlinear metric can be approximated by:

$$m(y, x|\mathbf{J}, \alpha) = \frac{2\alpha\sqrt{e_x}}{N_0} \quad (6.31)$$

The bit error rate performance of this system is difficult to analyze, so we have used Monte Carlo simulation to obtain its performance.

6.3.3.3 Weighted Soft Decision Metric, Imperfect CSI

In practical systems, CSI is not directly known by the receiver but CSI can be obtained by application of maximum-likelihood or suboptimal estimation techniques. Estimation procedures produce imperfect CSI, and so the performance of decoding metrics developed for ideal CSI will suffer some degradation in practice. The amount of degradation depends on the quality of the CSI estimates.

For a NC-BFSK receiver, the channel state information can be estimated by using only the output of energy detector. For NC-BFSK signaling with square-law detection, the signal power for a slot can be estimated by accumulating the larger decision variable, e_i , for each received symbol in the slot. This involves hard decision demodulation and is a feature of decision-directed estimation. For an orthogonal signaling scheme such as NC-BFSK, one way to form an estimate of the noise (or interference) power for a slot is to accumulate the smaller decision variable, e_j , in the slot. The quality of the signal power and noise power estimates depends on the sample size of the estimator, which is equal to the number of symbols per slot.

To model the CSI estimation errors, we assume a high SNR situation in which

most of the demodulator decisions are correct. The estimates of the actual weight factors, $\{w_k(z)\}$, are denoted by $\{\hat{w}_k(z)\}$, where $\hat{w}_k(0)$ and $\hat{w}_k(1)$ are random variables. To determine the degradation due to imperfect estimates, we developed a simulation to perform perturbation analysis. The simulation models the random nature of $\{\hat{w}_k(z)\}$ in the weighted soft decision decoding metric. The simulation results will be discussed in Section 6.4.

6.3.4 Quantized Metric (Single Quantization Interval)

We consider three slightly different quantized decoding metrics. For the first metric, called a linearly quantized metric (LQ metric), each sampled energy detector output is uniformly quantized into one of q levels. That is,

$$y_m = \begin{cases} 0 & 0 \leq \sqrt{e_m} < v \\ 1 & v \leq \sqrt{e_m} < 2v \\ \dots & \dots \\ q-1 & (q-1)v \leq \sqrt{e_m} < qv \\ q & qv \leq \sqrt{e_m} \end{cases} \quad m = 1, 2 \quad (6.32)$$

One way to optimize the quantization interval v is through the Chernoff parameter. For example, when the metric, $m(y, x) = y_x$, is used, the coding parameter below is minimized to obtain the optimum quantization interval:

$$D(\mathbf{p}, \mathbf{J}) = \min_{\lambda \geq 0, v \geq 0} \sum_{z=0}^1 p(z) \left(\sum_{k=0}^q e^{k\lambda} p_0(k|v, z) \right) \left(\sum_{j=0}^q e^{-j\lambda} p_1(j|v, z) \right) \quad (6.33)$$

where

$$\begin{aligned} p_i(k|v, z) &= e^{-k^2 v^2 / 2\sigma_i^2} - e^{-(k+1)^2 v^2 / 2\sigma_i^2} \\ p_i(q|v, z) &= e^{-q^2 v^2 / 2\sigma_i^2} \end{aligned} \quad (6.34)$$

and

$$2\sigma_i^2 = \begin{cases} N_{jz} & i = 0 \\ \bar{E} + N_{jz} & i = 1 \end{cases} \quad (6.35)$$

For the second metric, CSI \mathbf{J} is assumed to be available at the receiver and the sampled detector output is multiplied by a weighting factor before quantization. The weighting factors are given in (6.28). This metric is referred to as the weight adaptive quantized (WAQ) metric. Optimization of the quantization interval for the WAQ metric can also be found by minimizing the coding parameter (6.33) with the following new definitions for $2\sigma_i^2$:

$$2\sigma_i^2 = \begin{cases} \left(1 + \frac{N_{jz}}{\bar{E}}\right)^{-1} & i = 0 \\ \bar{E} / N_{jz} & i = 1 \end{cases} \quad (6.36)$$

6.3.5 Quantized Metric (Multiple Quantization Intervals)

We will show that the LQ metric can be improved significantly by using two different quantization intervals, one for each channel state. The quantization intervals are optimized through the coding parameter given by:

$$\mathbf{J} = \min_{\lambda \geq 0, \vec{v} \geq 0} \sum_{z=0}^1 p(z) \left(\sum_{k=0}^q e^{k\lambda} p_0(k|v_z, z) \right) \left(\sum_{j=0}^q e^{-j\lambda} p_1(j|v_z, z) \right) \quad (6.37)$$

where $\vec{v} = [v_0 \ v_1]$ is a vector of two elements. Each element represents a quantization

interval for the corresponding channel state. (6.37) is just a generalization of (6.32). It can be expected that selecting one or two quantization intervals involves a trade-off between receiver complexity and code performance. We name this third quantized metric the interval adaptive metric (IAQ).

Similar to the other coding parameters, (6.33) and (6.37) can be substituted into the Union-Chernoff bound (6.10) to obtain upperbounds on decoded bit error probability for the corresponding quantized decoding metrics.

6.4 Numerical Results and Discussion

In this section, numerical results are given for the metrics considered in this chapter for two types of channels, namely the Rayleigh fading with broadband noise jammer channel and the Rayleigh fading with bi-level partial-band noise jammer channel. The code we consider is the rate-1/2, constraint length 6, binary convolutional codes. For the region of interest, the union bounds on bit error probability can be closely approximated by the first five or six terms in the summation.

6.4.1 Rayleigh Fading Channel

The error probability analysis of the hard and soft decision metric for this channel is presented in [29]. Here we start with error probability analysis for the VRT E&X metric. A numerical optimization program is used to determine the optimum

erasure threshold through the Chernoff bound parameter. The top graph in Figure 6-3

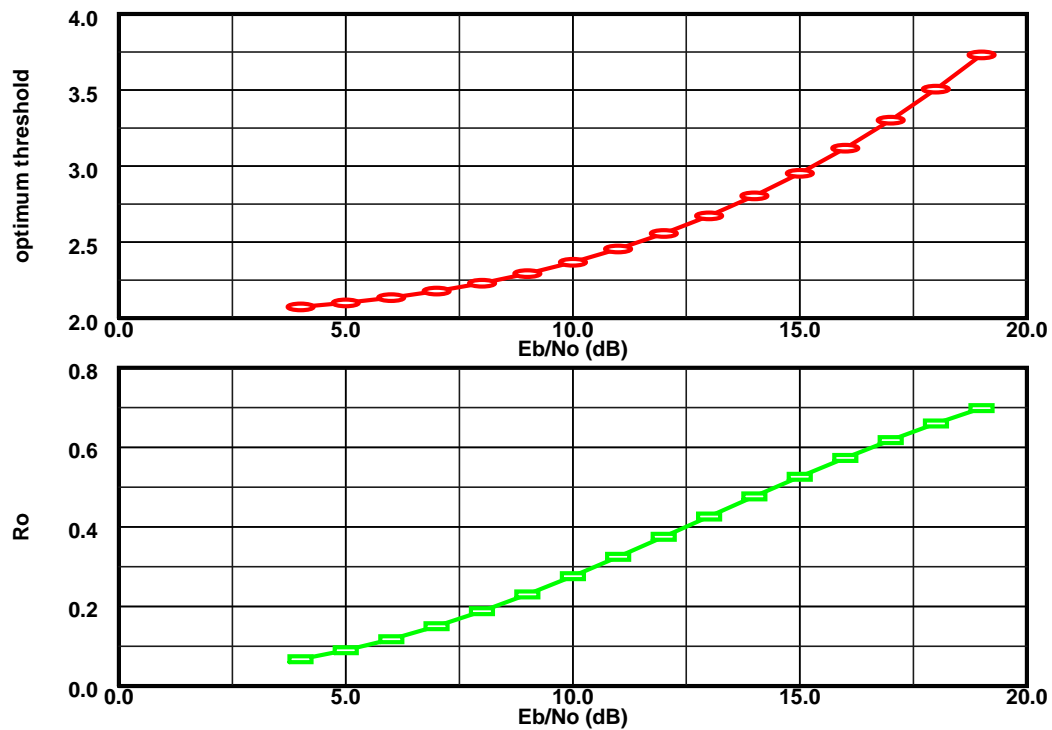


Figure 6-3 The optimum threshold and cutoff rate vs. SNR per bit for a binary coded system over the Rayleigh fading channel.

shows the optimum threshold as a function of the E_b/N_o for the Rayleigh fading channel. It shows that the optimum threshold increases as E_b/N_o increases. Intuitively, this says that as the channel becomes more reliable, the rate of declaring erasures should be reduced. Other results show that the system performance is not very sensitive to the setting of the threshold value and is quite robust against variations in SNR. The results also indicate that for a rate-1/2 code, the optimum threshold should be approximately 2.75 and the required E_b/N_o to achieve low decoded BER is approximately 14 dB. These results have been confirmed by simulation results shown in the next figure.

What is the comparative performance of different metrics? Figure 6-4 shows the

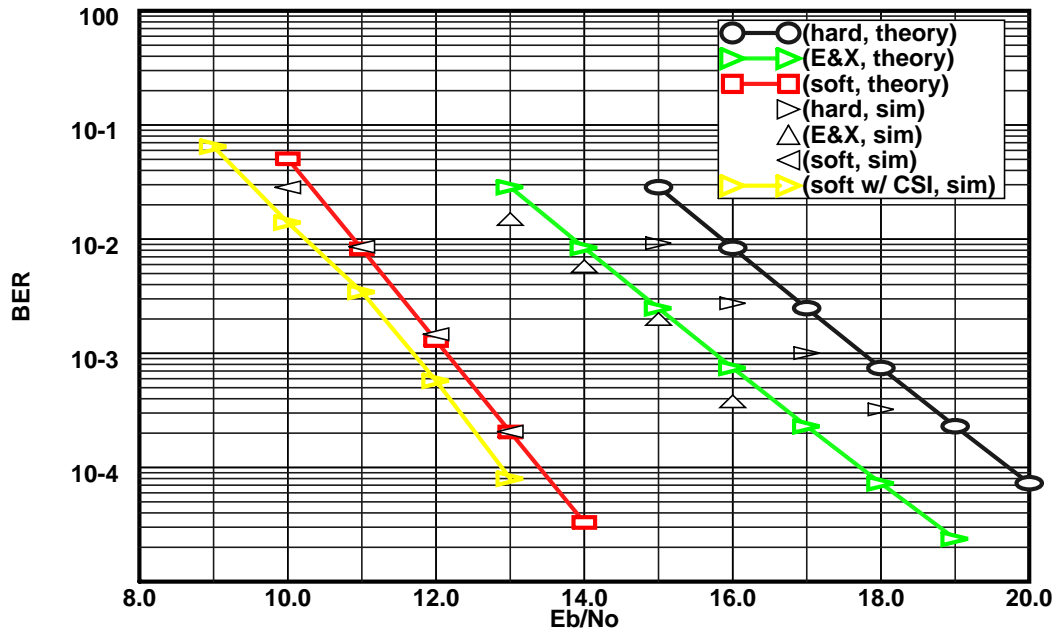


Figure 6-4 Coding gain comparison of four different metrics for $L=6$, $k=1$, $n=2$ convolutional code over the Rayleigh fading channel.

analytical and simulation BER vs. E_b/N_o curves for four different decoding metrics for the Rayleigh fading channel. Note that the simulation and theoretical results are in close agreement. As for the SNR requirement at 10^{-3} , one can observe that the gain of E&X decoding over hard decision decoding is approximately 1 dB. The gain of soft decision decoding over hard decision decoding is approximately 5 dB. The soft metric with CSI, α and J , improves the coding gain by another 0.5 dB over the soft metric without CSI.

How many bits are required for the LQ metric to approach the performance of

soft decision decoding? Figure 6-5 shows the optimum quantization interval and the

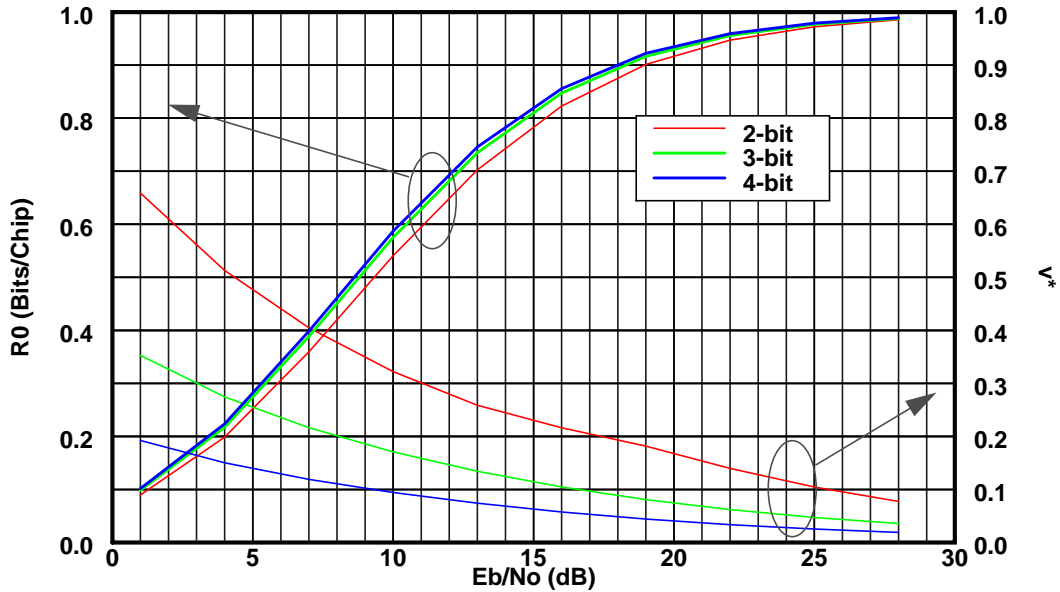


Figure 6-5 The optimum quantization interval and the corresponding cutoff rate vs. SNR for a binary coded system over a Rayleigh fading channel. (for 3 different number of quantization bits)

cutoff rate vs. SNR for the linearly quantized (LQ) metric with different number of quantization bits. To obtain the cutoff rate performance for this system, (6.33) is minimized with a numerical optimization program. The average received symbol energy was normalized to one in the optimization program. At rate 1/2, the difference in the SNR requirements for 2-bit and 3-bit quantization is about 0.5 dB and the difference between 3-bit and 4-bit quantization is negligible. Thus, the results show that, for the Rayleigh fading channel, three-bit quantization is sufficient to obtain most of the performance benefit of infinite precision soft decision decoding.

Figure 6-6 shows the performance for LQ decoding metrics in comparison to

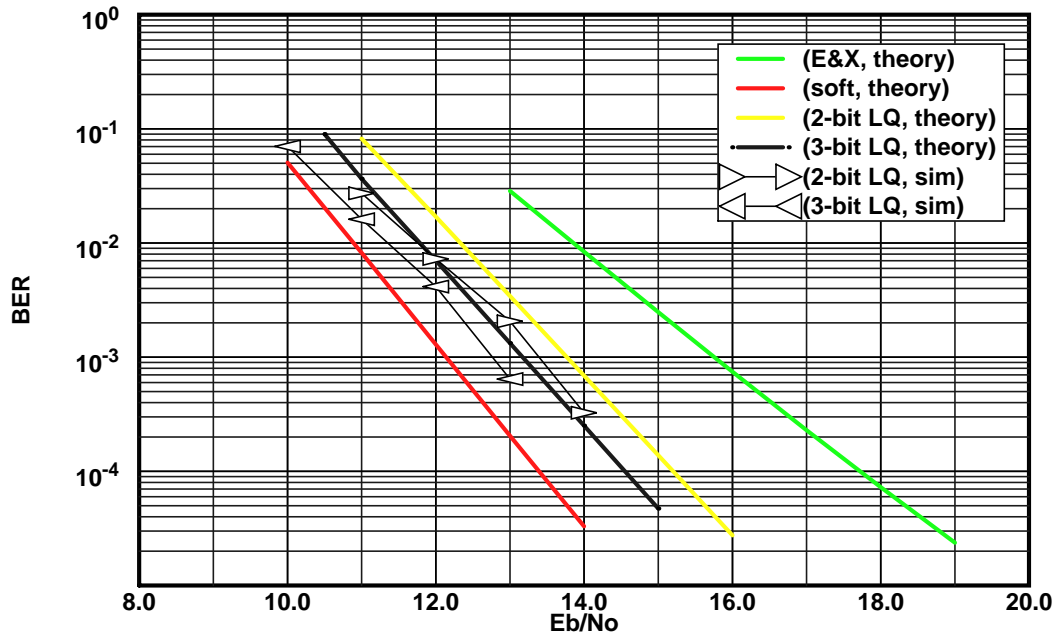


Figure 6-6 Coding gain comparison of four different metrics for L=6, k=1, n=2 convolutional code over the Rayleigh fading channel.

other decoding metrics. Note that the simulation and theoretical results for the LQ metric are in close agreement. At 10^{-3} , the coding gain of 2-bit LQ metric decoding over E&X decoding is approximately 2 dB and the gain of soft decision decoding over 3-bit LQ metric decoding is approximately 1 dB.

6.4.2 Rayleigh Fading, Bi-Level Partial-Band Jammer Channel

For the Rayleigh fading, bi-level partial-band jammer channel, Figure 6-7

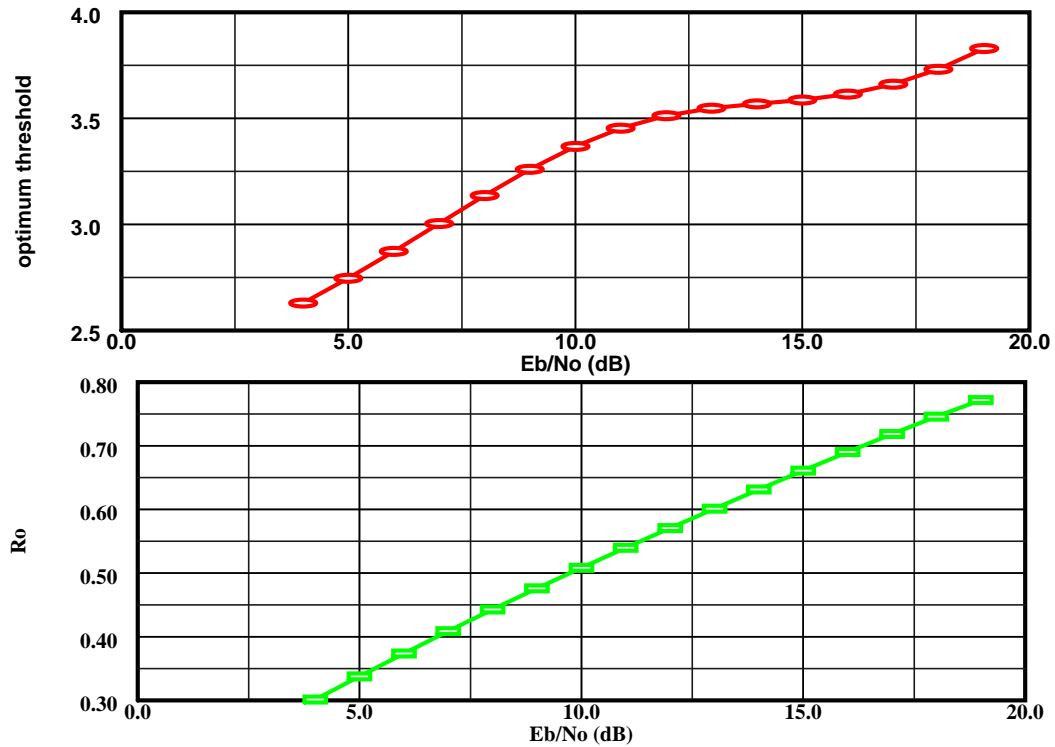


Figure 6-7 The optimum threshold and cutoff rate vs. SNR per bit for a binary coded system in a Rayleigh fading, bi-level partial-band jammer channel ($\rho = 0.25$, $f=0.90$).

shows the optimum threshold as a function of the E_b/N_o . The results show that the optimum threshold increases as E_b/N_o increases. The optimum threshold is approximately 3.4 and the required E_b/N_o to achieve low BER is approximately 10 dB.

Figure 6-8 shows the analytical and simulation BER vs. E_b/N_o curves for three

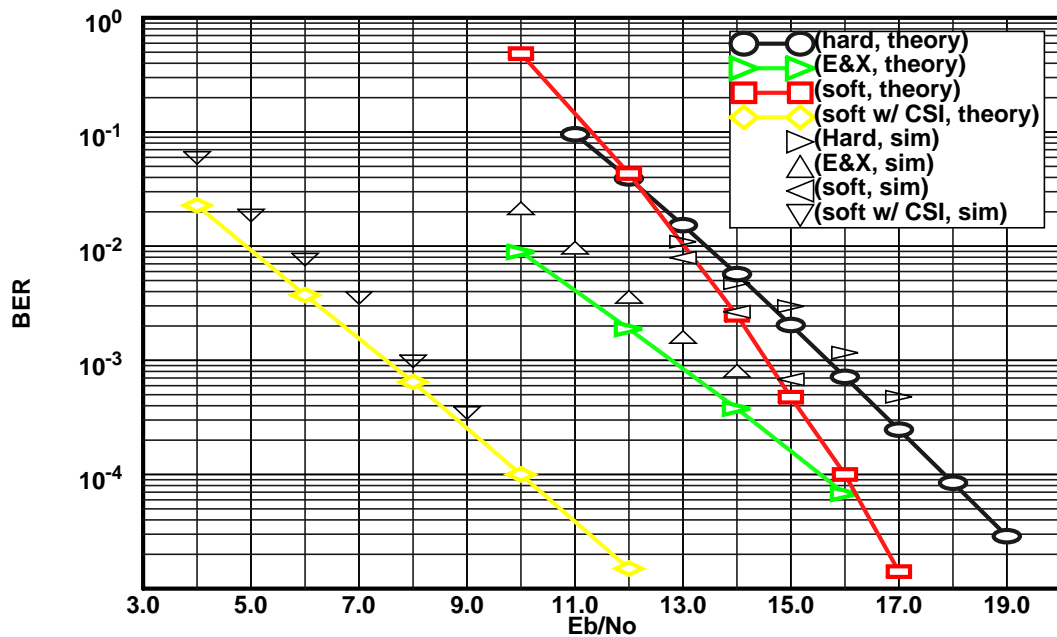


Figure 6-8 Coding gain comparison of three metrics using $L=6$, $k=1$, $n=2$ convolutional code over Rayleigh fading, bi-level partial-band jammer channel ($\rho = 0.25$, $f=0.90$).

different decoding metrics for the Rayleigh fading, bi-level partial-band noise jammer channel. Considering the SNR requirement at 10^{-3} , we see that the gain of E&X decoding over hard decision decoding is approximately 2 dB. And the gain of soft decision decoding over hard decision decoding is approximately 1 dB. Compared to the previous result for the Rayleigh fading channel, we see that soft decision decoding without CSI is more effective than E&X decoding against broadband noise but E&X decoding is more effective against narrowband noise than soft decision decoding without CSI. The soft metric with CSI, J , improves the coding gain by 5.5 dB over the E&X metric. This shows that using CSI in the decoding metric is more important when the channel noise characteristic is time-varying.

In a practical system perfect CSI is unavailable. However, the noise variance and bit energy could be estimated using the detector outputs as described in the previous section. With this type of estimator, the channel parameter estimates, N_g and \bar{E} are Chi-Square distributed. The variance of the Chi-Square distribution depends on N , the number of independent samples in the estimator. Figure 6-9 illustrates the performance degradation for the weighted soft metric due to the imperfect channel parameter estimation.

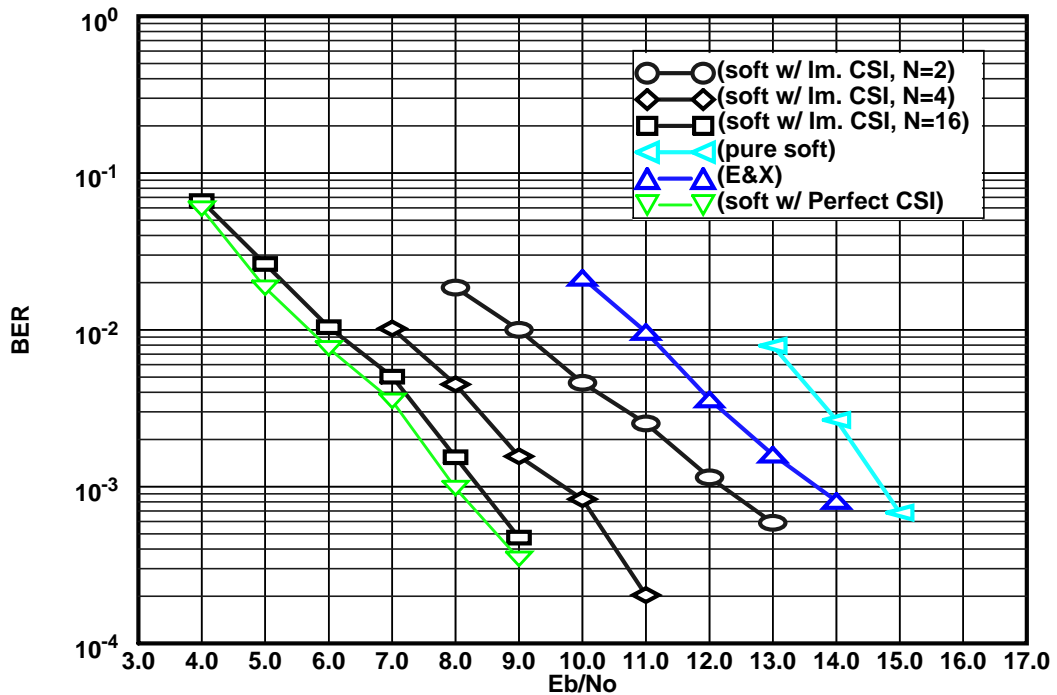


Figure 6-9 Comparison of weighted soft metrics with perfect CSI and imperfect CSI decoding for $L=6$, $k=1$, $n=2$ convolutional code for Rayleigh faded, bi-level partial-band jammer channel ($\rho = 0.25$, $f=0.90$).

The data shows that although the unreliable channel state estimates does degrade the performance of the weighted soft metric, a relatively small number ($N=16$)

suffices for good decision quality, which results in loss of less than 1 dB at 10^{-3} BER. Even with only two samples per estimate, the weighted soft metric with imperfect CSI still performs better than the E&X metric.

Next, we present numerical result for the different quantized metric. Figure 6-10 shows the cutoff rates for three different quantized metrics. To obtain these cutoff rates, we also found the optimum quantization intervals. Figure 6-11 shows the optimum quantization intervals for the IAQ metric and Figure 6-12 shows the optimum quantization interval for the WAQ and LQ metrics. The cutoff rate for E&X metric is included for comparison. At rate one-half, the data show that the E&X metric has 1.5 dB better coding gain than the 2-bit LQ metric. The data also indicate that the two adaptive quantized metrics have similar performance and both have 2 dB better coding gain than the E&X metric. The fact that the two adaptive quantized metrics are equivalent in performance is interesting. The results from cutoff rate analysis and simulation seems to imply that the interval adaptive quantized metric can be transformed to any other decoding metrics by simply changing the quantization interval and the number of quantization bits of the IAQ metric.

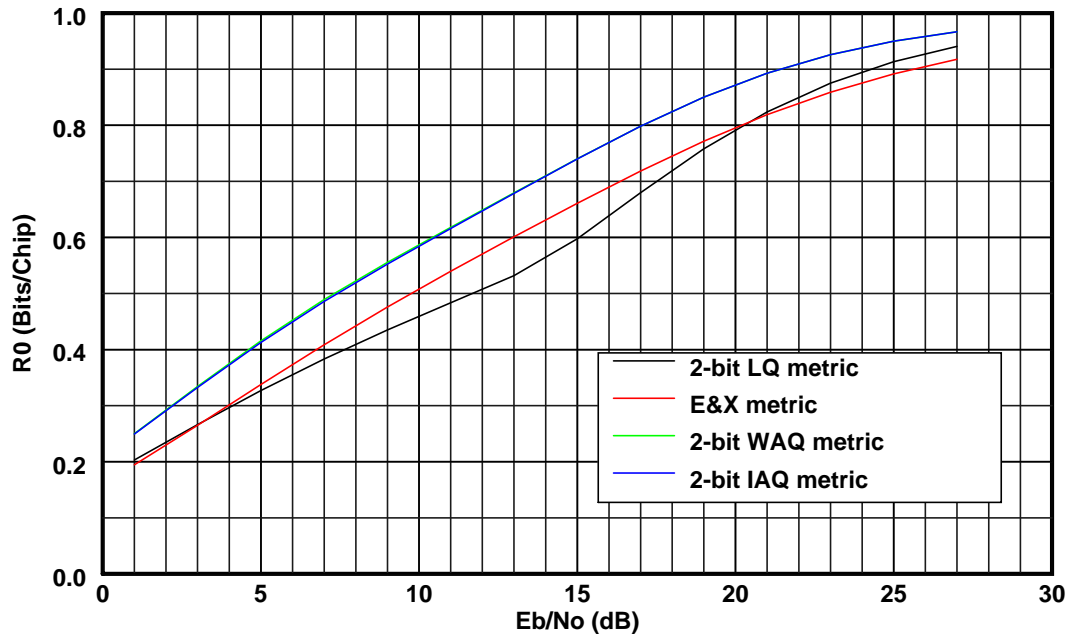


Figure 6-10 Cutoff rate vs. SNR per bit for quantized metric decode NC-BFSK system over Rayleigh fading bi-level, partial-band jammer channel ($\rho = 0.25$, $f=0.90$).

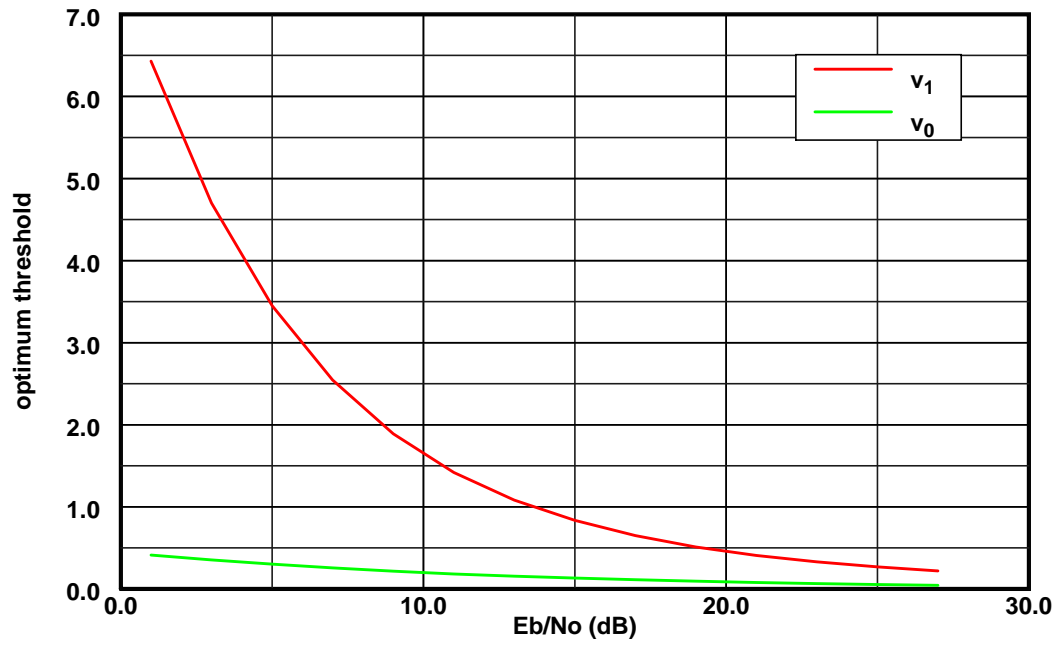


Figure 6-11 Optimum quantization interval vs. SNR per bit for IAQ metric decode NC-BFSK system over Rayleigh fading bi-level, partial-band jammer channel ($\rho = 0.25$, $f=0.90$).

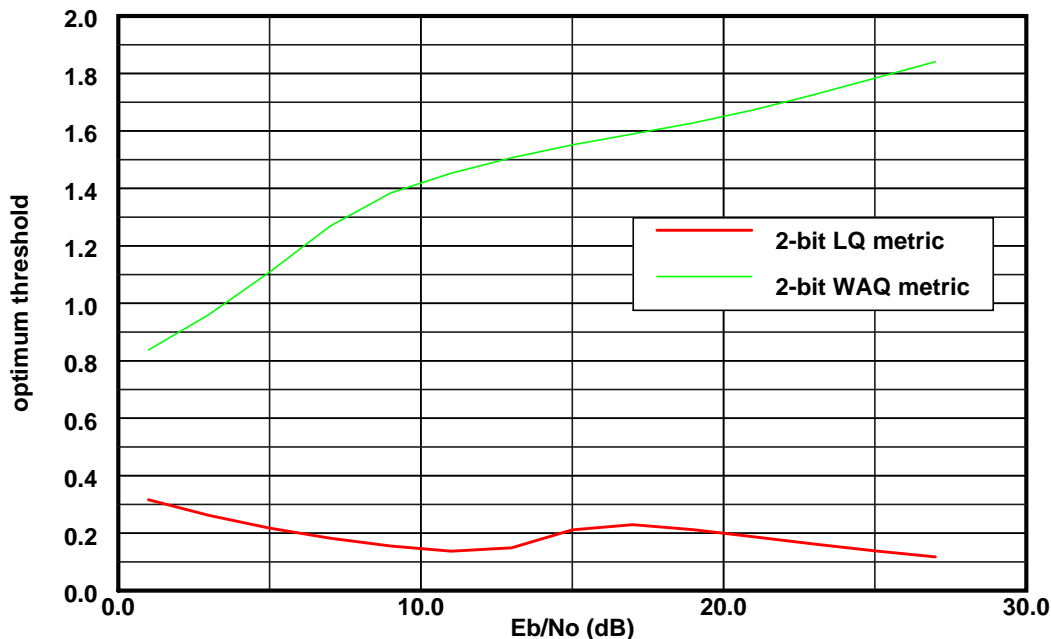


Figure 6-12 Optimum quantization interval vs. SNR for two quantized metric decoded NC-BFSK system over Rayleigh fading bi-level, partial-band jammer channel ($\rho = 0.25$, $f=0.90$).

Although the two adaptive metrics give the same coding performance, their implementation costs are different. Selecting which metric to implement in the receiver requires an understanding of the trade-off in hardware complexity. The WAQ metric requires a multiplier and a ROM to store the look-up table for the optimum quantization intervals. The IAQ metric does not require a multiplier but does demand twice as much memory for the look-up table since it uses two different quantization levels for each set of channel parameters. In custom VLSI design, a ROM larger than a few hundred bits would typically be more expensive than an 8-bit multiplier both in terms of area and in terms of complexity. Considering the memory requirements in the two cases, we believe that the WAQ metric would be less costly to implement.

It is known that the branch metric computation unit for pure soft decision

decoding over Rayleigh fading channels consists of a uniform quantizer with fixed thresholds and perhaps an automatic gain controller (AGC) to compensate for fading. For the WAQ metric, the branch metric computation unit should consist of a uniform quantizer with adjustable thresholds, a multiplier, a look-up table and some channel parameter estimators, such as the SNR estimator. We note that the cost of implementing channel estimation might be shared with the other units in the receiver that would require channel measurements. Compared to the pure soft decoding metric, the additional complexity for implementing an adaptive metric is not excessive if the look-up table is relatively small. Next, we describe an adaptive algorithm for the WAQ metric.

6.5 Adaptive Algorithm and Performance Results for the WAQ metric

To adapt the WAQ metric, we can make use of a training sequence to determine the characteristics of the channel. We assume that the parameters f , ρ , \bar{E} and N_o can be reliably estimated during the channel probing phase. The estimated channel parameters are used to index a look-up table, selecting the appropriate quantization interval. The look-up table stores the optimum quantization interval pre-computed by the cutoff rate analysis presented in Section 6.3.4. To track the channel, the channel estimates can be periodically updated by using a decision-directed estimation scheme based on the received data sequence.

In designing the look-up table, the size of the table should be minimized while meeting some accuracy constraint. In essence, the look-up table is used to approximate a multivariate function. From simulation and analysis, we determined that the error in

generating the optimum quantization interval must be less than 20% in order to guarantee that the BER performance degradation from using an approximated, suboptimal threshold would be no greater than 20%. A 20% increase in BER corresponds roughly to a SNR degradation of 1 dB.

As an example of how the look-up table should be designed and how the size of the table can be computed, consider a bi-level partial-band jammer channel where E_b/N_o varies between 10 and 15 dB. The look-up table contains byte-sized entries of the optimum quantization intervals for discrete values of the triplet $(E_b/N_o, f, \rho)$. Each coordinate in the triplet represents one axis in a three dimensional domain. If the accuracy criterion could be met by dividing each axis into ten uniformly spaced segments, then the look-up table would require exactly one kilobyte of memory.

We now illustrate the benefit of using the weighted adaptive quantized metric through our original motivational example given in Section 6.1. The performance of the WAQ metric is compared to the other metrics shown in Figure 6-1. The optimum thresholds for the WAQ metric with 16 quantization levels are stored in a small look-up table. 16 levels was found to give performance sufficiently close to infinite precision soft decision decoding. In this example, E_b/N_o and f are fixed so that the look-up table can be greatly simplified. The look-up table contains only 11 entries, each corresponding to one value in the sequence $\rho \in \{0, 0.1, 0.2, \dots, 1.0\}$. As the channel parameter ρ changes slowly, the quantization interval and the weight coefficients of the WAQ metric automatically adapts to the new channel condition. The rate of change is

on the order of thousands of channel symbol intervals. Figure 6-13 shows that the

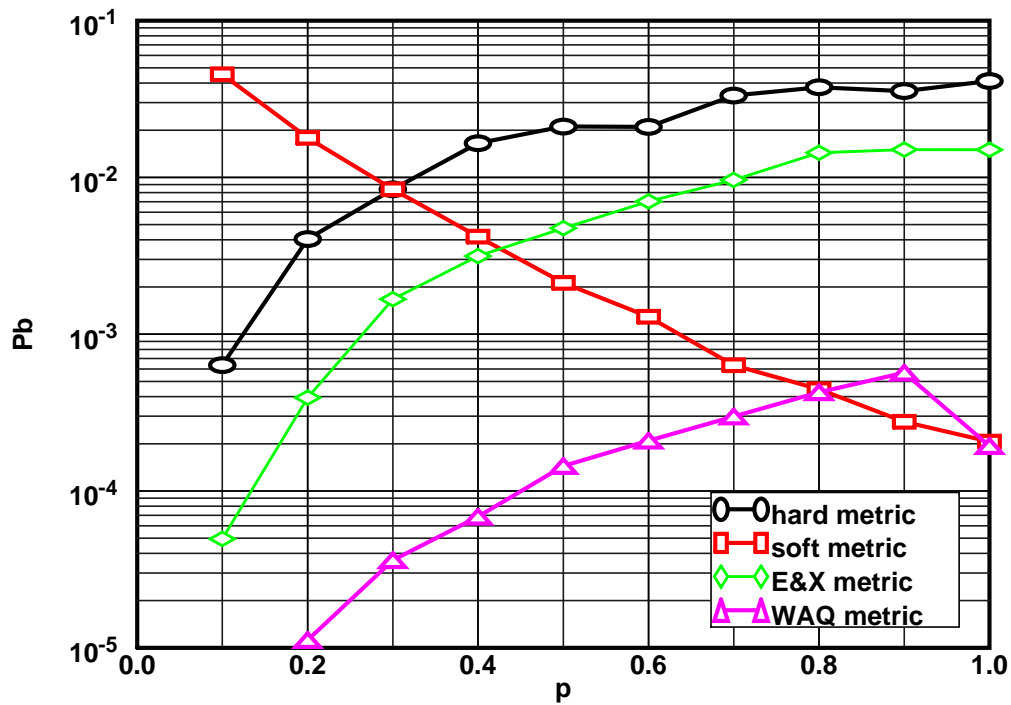


Figure 6-13 Error probability for four different decoding metrics in a NC-BFSK system over a Rayleigh fading and bi-level partial-band jammer channel ($f=0.90$, $E_b/N_0=13$ dB).

system with WAQ metric can maintain a 10^{-3} or lower BER for all ρ . It shows tremendous improvement over the E&X metric when $\rho = 1$ and over the soft metric when $\rho = 0.2$. In general, the performance curve for the WAQ metric tracks the lower envelope formed by the curves for the E&X and soft metrics. Thus, using the WAQ metric results in significant performance improvement over the standard fixed metrics over the range of ρ .

6.6 Summary

In summary, we analyzed the performance of conventional and new adaptive decoding metrics with convolutional coding in a Rayleigh fading and bi-level partial-band noise jammer channel and derived new tighter probability of error performance bounds in some cases. More importantly, we showed that using the weighted adaptive decoding metric for the Rayleigh fading, bi-level partial-band noise jammer channel can improve the performance of convolutional codes significantly over using conventional metrics. Based on the results from cutoff rate analysis and simulation, we observed that the adaptive quantized metric could be made to perform like standard fixed decoding metrics by setting the quantization interval and the number of quantization bits of the adaptive metric to the appropriate values. Thus, the adaptive metric combines the features of standard hard, soft and E&X metrics. A simple algorithm for adapting the metric was given and its implementation was considered.

The result of the thesis should motivate the consideration of adaptive decoding metric for other channels in which the potential performance gain may be much greater. Improving the adaptation algorithm is another possible research area. For example, we note that it might be possible to implement a supervised learning neural network (SLNN) co-processor to learn the relationship between channel statistical information and the optimum quantization interval [48]. Implementing a SLNN, rather than a memory look-up table, to generate the optimum quantization interval function might provide a more cost effective solution when confronted with highly variable propagation conditions.

Chapter 7

CONCLUSION

The purpose of this study is to develop and validate the system design techniques proposed for the UCLA prototype low-power handheld transceiver. The proposed architecture incorporates many advanced system techniques, such as antenna diversity, slow frequency-hopped/code division multiple access (SFH/CDMA), channel coding, and adaptive power control. Although these system techniques are developed for a particular transceiver, the techniques are general enough to be applicable to other commercial and military wireless communication applications. Our study focused on the system tradeoff issues in distributed power control implementation, channel code selection and adaptive decoding metric formulation.

Our study is restricted to the SFH/CDMA radio communication channel, in which the principal impairments are signal strength fluctuations due to log-normal shadowing and nonselective Rayleigh fading, and multiple access interference from other radios. To achieve robust transmission and maximize capacity without resorting to high transmitter power, the following advanced system techniques are used. Two

antennas with receive branch diversity combining are employed to provide polarization/space diversity. Frequency hopping combined with error-control coding is implemented to provide both frequency and interferer diversity. Adaptive power control is used so that the transmitted power required for reliable communication is minimized.

Our investigation has generated interesting conclusions and new results. Some new results include the specification and validation of a distributed power control scheme for SFH/CDMA systems, the determination of the sufficient transmit power dynamic range to prevent significant system capacity loss and the development of heuristic algorithms for reducing call dropping in a power controlled network with dynamic power range restrictions. Another result is the development of a low-delay channel coding scheme and the demonstration of the benefits of dual antenna diversity in combination with coding. In addition, we formulated an adaptive metric that can track variations in channel statistics, accommodating rapid changes in interference levels, and designed a simple algorithm for adapting the metric to the changing channel conditions. We have concluded that adapting the metric according to the channel condition provides significant performance gain over standard fixed decoding metrics, such as the soft decision and erasure and error decoding metrics.

Many questions emerge from our study of system issues for the wireless transceiver. The result of our thesis should motivate the consideration of adaptive decoding metric for other channels in which the potential performance gain may be much greater. In general, the effect of mobility on system capacity needs to be examined by incorporating more complex system models. For example, handoff issues could be studied in conjunction with power control. Better propagation channel modeling might be required to more accurately simulate microcellular environments. The use of other modulation schemes might be considered to improve transmission

throughput. Finally, we have not addressed the potential problem with strict time synchronization requirements for FH/CDMA systems. This problem and many others which we have not mentioned provide new research opportunities. At the present time, numerous researchers have already begun answering some of these very important questions.

The research activities in wireless communication will continue to be strong for the immediately foreseeable future. For example, a major research program is currently in progress at UCLA to develop a high-speed transceiver [32]. In this new project, low power design is not a major objective and hence, more sophisticated system techniques, such as adaptive beam forming and equalization, could be implemented to enable high-speed communication. Although SFH/CDMA is employed in both the UCLA high-speed and low-power transceiver projects, the merits of various multiple access schemes for wireless personal communications are still the subject of considerable dispute. The research on advanced communication techniques for building better wireless personal systems will fuel this intense debate for years to come.

Appendix A

Frequency Reuse with Latin-Squares

Here we consider combining frequency reuse with the latin-square construction for multi-cell or multi-cluster systems. Suppose the reuse factor is one-third, then the frequency spectrum is divided up into three disjoint subsets of subbands. These sets are denoted by $\{B_l, 0 \leq l \leq 2\}$ and l is called the reuse subset index. Each cell is assigned a single reuse subset, B_l , which contains the frequency slots the users in that cell may hop over. Furthermore, to eliminate adjacent channel interference, the bands of each reuse subset are interleaved with bands of the other subsets. Figure A-1 shows how a 1/3 reuse pattern can be imposed on a 19 cell network:

There are different ways to assign unique cell identification numbers, a , to each cell (clusters). We want the assignment to yield a simple formula for finding the frequency slot number in each hop. By sequentially labeling the cells in each cluster as in Figure A-1, we can obtain $l(a)$, which give the reuse set index as a function of the cell identification number:

$$l(a) = (a - 1)_{\text{mod } r} \quad (\text{A.1})$$

l will also be called the frequency offset because it determines the relative position of the subbands of each reuse set in the system bandwidth.

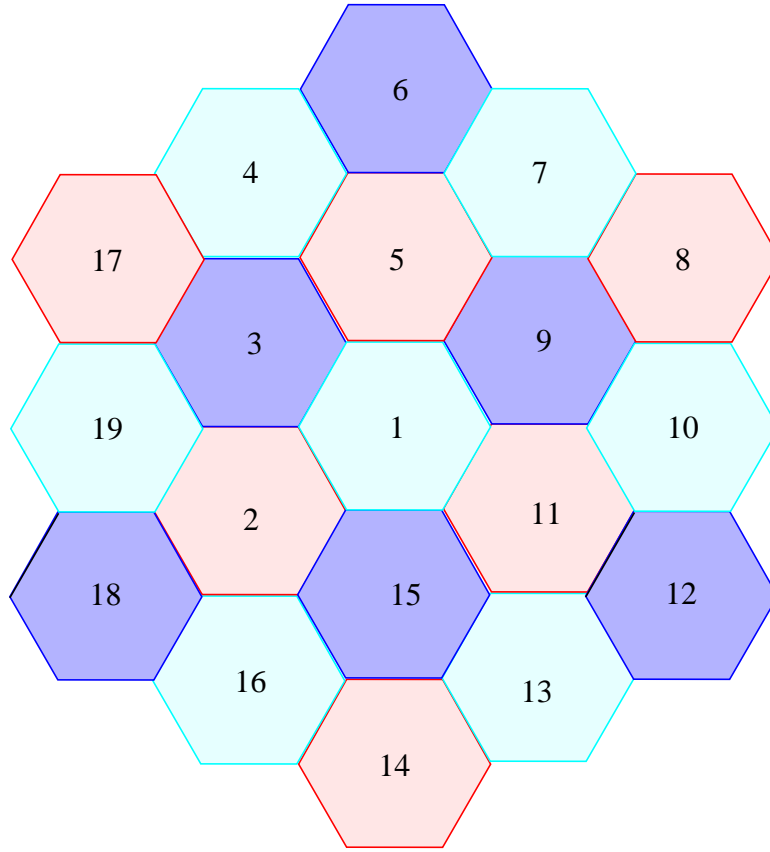


Figure A-1 19 Hexagonal Cell Layout (Frequency Reuse Factor of 1/3)

Consider the following example. Suppose the base-station number of the k th user with mobile id $m^{(k)}$ is $a^{(k)}$, the frequency slot number in the i th hop will be given by the following formula:

$$j = (m^{(k)} - a^{(k)}i)_{\text{mod } n} \times r + l(a^{(k)}) \quad (\text{A.2})$$

The mobile id is given by

$$m^{(k)} = \begin{cases} \left(a^{(k)}i + \frac{j}{r} \right)_{\text{mod } n} & \text{if } (j)_{\text{mod } r} = (a^{(k)})_{\text{mod } r} \\ 0 & \text{otherwise} \end{cases} \quad (\text{A.3})$$

For example, consider a system with the parameter $n = 8$. The hopping patterns used for cells one through six is shown in Figure A-1. Rows with identical shading in the hopping pattern matrix are from the same reuse set.

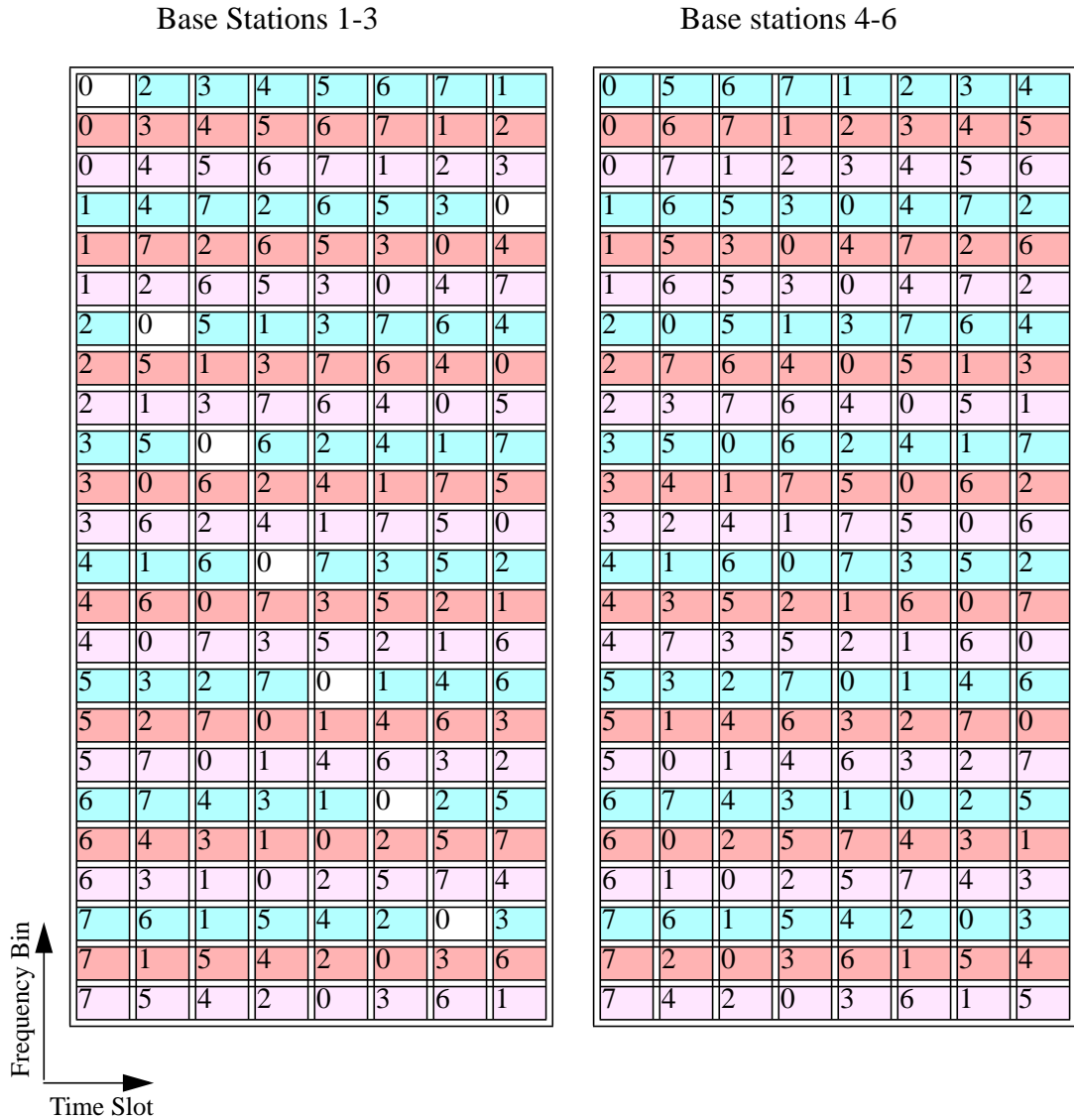


Figure A-2 Hopping pattern by Latin-square construction ($n = 8$ and frequency reuse factor of $1/3$)

Appendix B

Derivation of the Exact Pair-wise Error Probability

In this Appendix we derive the exact pair-wise error probability for soft decision decoding over a Rayleigh fading, bi-level partial-band jammer channel. Without loss of generality we consider the decision variable, $y \equiv y_1$, conditioned on the event that given the number of transmitted symbols in the sequence is $m = m_1 + m_2$, where m_1 symbols have been transmitted over the 0-state channel and m_2 symbols in the 1-state channel. y can be written as:

$$y = \sum_{k=1}^{m_1} e_{1k}^{(1)} + \sum_{l=1}^{m_2} e_{1l}^{(2)} \quad (\text{B.1})$$

The characteristic function of the decision variable y is defined as:

$$\Psi(s) = E[e^{jsy}] = E\left[\exp\left(js\left(\sum_{k=1}^{m_1} e_{1k}^{(1)} + \sum_{l=1}^{m_2} e_{1l}^{(2)}\right)\right)\right] \quad (\text{B.2})$$

Since $\{e_{1k}^{(1)}, e_{1l}^{(2)}\}$ are independent, (B.2) reduces to the product of the characteristic functions raised to some powers. That is,

$$\Psi(s) = \left\{ \frac{1}{\sigma_{1,0}} \right\}^{m_1} \left\{ \frac{1}{s - \frac{1}{\sigma_{1,0}}} \right\}^{m_2} \quad (\text{B.3})$$

where $\sigma_{1,z} = \bar{E} + N_{j_z}$ if an all zero sequence was transmitted.

After expansion of (B.3) by partial-fractions and taking the inverse fourier transform, we obtain the pdf:

$$p(y) = \left(\frac{1}{\sigma_{1,1}} \right)^{m_1} \left(\frac{1}{\sigma_{1,2}} \right)^{m_2} \times \left[\sum_{z=1}^2 \sum_{s=1}^{m_z} \frac{(-1)^{s-1} (m_{\hat{z}} + s - 2)!}{(s-1)! (m_z - s)! (m_{\hat{z}} - 1)!} \left(\frac{1}{\sigma_{1,z} - \frac{1}{\sigma_{1,\hat{z}}}} \right)^{m_{\hat{z}} + s - 1} y^{m_z - s} e^{-\frac{y}{\sigma_{1,z}}} \right] \quad (\text{B.4})$$

In general, the pdf for y_l is given by (B.4).

Appendix C

Glossary

C.1 List of Acronyms and Abbreviations

AMPS	Advanced Mobile Phone Service
AWGN	Additive white Gaussian noise
BER	Bit error rate
CDMA	Code division multiple access
DECT	Digital European Cordless Telecommunications
FCC	Federal Communications Commission (U. S.)
FDMA	Frequency division multiple access
FEC	Forward error correction (Channel coding)
FM	Frequency modulation
FSK	Frequency shift keying
GSM	Groupe Spécial Mobile or Global System for Mobile Communication
IS-54	Interim Standard 54 (TIA/EIA TDMA cellular standard, U. S.)
IS-95	Interim Standard 95 (TIA/EIA CDMA cellular standard, U. S.)
ISDN	Integrated Services Digital Network

ISM	Industrial, Scientific, and Medical (bands, devices)
LAN	Local area network
NCFSK	Non-coherent frequency shift keying
PBX	Private branch exchange
PCN	Personal Communications Network (Europe)
PCS	Personal Communications Services (U. S.)
PDC	Personal Digital Cellular (Japan)
PSTN	Public Switched Telephone Network
SIR	Signal-to-interference ratio
SNR	Signal-to-noise ratio
TDMA	Time division multiple access
TIA	Telecommunications Industry Association (U. S.)
UCLA	University of California, Los Angeles

C.2 Definitions

Availability: The probability or fraction of time that a system is available for use.

Baud: The unit of symbol rate in modulation.

Bit error rate: The ratio of the number of bits incorrectly received to the total number of bits transmitted.

BCH Codes: A large class of cyclic codes that include both binary and nonbinary alphabets.

Block codes: A type of code in which blocks of k information symbols are encoded into corresponding block of n symbols ($n > k$). Each block of n symbols constitute a code word.

Capacity: Maximum number of users a system can support.

Cellular Radio: A system in which a service area is divided into smaller areas, called cells and portions of the radio spectrum may be shared by different cells.

Channel: An allocation of the physical (frequency and time) resources of a transmission medium for communications.

Channel coding: Adding controlled redundancy to the information sequence to improve reliability of data transmitted through a noisy channel.

Coherent detection: Detection using a reference signal that is synchronized in frequency and phase to the transmitted signal.

Convolutional codes: A type of code in which output sequence consists of a selected set of linear combinations of the input sequence.

Code division multiple access: A way of sharing a common spectrum in which signals from different transmitters are distinguished by a code known to the intended receiver.

Dispersion: The spreading, separation or scatter of a waveform during transmission.

Distortion: Any departure from a specified input/output relationship.

Diversity: The reception of different versions of the same information, each with independent fading levels.

Doppler: A shift in the observed frequency of a signal caused by variation in the path lengths between the transmitter and receiver.

Fading: The variation of the intensity or relative phase of any frequency component of a received signal due to changes in the characteristics of the propagation path with time.

Flat fading: Fading resulting in similar attenuation of all frequency components of signal.

Frame: A set of consecutive time slots in which the position of each slot can be identified in reference to the frame start time.

Frequency diversity: A transmission technique used to minimize the effects of fading wherein the same information signal is transmitted and received simultaneously

on two or more independent carrier frequencies.

Frequency-hopping: A spread spectrum technique in which the available channel bandwidth is subdivided into a large number of frequency slots. In any signaling interval, the transmitted signal occupies one or more of the available frequency slots.

Frequency-selective fading: Fading in which not all frequency components of the received radio signal are attenuated equally.

Frequency-shift keying (FSK): A form of frequency modulation in which discrete frequencies are used to represent a digital signal.

Hard decoding: The decoder operates on the hard decisions made by the demodulator.

Integrated services digital network (ISDN): An integrated digital network which can establish connection for data and telephony services using the same transmission equipment.

Interference: Undesired signals in the communication channel.

Interleaving: A method of spacing successive symbols of a given codeword at wide intervals in time to overcome burst errors.

Medium: A substance regarded as the means of signal transmission.

Modulation: The process of varying certain characteristics of a carrier in accordance with a message signal.

Multipath: The large set of propagation paths that the transmitted signal takes to the receiver. The multiple paths could be caused by scattering.

Multipath fading: Fading that results when radio signals reach the receiving antenna by two or more paths.

Multiple-Access: A sharing scheme that enables dispersed users to simultaneously access a common channel resource.

Network: An organization of terminals capable of intercommunication.

Noncoherent detection: Any form of detection that does not require a phase reference.

Outage: A condition wherein a user is deprived of service due to unavailability of the communication system.

Personal Communication Services (PCS): For standard purposes, it is an umbrella term to describe services and supporting systems that provide users with the ability to communicate anytime, anywhere, and in any form.

Power Control: A technique employed to adjust the transmit power from every radio link to the minimum level required for reliable transmission.

Quantization: A process in which the continuous range of values of a signal is divided into nonoverlapping but not necessarily equal subranges and to each subrange a discrete value of the output is uniquely assigned. Whenever the signal value falls within a given subrange, the output has the corresponding discrete value.

Receiver: A device that converts signals used for transmission back to information signals.

Reed Solomon Codes: A class of non-binary block codes with good distance properties.

Spread Spectrum: A signaling scheme in which the transmission bandwidth is much greater than the information rate.

Soft decoding: The decoder uses the unquantized samples output from the demodulator to recover the information sequence.

Transmitter: A device that converts information signal to electrical or optical signals for transmission purposes.

Transceiver: A contraction of “transmitter/receiver.” The term is used when a communication device can both transmit and receive.

White noise: Noise whose frequency spectrum is uniform over a wide frequency band.

Wireless Communications: Covers approaches to communication without wires.

Bibliography

- [1] D. Avidor and J. Omura, "Analysis of FH/MFSK systems in non-uniform Rayleigh fading channels," in Proc. MILCOM '82, pp. 28.3.1-28.3.6.
- [2] D. M. Black, and D. O. Reudink, "Some characteristics of mobile radio propagation at 836 MHz in the Philadelphia area," IEEE Trans. Veh. Tech., vol. VT-21, pp. 45-51, 1972.
- [3] R.E. Blahut, *Theory and Practice of Error Control Codes*. New York: Addison-Wesley, 1983.
- [4] S. C. Chen, N. Bambos, and G. J. Pottie, "On Distributed Power Control for Radio Networks," Proc.of IEEE ICC '94., pp. 1281-1285, vol. 3., May 1994.
- [5] K. Cheun and W. E. Stark, "Performance of Robust Metric with Convolutional Coding and Diversity in FHSS Systems under Partial-Band Noise Jamming," IEEE Trans. Commun., vol. COM-41, pp. 200-209, Jan. 1993.
- [6] C. C. Clark, and J. B. Cain, *Error Correcting Coding for Digital Communications*, Plenum Press, New York, 1981.
- [7] G. R. Cooper and R. W. Nettleton, "A spread-spectrum technique for high-capacity mobile communications," IEEE Trans. Veh. Tech., vol. 27, no. 4,

pp. 264-275, Nov. 1978.

- [8] D. C. Cox,, “Wireless network access for personal communications,” IEEE Commun. Mag., pp. 96-115, Dec. 1992.
- [9] D. C. Cox, “Universal digital portable radio communications,” proc. IEEE, vol. 75, pp. 436-477, April 1987.
- [10] G. J. Foschini and Z. Miljanic. “A Simple Distributed Autonomous Power Control Algorithm And Its Convergence,” IEEE Trans. on Veh. Tech., vol. 42: pp. 641-646, 1993.
- [11] M. Gerla and J. T. C. Tsai, “A Distributed Mobile Wireless Infrastructure for Wireless Applications,” Fifth WINLAB Workshop on Third Generation Network, April 1995.
- [12] K. S. Gilhousen, I. M. Jacobs, R. Padovani, A. J. Viterbi, L. A. Weaver, Jr., and C. E. Wheatley, III, “On the capacity of a cellular CDMA system,” IEEE Trans. Vehic. Technol., vol. 40, pp. 303-312, May 1991.
- [13] D. J. Goodman, P. S. Henry, and V. K. Prabu, “Frequency-hopped multilevel FSK for mobile radio,” Bell Sys. Tech. J., vol. 59, pp. 1267-1275, Sept. 1980.
- [14] V H. MacDonald, “The cellular concept,” Bell Syst. Tech. J., vol. 58, no. 1, Jan 1979.
- [15] M. F. Ibrahim, and J. D. Parsons, “Signal strength prediction in build-up areas, Part I; median signal strength,” IEE Procs., vol. 130, Pt. F, No. 5, pp. 377-384, 1984.

- [16] R. Kohno, R. Meidan, and L. B. Milstein, "Spread Spectrum Access Methods for Wireless Communications," *IEEE Commun. Mag.*, pp. 58-67, Jan. 1995.
- [17] A. D. Kucar, "Mobile radio: An overview," *IEEE Commun. Mag.*, pp. 72-85, Nov. 1991.
- [18] J. S. Lee, R. H. French, and L. E. Miller, "Probability of error analyses of a BFSK frequency-hopped system with diversity under partial-band jamming interference-Part I: performance of square-law linear combining soft decision receiver," *IEEE Trans. Commun.*, vol. COM-32, pp. 645-653, June 1984.
- [19] V. O. K. Li and X. Qiu, "Personal Communication Systems (PCS)," *Proc. of IEEE*, vol. 83, no. 9, pp. 1210- 1245, Sept. 1995.
- [20] S. Lin and D.J. Costello, *Error Control Coding: Fundamentals and Applications*. Englewood Cliffs, NJ: Prentice-Hall, 1983.
- [21] V. S. Lin and G. J. Pottie, "Channel Coding for a Frequency-Hopped Wireless Transceiver," *Proc. of the 1993 Canadian Workshop on Information Theory*, Ottawa, Canada, pp. 109-124, 1994.
- [22] V. S. Lin and G. J. Pottie, "Implementation of Distributed Power and Admission Control for a Frequency-Hopped Wireless Transceiver," Submitted to *IEEE Trans. Vehic. Technol.*
- [23] J. L. Massey, "Coding and modulation in digital communications," *Proc. Int. Zurich Seminar on Digital Communications*, pp. E2(1)-E2(4), 1974.
- [24] D. Mitra, "An Asynchronous Distributed Algorithm For Power Control In

Cellular Radio Systems,” Proc. Fourth Winlab Workshop on Third Generation Wireless Information Network, October 1993.

- [25] J. Min, A. Rofougaran, V. Lin, M. Jensen, A. Abidi, G. Pottie, and Y. Rahmat-Samii, “A Low-Power Handheld Frequency-Hopped Spread Spectrum Transceiver Hardware Architecture,” Virginia Tech Symposium on Wireless Personal Communications, Blackburg, VA, p. 10/1-8, June 1993.
- [26] J. S. Min and H. Samueli, “Analysis and Design of A Frquency-Hopped Spread Spectrum Transceiver for Wireless Personal Communications,” Submitted to IEEE Trans. on Veh. Tech.
- [27] J. D. Parson, *The Mobile Radio Propagation Channel*, New York, NY: Wiley & Sons, 1991.
- [28] G. J. Pottie and A. R. Calderbank, “Channel Coding Strategies for Cellular Radio,” IEEE International Symposium on Information Theory, San Antonio, TX, Jan. 1993. (submitted to IEEE Trans. on Veh. Tech.).
- [29] J. G. Proakis, *Digital Communications*, new york: McGraw-Hill, 1983.
- [30] Y. Okurmura, E. Ohmori, T. Kawano, and K. Fukuda, “Field strength and its variability in the VHF and UHF land mobile radio service,” Review Elec. commun. Lab., vol. 16, No. 9-10, pp. 825-873, 1968.
- [31] S. Stein, “Fading channel issues in system engineering,” IEEE JSAC, vol. 5, no. 2, pp. 68-??, Feb. 1987.
- [32] H. Samueli, et. al, “Hardware Technologies for Adaptive High Bit-Rate Wireless Transceivers,” Technical and Management Proposal to ARPA,

UCLA, 1993.

- [33] H. Samueli, et. al, "Hardware Technologies for Robust Personal Communication Transceivers," Semi-Annual Technical Report to ARPA, UCLA, 1994.
- [34] G. L. Stuber, J. W. Mark, and I. F. Blake, "Diversity and Coding for FH/MFSK Systems with Fading and Jamming - Part I: Multichannel Diversity," IEEE Trans. Commun., vol. COM-35, pp 1329-1341, Dec. 1987.
- [35] G. L. Stuber, L. B. Yiin, E. M. Long, K. Yang, "Outage Control in Digital Cellular Systems," IEEE Trans. on Veh. Tech., vol. 42, pp. 177-197.
- [36] M. K. Simon, J. K. Omura, R. A. Scholtz, and B. K. Levitt, *Spread Spectrum Communications Volume I*. Rockville, MD: Computer Science 1985.
- [37] M. K. Simon, J. K. Omura, R. A. Scholtz, and B. K. Levitt, *Spread Spectrum Communications Volume II*. Rockville, MD: Computer Science 1985.
- [38] W. E. Stark, "Coding for frequency-hopped spread-spectrum communication with partial-band interference - Part II," IEEE. Trans. Commun., vol. COM-33, pp. 1045-1057, Oct. 1985.
- [39] G. L. Turin, "Introduction to spread-spectrum antimultipath techniques and their application to urban digital radio," Proc. IEEE, vol. 68, no. 3, pp. 328-353, Mar. 1980.
- [40] A. J. Viterbi, "A robust ratio-threshold technique to mitigate tone and partial-band jamming in coded MFSK systems," MILCOM '82, Oct. 18-20, 1982.

- [41] A.J. Viterbi, J.K. Omura, *Principles of Digital Communication and Coding*. New York: McGraw-Hill, 1979.
- [42] A. J. Viterbi, "When not to spread spectrum - A sequel," *IEEE Commun. Mag.*, vol. 23, pp. 12-17, Apr. 1985.
- [43] A. J. Viterbi, "Wireless digital communication: A view based on three lessons learned," *IEEE Commun. Mag.*, vol 29, no. 9, pp. 33-36, Sept. 1991.
- [44] A. J. Viterbi, "The Evolution of Digital Wireless Technology from Space Exploration to Personal Communication Services," *IEEE Trans. on Veh. Tech.*, vol 43, no 3, pp. 638-644, Aug. 1994.
- [45] A.D. Whalen, *Detection of Signals in Noise*. San Diego: Academic Press, Inc., 1971.
- [46] J. M. Wozencraft, and I. M. Jacobs, *Principles of communication engineering*, NY: John Wiley & Sons, 1965.
- [47] J. M. Wozencraft, and R. S. Kennedy, "Modulation and demodulation for probabilistic coding," *IEEE Trans. Inform. Theory*, Vol. IT-12, pp. 291-297, July 1966.
- [48] Y.-J. Wu, P. M. Chau, and R. Hecht-Nielsen, "A Supervised Learning Neural Network Coprocessor for Soft-Decision Maximum-Likelihood Decoding," *IEEE Trans. Neural Net.*, vol. 6, no. 4, pp. 986-992, July 1995.
- [49] Z. Zolghadr, and B. Honary, "Digital Matched-Correlator Automatic Gain Control Scheme Applicable to MFSK Modems," *IEE Proc.-1*, vol. 138, no. 2, pp. 123-131, April 1991.